R-ED 11117

SCOUT
SYSTEM DESIGN
REPORT

Honeywell
Aeronautical Division

LOS ANGELES, CALIFORNIA

Honeywell
Aeronautical Division

1915 ARMACOST AVENUE
WEST LOS ANGELES, CALIF.

SCOUT SYSTEM DESIGN REPORT

Prepared by: *C. L. Smith*
Systems Analysis Engineer

Approved by: *R. L. Pynearson*
Senior Project Engineer

Approved by: *D. C. Gerrish*

D. C. Gerrish, Manager

FOREWORD

This document is submitted to Chance Vought Corporation as a requirement of contract No. CV 300. Two supplements to this document, which will be published in the early part of 1961, will complete the above requirement.

The first supplement will be entitled "SCOUT System Design Report, Supplement I, Basic System Design Data." This document will contain charts and graphs which represent basic characteristics of the airframe and engines. The second supplement will be entitled "SCOUT System Design Report, Supplement II, Design Data Used in Selection of System Parameters." This document will contain charts and graphs which represent the "large payload" design effect on the system.

TABLE OF CONTENTS

LIST OF ILLUSTRATIONS

LIST OF TABLES

INTRODUCTION

The SCOUT is a four-stage, solid fuel, rocket research vehicle capable of carrying moderate size payloads to high altitudes or of placing them in orbits. The SCOUT vehicle is guided along a zero-lift trajectory by a stored program of attitude commands, and it derives its attitude from three body-mounted gyros. Ignition signals for each stage except the first are provided by a timer in the guidance unit. The vehicle is controlled from launch to second-stage ignition by movable jet vanes and aerodynamic surfaces. The second and third stages are controlled by hydrogen peroxide reaction jets, while the fourth stage attitude is maintained by spin stabilization only.

This report presents the methods and results of the system design of the SCOUT controls for the first three vehicles. These early SCOUTS were characterized by a 20-inch diameter fourth-stage and by a payload weight of 150 lbs. The analysis of the fourth vehicle, which has a different fourth-stage structure, will follow this report as an addendum.

SUMMARY

This report documents the considerations involved in the design of the SCOUT first, second, and third-stage control systems. The considerations of the control members of each stage as determined by disturbance moments, jet vanes, aerodynamic surfaces, and control-surface actuation are discussed.

Stabilization of the three axes of the first-stage is reviewed with respect to a description of the airframe, control system design, and the nominal control system.

The second and third-stage control systems are discussed with regard to the selection of control parameters for the first four vehicles. A description of the airframe is also included.

SECTION I

SCOUT FIRST-STAGE CONTROL SYSTEM

CONTROL MEMBERS

During first-stage operation the SCOUT is controlled by means of movable, aerodynamic surfaces and by jet vanes located in the engine exhaust. The aerodynamic surfaces, which are actually the tips of each of the four fins, are connected to the same shaft that drives the jet vanes. During the few seconds immediately following launch, the jet vanes provide most of the control; then as the dynamic pressure increases, the tip surfaces become more effective.

Disturbance Moments

The sizes of both the vanes and the tips were chosen to provide controlling forces adequate to overcome disturbance moments due to thrust misalignment, fin misalignment, and winds. Thrust misalignment moments, at the maximum specified angle of 0.25 degree, vary from 11,100 to 20,400 ft-lbs during flight. If both fins in one plane were misaligned the specified maximum of 0.15 degree, the resulting moment would reach a peak of about 16,600 ft-lbs. The disturbance moment due to wind is about 55,000 ft-lbs within the wind and attitude specifications for SCOUT.

In the body roll axis, disturbance moments are produced mainly by differential misalignment of the four fins. If each fin were misaligned the maximum allowable amount of 0.15 degree, the peak rolling moment

would be 1120 ft-lbs under conditions of an 80-degree vehicle launch angle.

Jet Vanes

The jet vane used on SCOUT produces an average lift of 48 lbs/deg deflection; the actual value depends upon the Algol engine thrust and the state of erosion of the vane surface. Static firing tests of the vane show normal erosion of about eight percent of the effective area during engine burning. This erosion causes the lift to decrease by the same amount. The lift (and hence the control moment) of the vane is quite linear with deflection over the range of deflections used.

Lift naturally decreases during the engine thrust decay after burning. Several jet vane designs were considered with a view to minimizing the hinge moment, reducing variations due to erosion, and preventing flame leakage into the drive-shaft area. The design chosen produces relatively low hinge moments which vary from initially unstable to stable moments in about 19 seconds. At engine ignition full deflection produces a diverging moment of 570 in-lbs, while just prior to engine tailoff, a 20-degree deflection results in a restoring moment of 475 in-lbs. Hinge moments are not predictable within a small range due to erosion of the vane and flame shield, and it is expected that bias and asymmetrical moments exist in operation.

The aerodynamic tip control surfaces produce lift dependent upon dynamic pressure and Mach number. Assuming an 80-degree launch angle, the total pitch or yaw control moment (which is a function of the vehicle center of mass) is plotted against time in figure 1. Note that the total control

R-ED 11117

- 4 -
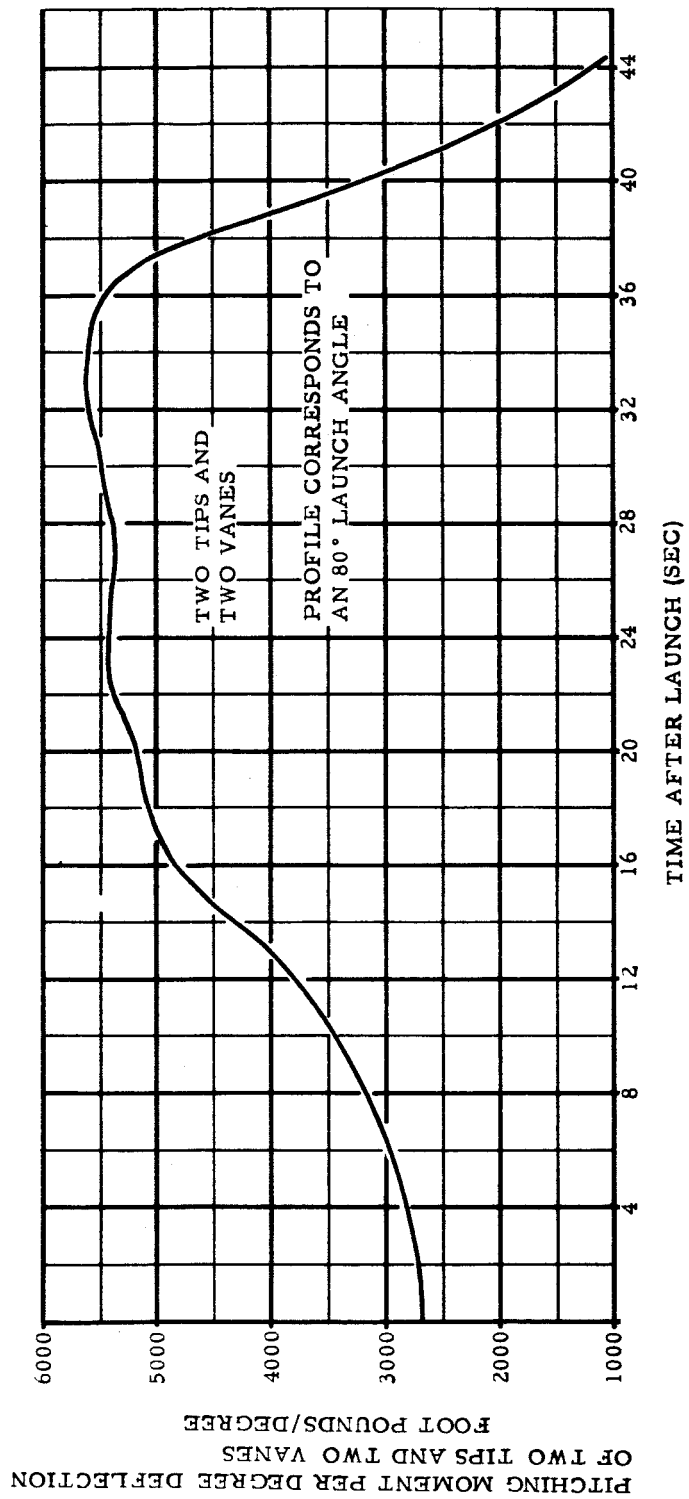
Figure 1 First-Stage Total Pitch Control Moment vs Time

moment per degree deflection varies from 2660 to 5600 ft-lbs ⁄ deg (a factor of 2.1) during powered flight. In roll the total control moment due to differential deflection of two surfaces and vanes varies from 1280 to 4460 ft-lbs during first-stage burning, as may be seen from the plot of figure 2.

Aerodynamic Surfaces

The aerodynamic tip controls are statically unstable at all Mach numbers, but above Mach 2 their hinge moment coefficient is very low. Hinge moments due to the tips are nonlinear with deflection, and are dependent upon the dynamic pressure, Mach number, and angle of attack. In the SCOUT design, total moments were calculated with a four-degree angle of attack of the most conservative sign. The most severe over-all hinge moment, occurring about 11 seconds after launch, is 600 in-lbs at 20 degrees of deflection and four degrees angle of attack. This is true for an 80-degree launch angle. The nonlinear relationship between hinge moment and deflection causes the equivalent "spring rate" of the control surfaces to be somewhat higher than indicated by the moment at 20 degrees of deflection. More complete data on basic items such as lift and moment coefficients will be given in SCOUT System Design Report, Supplement I.

Control Surface Actuation

Movement of the control surfaces on SCOUT is accomplished by means of a hydraulic piston actuator operated by an electro-hydraulic valve. These components, together with a power amplifier and a feedback
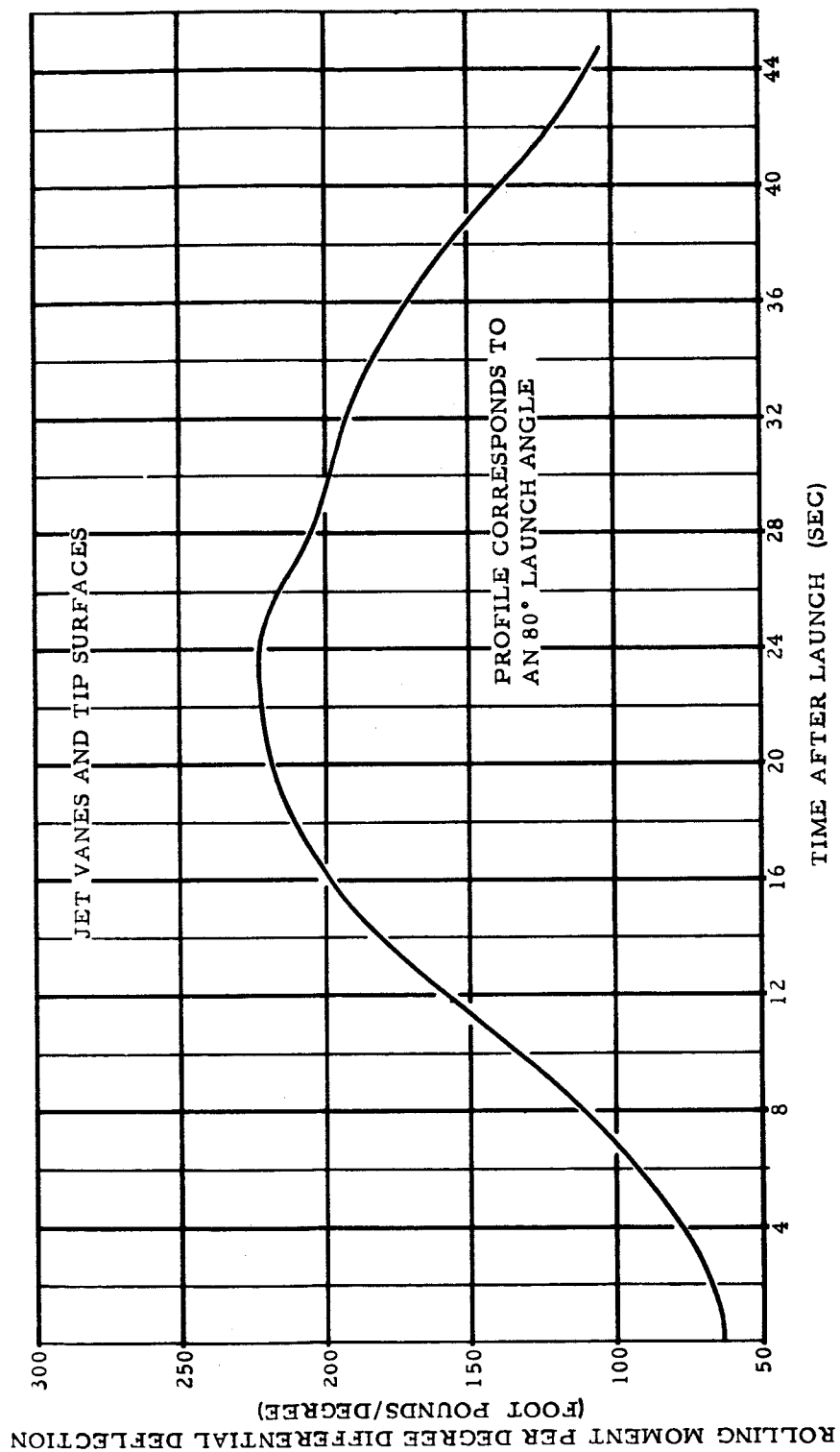
Figure 2 First-Stage Total Roll Control Moment vs Time

transducer, form a servo unit, one of which is used for each control surface. A block diagram of a SCOUT servo is given in figure 3. The actuator, valve combination must be chosen to be capable of overcoming the maximum expected hinge moment and providing a slewing rate adequate for control. Since the maximum hinge moment and slewing rate requirements were not known at the time of component selection, rather conservative values were chosen. Accordingly the SCOUT actuator and valve can produce a stall hinge moment of 1700 in-lbs and a no-load slewing rate of 250 deg/sec. These numbers are much greater than required, but are incorporated because of the ease of attaining them with a hydraulic servo. The reason, however, for leaving a sizable hinge moment margin is due partly to the uncertainty in requirement resulting from erosion, and partly due to the mere fact that the moment is sometimes unstable. The servo valve consists of a solenoid-driven flapper valve which directs hydraulic oil to position a four-way spool. The spool in turn controls the flow to the actuator. System operating pressure is obtained by means of a battery-driven electric pump, a hydraulic accumulator, and a regulator set at 3000 psi. The hydraulic actuator is a cylinder and piston having an effective area of 0.419 square inches and a total stroke of 0.86 inches. It acts at a moment arm (at zero deflection) of 1.375 inches and can produce a total angular control surface deflection of 37 degrees. The closed loop dynamic response of the servo depends upon amplifier and valve lags, the inertia of the load (vanes and tips), and the open-loop gain. With the SCOUT components, the lags are very small (less than one ms), so that at low gains, the gain alone determines the dynamic response. Without introducing extraneous lags, the servo exhibits primarily a first-order response up to frequencies of 50 or 60 rad/sec.
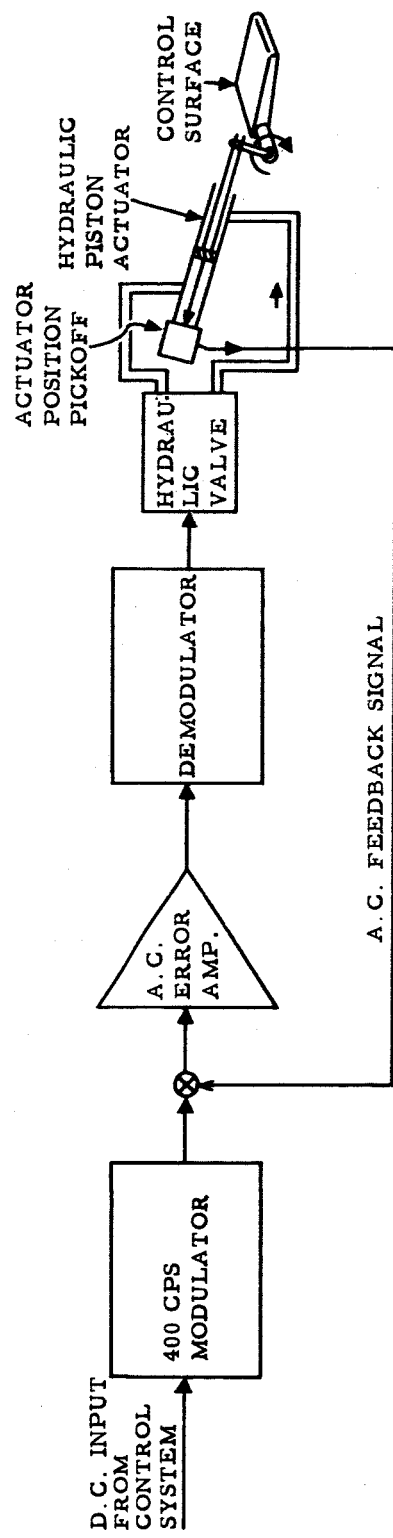
Figure 3 First-Stage Block Diagram of SCOUT Hydraulic Servo

If the loop gain is raised even more, the effect of the system lags begins to become evident, and the servo eventually becomes underdamped in the region of 100 to 150 rad/sec. Since it is necessary for the control designer to know the response of each component in his system as closely as possible, the servo loop gain on SCOUT was made variable. During the system design of the first stage, a servo response was determined which gave the best overall operation, and this was approximated in the actual equipment by adjusting the loop gain. The resultant behavior is nearly a simple, first-order response with a break frequency of 31 rad/sec. Within the region of operation, the simple break frequency varies directly with loop gain, and in fact, is numerically equal to it.

The response of the SCOUT servo depends upon external parameters such as hydraulic pressure and spring rate of the load as well as upon loop gain. The tolerance on supply pressure is ± 10 percent, which should allow a variation of ± 3 percent in the servo break frequency. The load affects the servo response in two ways. The effective spring rate due to hinge moment raises or lowers the natural frequency a slight amount merely by adding a position term to the characteristic equation. Also, the presence of a static load requires that the actuator assume a certain pressure level, which reduces the pressure drop across the valve and decreases its gain. Measurements of servo frequency response were made with large hinge moments and the results are shown in figure 4. Investigation of the effect of low hydraulic pressure indicated that deviations in response were within the measurement error.
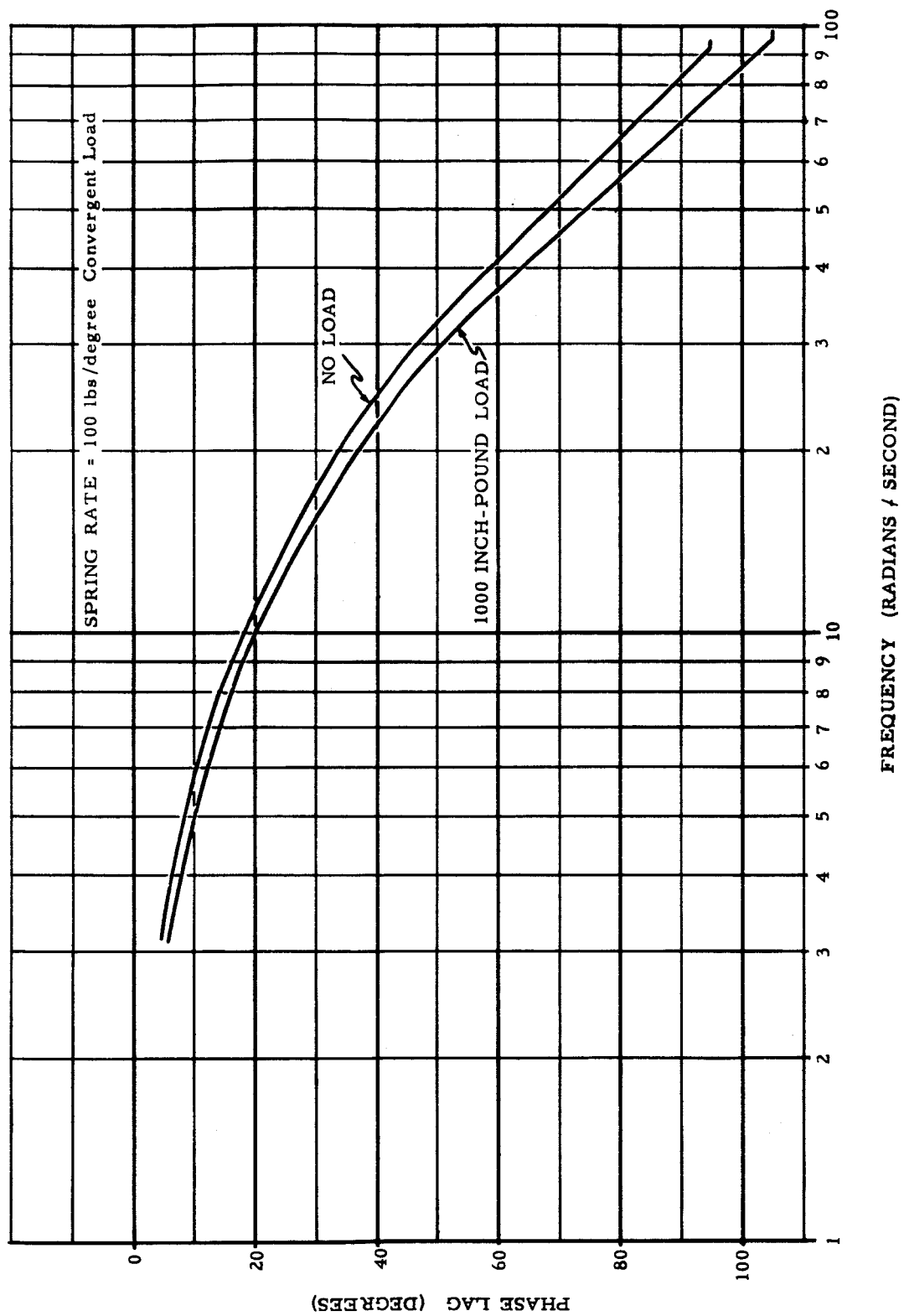
Figure 4 - Effect of Hinge Moment on First-Stage Servo Frequency Response

The choice of hydraulic rather than electric servo actuation was made at a time when the hinge moment, slewing rate, and frequency response requirements could only be estimated. The hydraulic servo has the advantage of being more than adequate in hinge moment while giving an adjustable response. The hydraulic servo is capable of first-order behavior up to relatively high frequencies, and due to its large margin of effectiveness, it is affected very little by load variations.

STABILIZATION

Pitch And Yaw Axes

Airframe Description: The SCOUT airframe, which must be stabilized by the control system is a long, slender body and is aerodynamically stable. The lift due to angle of attack is distributed over the body in a manner dependent on Mach number. For purposes of analysis the distribution was lumped at four body stations, this being practical since the loads tend to concentrate at the nose, the D-section flare, the B-section flare, and at the fins. The lumped distributions will be given in "SCOUT System Design Report, Supplement 1", for three Mach numbers.

To properly stabilize the SCOUT vehicle, the effects of body flexibility had to be considered. The first three body-bending modes were used to describe the deflections and angles at each body station. Bending

mode shapes, slopes, and frequencies will be given for several flight conditions in "SCOUT System Design Report, Supplement I." In flight the actual lift distribution is determined by the local angles of attack along the body, and these are affected by bending. Hence, the total description of the airframe is accomplished by writing the ordinary rigid equations of motion in conjunction with a set of wave equations for the body flexibility.

The SCOUT first-stage control system was designed by investigating the airframe behavior at several discrete conditions. These were launch, the transonic region, maximum dynamic pressure, and burn-out. These conditions were felt to be representative of the most severe points on the trajectory. The launch case was of interest because the bending frequencies were lowest there and because the effective control gain was low (due to both the absence of aerodynamic control and to the inertia center-of-mass situation). The transonic condition was considered because the static stability margin is very large near Mach one, and the tip controls are especially effective. Maximum dynamic pressure is of primary importance since the tip controls are very effective, the aerodynamic coupling of bending modes is large, and the moment due to angle of attack is near maximum. The burnout condition was used primarily to check the performance just prior to the first-stage coast; at that time the lift forces are small and the control effectiveness has been greatly reduced due to the loss of jet vane control.

The equations of motion of the vehicle are composed of aerodynamic and structural terms; the force on the body is the summation of lifts at the four aerodynamic load stations and these, in turn, are functions

of the local angles of attack. The angle of attack at each body station is that of the rigid airframe plus that due to bending. Bending produces two angle-of-attack terms at each station; one is the actual bending slope (the sum of the slopes due to each of the three modes), and the other is that caused by the bending deflection rate.

In writing the airframe equations in the pitch plane, standard terminology has been used wherever possible. Capital M's refer to moments and Z's to displacement. The wave description of structural deflection is $w(x, t) \equiv \varphi(x) z(t)$ where w is the generalized deflection at time, t, and body station, x. φ is the normalized bending mode shape and z is the normalized time response. Subscripts refer to the number of the mode and to the number of the body station, in that order. Thus φ_{ij} is the normalized deflection of the ith bending mode at the jth body station. The matrix of pitch equations of motion at a particular flight condition is given in figure 5 for force applied by a control surface deflection, δ.

Here α is the rigid-body angle of attack, $\dot{\theta}$ the rigid pitch rate, V is the vehicle velocity, and S is the Laplace (complex frequency) operator. Coefficients such as $Z_1\dot{z}_2$ refer to forces exciting the first mode due to rate of deflection of the second, while the coefficient $Z_1 z_1$, for example, is the square of the natural frequency of the first mode including aerodynamic influence. The coefficients are defined in table 1.

$$
\begin{bmatrix}
-S + \dfrac{Z_\alpha}{V} & 1 & \dfrac{Z_{\dot{z}_1}}{V}S + \dfrac{Z_{z_1}}{V} & \dfrac{Z_{\dot{z}_2}}{V}S + \dfrac{Z_{z_2}}{V} & \dfrac{Z_{\dot{z}_3}}{V}S + \dfrac{Z_{z_3}}{V} \\[2ex]
M_\alpha & -S + M_{\dot{\theta}} & M_{\dot{z}_1}S + M_{z_1} & M_{\dot{z}_2}S + M_{z_2} & M_{\dot{z}_3}S + M_{z_3} \\[2ex]
Z_{1\alpha} & Z_{1\dot{\theta}} & -S^2 + Z_{1\dot{z}_1}S + Z_{1z_1} & Z_{1\dot{z}_2}S + Z_{1z_2} & Z_{1\dot{z}_3}S + Z_{1z_3} \\[2ex]
Z_{2\alpha} & Z_{2\dot{\theta}} & Z_{2\dot{z}_1}S + Z_{2z_1} & -S^2 + Z_{2\dot{z}_2}S + Z_{2z_2} & Z_{2\dot{z}_3}S + Z_{2z_3} \\[2ex]
Z_{3\alpha} & Z_{3\dot{\theta}} & Z_{3\dot{z}_1}S + Z_{3z_1} & Z_{3\dot{z}_2}S + Z_{3z_2} & -S^2 + Z_{3\dot{z}_3}S + Z_{3z_3}
\end{bmatrix}
\begin{bmatrix} \alpha \\ \dot{\theta} \\ z_1 \\ z_2 \\ z_3 \end{bmatrix}
= \delta
\begin{bmatrix} -\dfrac{Z_\delta}{V} \\[2ex] -M_\delta \\[1ex] -Z_{1\delta} \\[1ex] -Z_{2\delta} \\[1ex] -Z_{3\delta} \end{bmatrix}
$$

Figure 5 Matrix of Pitch Equations of Motion

$$\frac{Z_a}{V} = \frac{-qS}{mV} \sum_j C_{La_j} - \frac{T}{mV}$$

$$\frac{Z\dot{z}_i}{V} = \frac{qS}{mV^2} \sum_j C_{La_j} \phi_{ij} \quad \text{for } i = 1, 2, \text{ and } 3$$

$$\frac{Zz_i}{V} = \frac{-qS}{mV} \sum_j C_{La_j} \phi'_{ij} - \frac{T}{mV} \phi'_{iT}$$

$$\frac{Z_\delta}{V} = \frac{-qS}{mV} C_{L\delta} - \frac{K_\delta}{mV}$$

$$M_a = \frac{qS}{I} \sum_j C_{La_j} \bar{x}_j$$

$$M_{\dot\theta} = \frac{-qS}{VI} \sum_j C_{La_j} \bar{x}_j^2$$

$$M_{z_i} = \frac{qS}{I} \sum_j C_{La_j} \bar{x}_j \phi'_{ij} + \frac{T}{I}\left(\bar{x}_T \phi'_{iT} - \phi_{iT}\right)$$

$$M_{\dot z_i} = \frac{-qS}{VI} \sum_j C_{La_j} \bar{x}_j \phi_{ij}$$

$$M_\delta = \frac{qS}{I} C_{L\delta} \bar{x}_\delta + \frac{K_\delta \bar{x}_\delta}{I}$$

$$Z_{ia} = \frac{qS}{m_i} \sum_j C_{La_j} \phi_{ij}$$

$$Z_{i\dot\theta} = \frac{-qS}{m_i V} \sum_j C_{La_j} \bar{x}_j \phi_{ij}$$

$$Z_{i\dot z_i} = -2\zeta_i \omega_i \frac{-qS}{m_i V} \sum_j C_{La_j} \phi_{ij}^2$$

$$Z_{i z_i} = -\omega_i^2 + \frac{qS}{m_i} \sum_j C_{La_j} \phi'_{ij} \phi_{ij}$$

$$Z_{i\dot z_k} = \frac{-qS}{m_i V} \sum_j C_{La_j} \phi_{ij} \phi_{kj}$$

$$Z_{i z_k} = \frac{qS}{m_i} \sum_j C_{La_j} \phi_{ij} \phi'_{kj}$$

$$Z_{i\delta} = \frac{qS}{m_i} C_{L\delta} \phi_{i\delta} + \frac{K_\delta \phi_{i\delta}}{m_i}$$

where:

q = dynamic pressure

S = reference area for the lift coefficient

V = vehicle velocity

I = vehicle inertia

m = vehicle mass

C_{La_j} = lift coefficient at the jth body station due to angle of attack

$\bar{x}_j$ = distance from the jth body station to the center of mass, positive if j is forward of the center of mass

ϕ' = mode slope

m_i = generalized mass of the ith mode

i, k = mode numbers

subscript δ = the control surface station

subscript T = the engine thrust station (the nozzle throat)

$C_{L\delta}$ = lift coefficient of the aerodynamic control surfaces per unit deflection

K_δ = lift of the jet vanes per unit deflection

T = engine thrust

ω_i = natural bending frequency of the ith mode

ζ_i = structural damping ratio of the ith mode

Table 1   Coefficients of Pitch Equations of Motion for First Stage

Note that the engine thrust level appears in the moment coefficients. This is necessary to account for the effect of tail deflections due to bending which tilt the thrust vector away from the center of mass. Many of the coefficients are negligibly small when practical data is used. Nevertheless all of the terms were retained during the SCOUT design since they do not add significantly to the work and they can become important under certain circumstances.

Control System Design: The control system for the SCOUT first-stage consists of rate and position gyros, a servo, a compensation network, and of course, the airframe. Each of these items has its own dynamic response which contributes to the complexity of the analysis. Because of the body flexibility, combinations of some of the component dynamics are not simple. For instance the rate and position gyros are located at different body stations, so that the angles and rates they detect are different mixtures of bending slope and rigid-body motion. The actual inputs seen by each gyro are:

$$\text{position input} \qquad \dot{\theta}_{G_{in}} = \dot{\theta} + \sum_i \left(\phi'_{iG} \right) \left(\dot{z}_i \right)$$

$$\text{rate input} \qquad \dot{\theta}_{RG_{in}} = \dot{\theta} + \sum_i \left(\phi'_{iRG} \right) \left(\dot{z}_i \right)$$

A block diagram of the pitch system is shown in figure 6. The dynamic response of the position gyro is that of a simple time constant of 0.4 ms, while the rate gyro responds as a second-order device with a natural frequency of 22 cps and a damping ratio of 0.5.
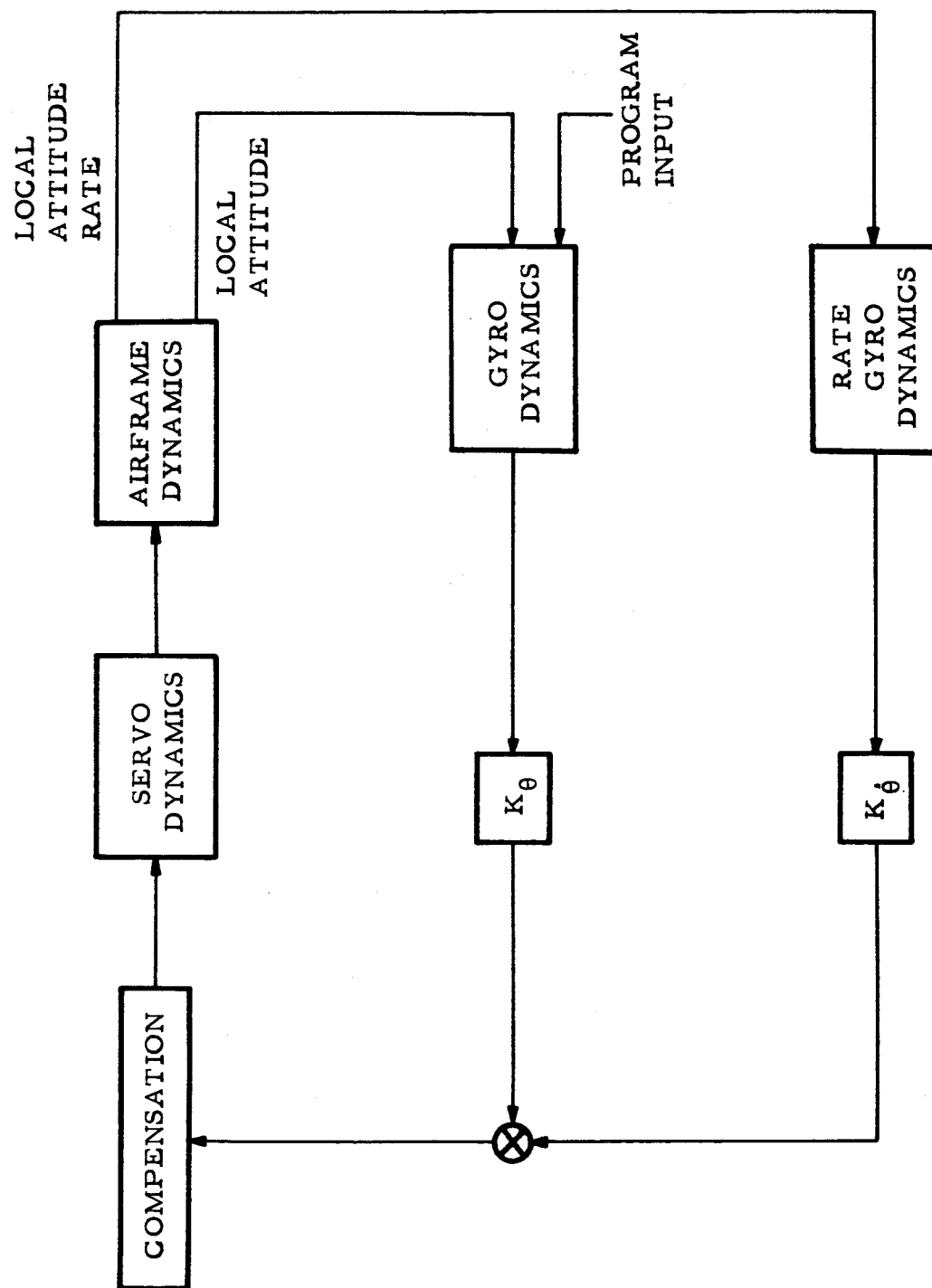
Figure 6 First-Stage Block Diagram of the Pitch Control System

The dynamic behavior of the servo system and the compensation device are, within certain limits, under the control of the designer. In general each can be represented by equations of second order or less, although higher order compensation terms have been considered.

The SCOUT control problem was attacked by considering the entire set of airframe and control equations together. In the pitch plane this results in a twelfth-order square matrix, the eigenvalues of which are the roots of the closed loop system equation. The zero matrix is shown in figure 7.

In representing equations this way several assumptions are made. First, the aerodynamic and structural coefficients are considered to be constant at the time the equations were written, i.e., they are invariant with time. Second, the coefficients are assumed to be invariant with the dependent variable, making the equations linear. Strictly speaking, both assumptions are false but their effect can be estimated. Changes with time are always too small to be a significant problem, but nonlinearities are important in some cases. The values of $C_{L\alpha}$ and $C_{L\delta}$ are both dependent upon their variables, and for stability analysis, their greatest values were used (corresponding to zero angle of attack or control deflection).

The design latitude included selection of rate and position gains, of course, and as much variation in servo response as could be reasonably justified with electric or hydraulic actuators. Synthesis of the control system was accomplished by determining the most advantageous servo behavior, gains, compensation, and as it developed later, location of

	α	θ	a_1	a_2	a_3	b	$[\delta_c]_{FILTER\ OUT}$	δ_c	$[\dot\theta_{RG}]_{IN}$	$[\dot\theta_{RG}]_{OUT}$	$[\theta_G]_{IN}$	$[\theta_G]_{OUT}$
FORCE EQUATION	$-S + \frac{Z_\alpha}{V}$	1	$\frac{Z_{a_1}S}{V} + \frac{Z_{s_1}}{V}$	$\frac{Z_{a_2}S}{V} + \frac{Z_{s_2}}{V}$	$\frac{Z_{a_3}S}{V} + \frac{Z_{s_3}}{V}$	$\frac{Z_\delta}{V}$	0	0	0	0	0	0
MOMENT EQUATION	M_α	$-S + M_{\dot\theta}$	$M_{a_1}S + M_{s_1}$	$M_{a_2}S + M_{s_2}$	$M_{a_3}S + M_{s_3}$	M_δ	0	0	0	0	0	0
FIRST BENDING MODE EQUATION	$Z_{1\alpha}$	$Z_{1\dot\theta}$	$-S^2 + Z_{1a_1}S + Z_{1s_1}$	$Z_{1a_2}S + Z_{1s_2}$	$Z_{1a_3}S + Z_{1s_3}$	$Z_{1\delta}$	0	0	0	0	0	0
SECOND BENDING MODE EQUATION	$Z_{2\alpha}$	$Z_{2\dot\theta}$	$Z_{2a_1}S + Z_{2s_1}$	$-S^2 + Z_{2a_2}S + Z_{2s_2}$	$Z_{2a_3}S + Z_{2s_3}$	$Z_{2\delta}$	0	0	0	0	0	0
THIRD BENDING MODE EQUATION	$Z_{3\alpha}$	$Z_{3\dot\theta}$	$Z_{3a_1}S + Z_{3s_1}$	$Z_{3a_2}S + Z_{3s_2}$	$-S^2 + Z_{3a_3}S + Z_{3s_3}$	$Z_{3\delta}$	0	0	0	0	0	0
SERVO TRANSFER FUNCTION	0	0	0	0	0	$S^2 + (2\zeta\omega_s)S + \omega_s^2$	$-\omega_s^2$	0	0	0	0	0
FILTER TRANSFER FUNCTION	0	0	0	0	0	0	$S^2 + (2\zeta\omega_p)S + \omega_p^2$	$-S^2 + (2\zeta\omega_o)S - \omega_o^2$	0	0	0	0
RATE GYRO INPUT	0	1	$\phi'_{1RG}S$	$\phi'_{2RG}S$	$\phi'_{3RG}S$	0	0	0	-1	0	0	0
RATE GYRO TRANSFER FUNCTION	0	0	0	0	0	0	0	0	$-\omega_{RG}^2$	$S^2 + (2\zeta\omega_{RG})S + \omega_{RG}^2$	0	0
ATTITUDE GYRO INPUT	0	-1	$\phi'_{1G}S$	$\phi'_{2G}S$	$\phi'_{3G}S$	0	0	0	0	0	-S	0
ATTITUDE GYRO TRANSFER FUNCTION	0	0	0	0	0	0	0	0	0	0	$-\frac{1}{\tau_G}$	$\frac{1}{S + \tau_G}$
CONTROL EQUATION	0	0	0	0	0	0	0	-1	0	$K_{\dot\theta}$	0	K_θ

Figure 7 Matrix of Pitch Airframe and Control Equations for First Stage

the gyros in the airframe. Discrete changes in control gains during the flight were left as a possibility. These parameters were to be chosen so that predetermined design criteria could be met in spite of variations and tolerances.

During the design it was intended that the "nominal system" (that system for which no allowance was made for component variation, parameter tolerances, or accuracy of basic data) should maintain gain and phase margins of stability of 12 db and 30 degrees, respectively. The criteria was later changed to 10 db and 20 degrees in the presence of the worst parameter variation. Other factors of importance were high loop gain and good damping. In order to cope with steady or slowly varying disturbances such as thrust misalignment, winds, and fin misalignment, the control gain should be large. Sudden moments from gusts or sharp changes in thrust misalignment are controlled better if the effective overall damping ratio is high enough to prevent more than one overshoot. It was decided that the control gain should be kept above five if possible and that the damping ratio of the "rigid-body" response (the response in the region of 0. 5 cps) should exceed 0. 2. Actually the transient response is so complex (since it includes all the bending frequencies and several control frequencies and time constants) that damping ratio has little meaning. Higher damping than 0. 3 or 0. 4 was deemed unnecessary since the wavelength of the oscillations is very long and since the pitch-over maneuver is more accurate at low damping. The settling time was maintained as low as possible, however, at frequencies of three cps and lower.

Originally there were two outstanding difficulties connected with stabilization of the first stage: the unfavorable phase shift introduced to the gyros by the second body-bending mode, and the proximity in frequency of the first bending mode and the rigid-body response at conditions of high q (dynamic pressure). The second mode effect upon the gyros when mounted in Transition Section D (at body station 120) was quite severe. Attempts to filter the forward control loop by low-pass networks were handicapped by the adverse effect of the filter on the first mode behavior. If the proper combination of servo and lag compensation dynamics is chosen for the rigid and first bending frequencies, the second bending frequency is still not sufficiently attenuated. A combination low frequency lag and second-mode notch filter was considered which produced satisfactory response to a certain extent, but which allowed too much transmission at high frequency, thus making the system more susceptible to noise and to third-mode instability. It was decided that the best overall solution to the problem would be to reduce the second-mode coupling at its source by moving the rate gyros to a more favorable location. The location of the rate gyros is more critical than that of the displacement gyros, since a rate gyro output is higher at body-bending frequencies. The rate-gyro Gnat Package Assembly was located at body station 214 in Transition Section C because the second-mode normalized slope is very small at this location. Section C was preferred over locations of low slope in other sections because of the advantage of retaining the rate gyros through third-stage operation. Although the roll rate gyro location is not particularly critical, this gyro was also relocated since it is an integral part of the Gnat Package Assembly. By relocating the gyro package, the second-bending mode effect was reduced by almost 16 db.

As the concurrent selection of compensation and servo dynamics proceeded, it became clear that the additional response required was of low-pass nature. The root locus plot of figure 8 and the Bode plot of figure 9 show the situation at maximum q with no compensation and a perfect (instantaneous response) servo. The rate-to-position gain ratio, which produces a low-frequency real zero in the open-loop transfer function, has been arbitrarily set at 0.33. From the movement of the system roots as the loop gain is increased, it can be seen that considerable phase shift is needed at the first bending mode frequency. If one or more lag terms (poles) were added at low frequency, the first mode locus would start into the left half plane and the rigid-body locus would not bend so far to the left. Lag compensation thus involves a compromise in the behavior of the rigid body and the first bending mode, and the separation of their frequencies determines its feasibility. The shape of the locus is also affected by the location of the rate gain zero which is almost equal to the position-to-rate gain ratio. As this zero is moved closer to the origin the rigid-body locus is bent more to the left, improving the system damping. Unfortunately, such movement of the zero is accomplished by raising the rate gain, which increases the sensitivity to bending modes. Thus there is a practical lower limit to the frequency of the zero.

Because of the small frequency separation between the rigid and first modes there is little chance of compensating the first-mode locus by attenuation of the higher frequency. Accordingly, it was recognized that the servo and compensation dynamics together must produce sufficient phase shift at the first-mode frequency to stabilize the first mode without adversely affecting the rigid-body locus. The phase

NO NETWORK, IDEAL SERVO
POSITION TO RATE GAIN RATIO = 3

MAX. q CONDITION

SECOND
BENDING
MODE
$K_\theta = 15$

FIRST
BENDING
MODE

$K_\theta = $ 3 5 10

$j\omega$ (RAD/SEC)

RIGID BODY

$K_\theta = $ 15 10 5

3

σ (sec^{-1})
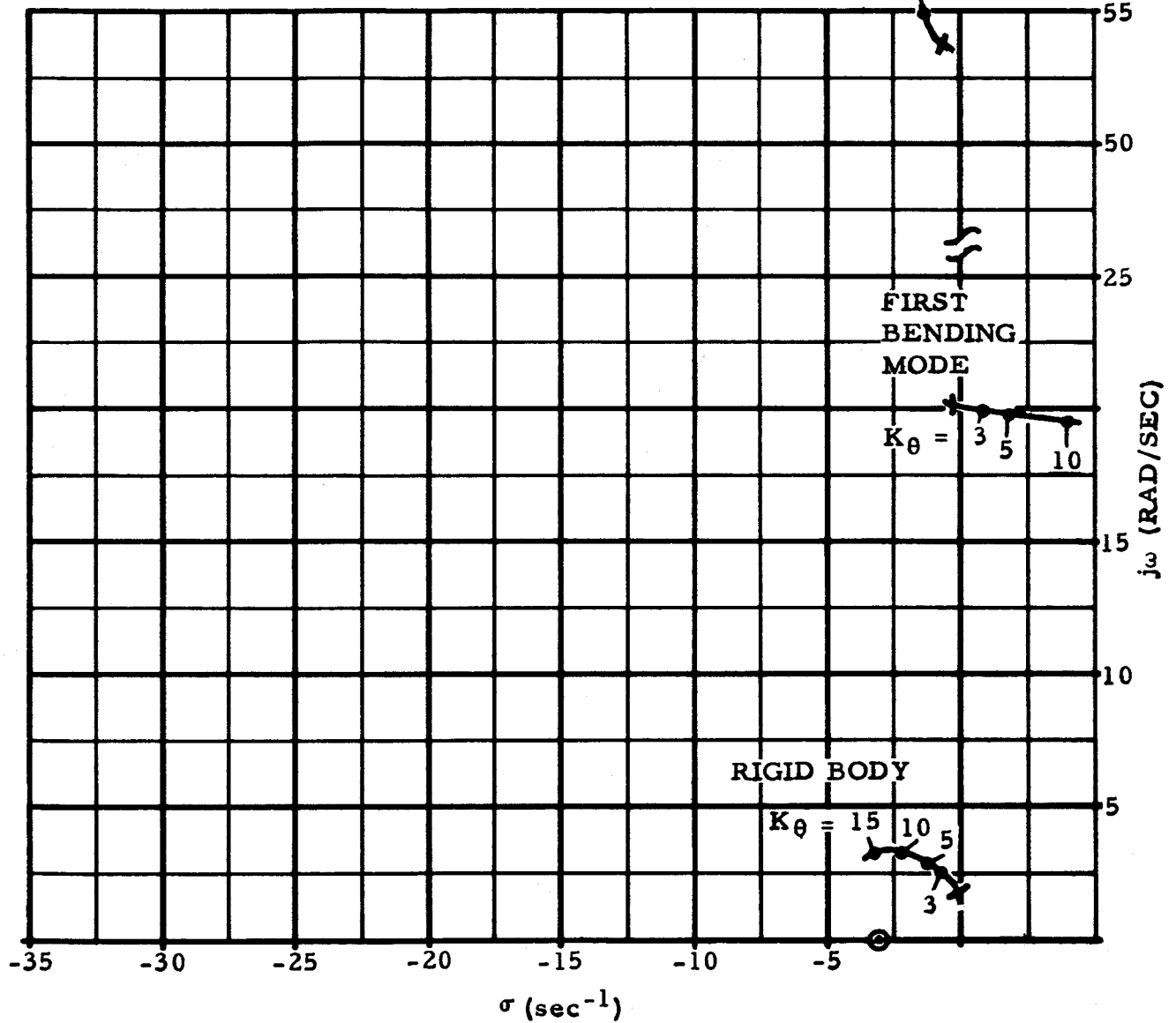
Figure 8 Root Locus Plot of Uncompensated First-Stage System
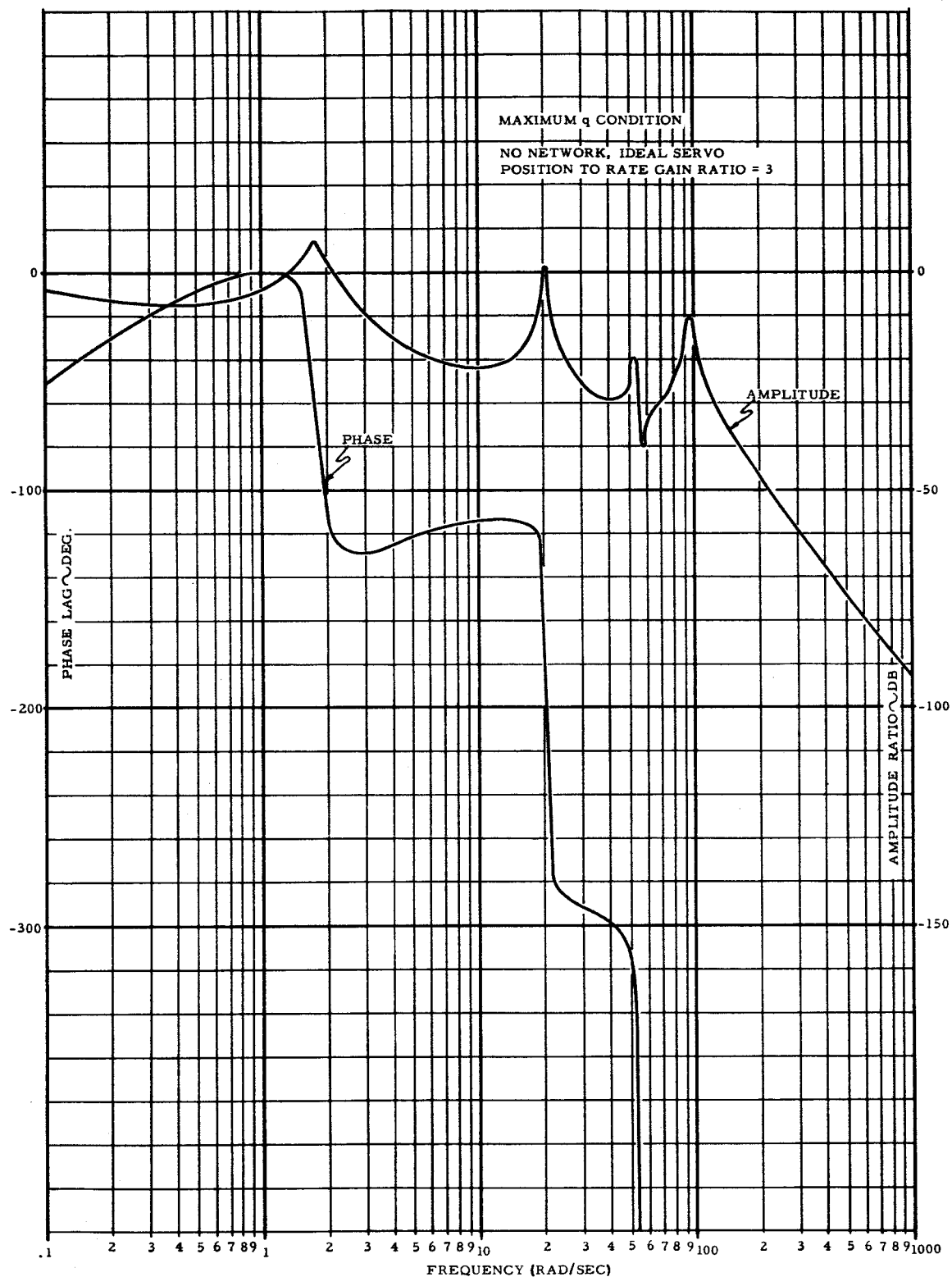
Figure 9 Bode Plot of Uncompensated First-Stage System

compensation reasoning is inferred in the Bode plot of figure 9. The amplitude plot naturally shows a peak at the first-mode frequency, and it is the purpose of the phase compensation to ensure that the phase plot crosses 180 degrees at a lower frequency.

The effort to determine suitable servo and compensation transfer functions was subject to several hardware constraints. The design of the main portion of the control system electronics had already progressed to a stage at which certain types of networks and mechanical components could not be incorporated. One such limitation was the attenuation allowable in the compensation network, which was to be kept below 20 db. The compensation had to be passive and preferably not require inductive components; moreover, its input and output impedance levels were restricted to certain ranges. The use of a hydraulic servo actuator had already been established, and it was highly desirable to use only position feedback and ac amplification. Thus the servo response could be easily altered only by varying its loop gain or using ac networks. In addition to requirements such as these, the second and third-stage control designs suggested many compromises. It had been determined, for example, that the rate-to-position gain ratio on stages two and three should be 0.4, making it desirable to use the same ratio on the first stage to avoid switching. Also, owing to stringent upper-stage reaction-jet fuel requirements, portions of the electronic circuitry common to the first and second stages could not be used for first-stage compensation devices.

A set of component dynamics was established which provided reasonable gain and phase stability margins and damping, and which could be

synthesized with the existing hydraulic servo and a simple, second-order
lag network. Three real poles were placed very close together near
a frequency of -31 nepers per sec. Two poles were to be generated
by the network and one pole by the servo. Tests of the servo actuator
have roughly verified predictions of the response obtainable. At
frequencies of interest (40 rad/sec and lower) the servo transfer
function was nearly characterized by a single pole which varied in
frequency directly with loop gain. Actually the early servos exhibited
higher-order poles at approximately -300 and -500 nepers per second.
The locations of these poles were rather unpredictable since they varied
from unit to unit as well as with loop gain. However, the problem of
considering these pole characteristics became unnecessary because it
was found that the poles moved to higher frequencies on later servos.
Because of the slight variation in servo high-frequency behavior, several
poles were included in the stability analysis to determine their effect.
By using a two-pole transfer function, the actual servo could be simu-
lated as closely as was necessary in a linear analysis.

The double-lag network could not be synthesized with its poles too
close together and still be passive and non-inductive. Accordingly the
two break frequencies were slightly separated; the nominal settings
being -29 and -33 nepers per second.

Nominal Control System: Figures 10 and 11 give the root-locus plot
and Bode plot of the nominal system at the maximum q condition.
The position-to-rate gain ratio which gives the best overall operation
is 3.0; it was considered better to use this more satisfactory ratio
and switch gains at second-stage ignition than to compromise it with

MAXIMUM DYNAMIC PRESSURE CONDITION
NOMINAL SERVO AND NETWORK
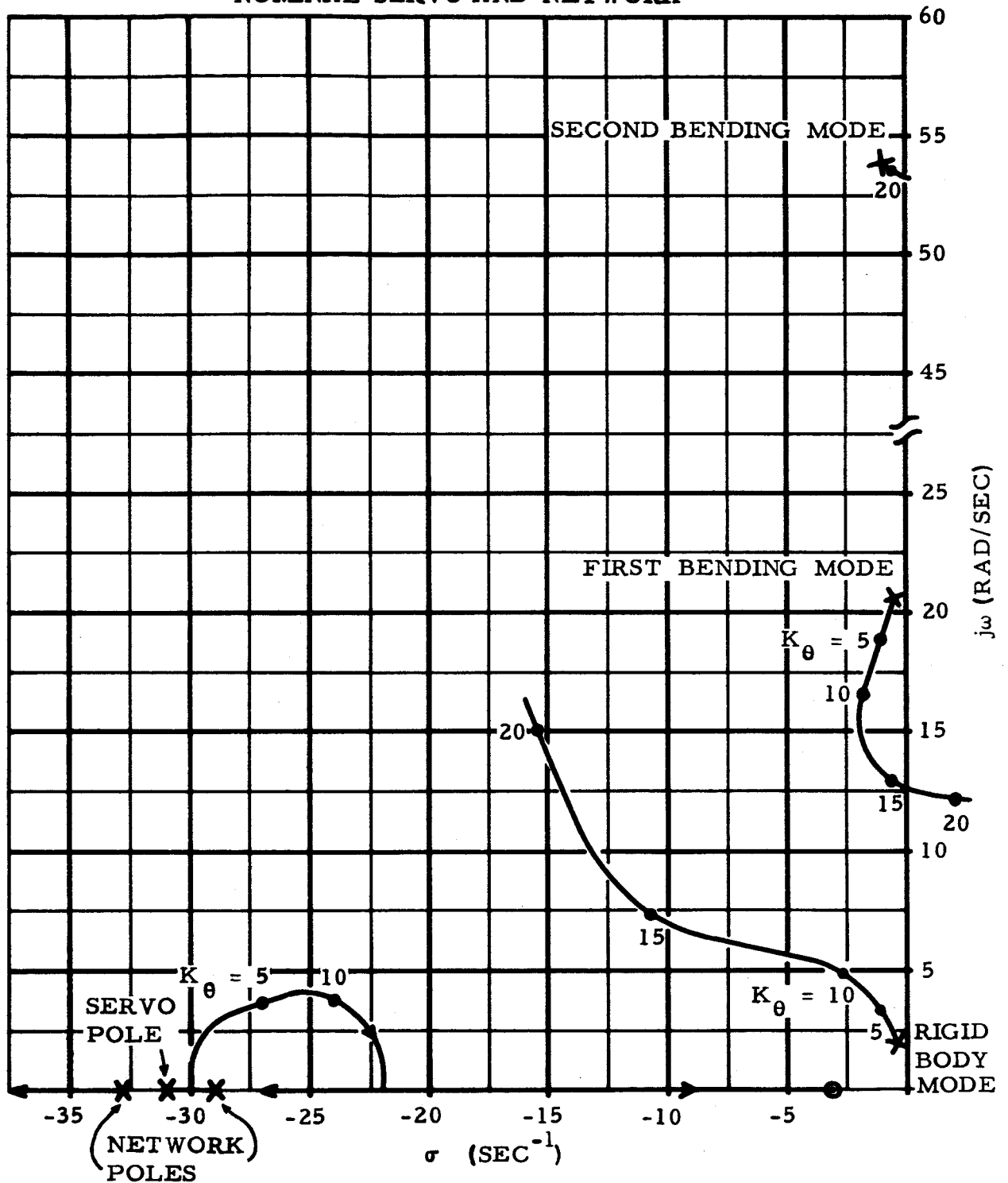
Figure 10 Root Locus Plot of Nominal First-Stage System at Maximum q Condition
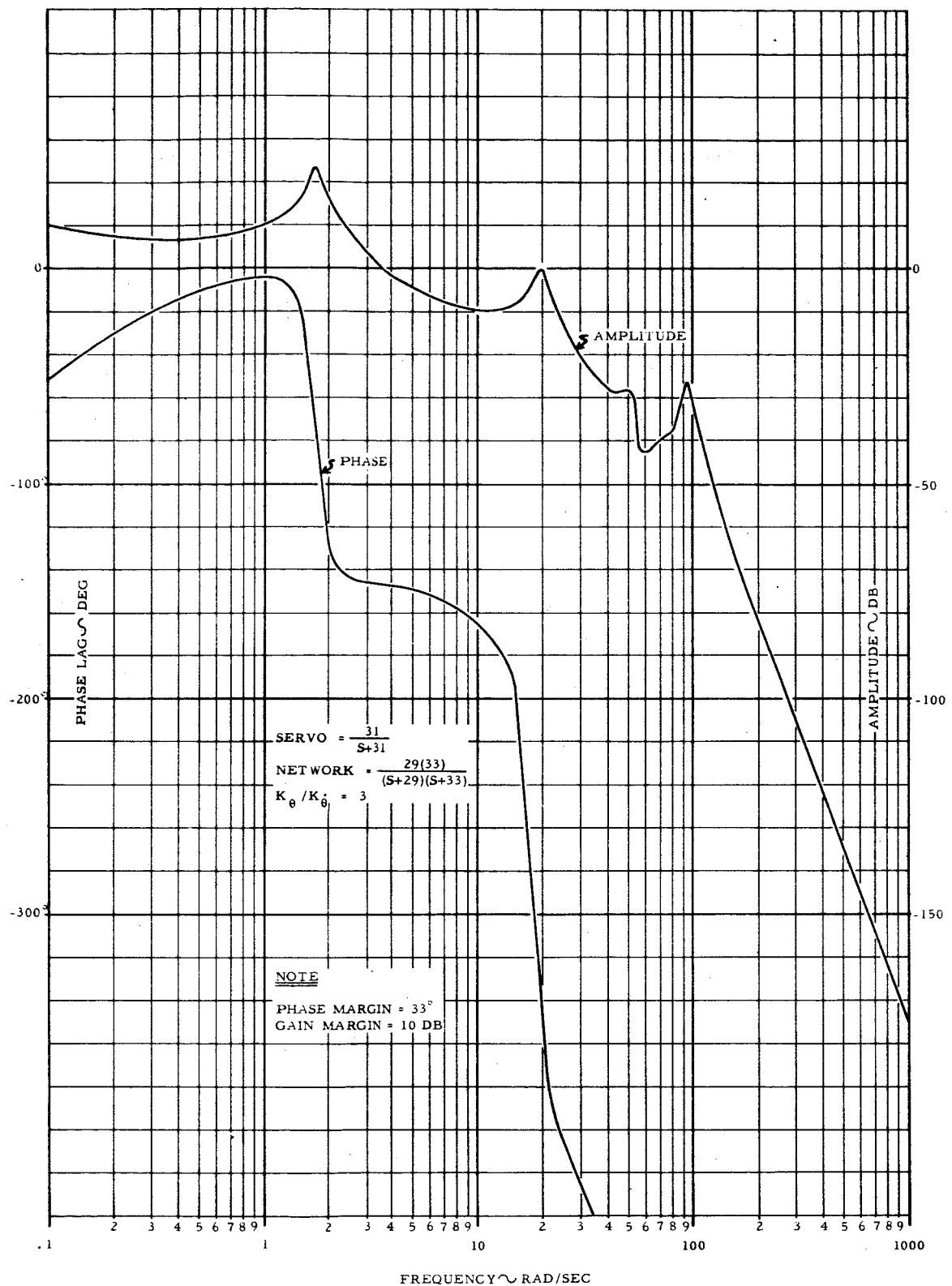
Figure 11   Bode Plot of Nominal First-Stage System at Maximum q Condition

a ratio which could include the upper stages. The nominal parameter values were chosen only after reviewing the effects of changes in each of them, as well as reviewing variations in basic data and in flight condition. Figure 12 through 16 show root-locus and Bode plots for the nominal system at launch, 17 seconds after launch, and at burnout (with jet vanes still fully effective). The nominal position gain is 5.0 degrees of control surface deflection per degree attitude error. Note that at launch the rigid-body locus becomes very damped at high gain, but at a gain of 5.0, the damping is poor. Because the gain margin is great at launch (due to the absence of aerodynamic tip control and the separation between rigid and first-mode frequencies), the gain might have been increased to 10.0 for the first few seconds of flight, thus improving the damping. It was felt, however, that although the damping was low, it was adequate and that the improvement could not justify the use of gain switching.

The stability of the SCOUT first-stage control system was checked at a variety of conditions. Variations of the following parameters were investigated:

- Bending frequency

- Maximum dynamic pressure

- Rate-gyro location

- Rate and position-gyro natural frequency

- Rate-gyro damping

- Servo dynamic response

NOMINAL SERVO AND NETWORK
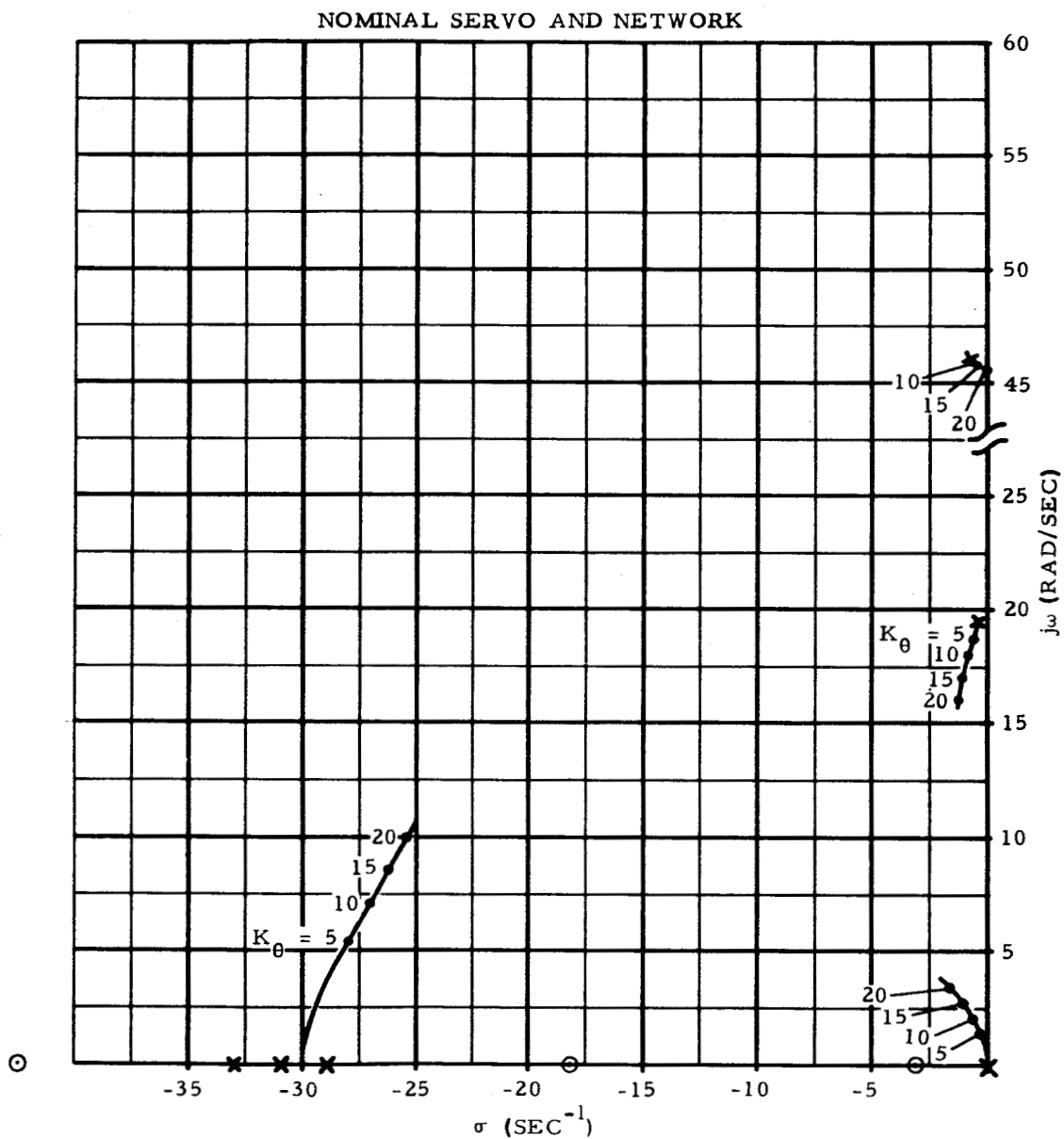
Figure 12 Root Locus Plot of Nominal First-Stage System at Launch

The plot contains the following annotations:

PHASE

AMPLITUDE

SERVO $= \dfrac{31}{S+31}$

NETWORK $= \dfrac{29(33)}{(S+29)(S+33)}$

$K_\theta / K_{\dot\theta} = 3$

PHASE LAG ∽ DEG

AMPLITUDE RATIO ∽ DB

FREQUENCY ∽ RAD/SEC
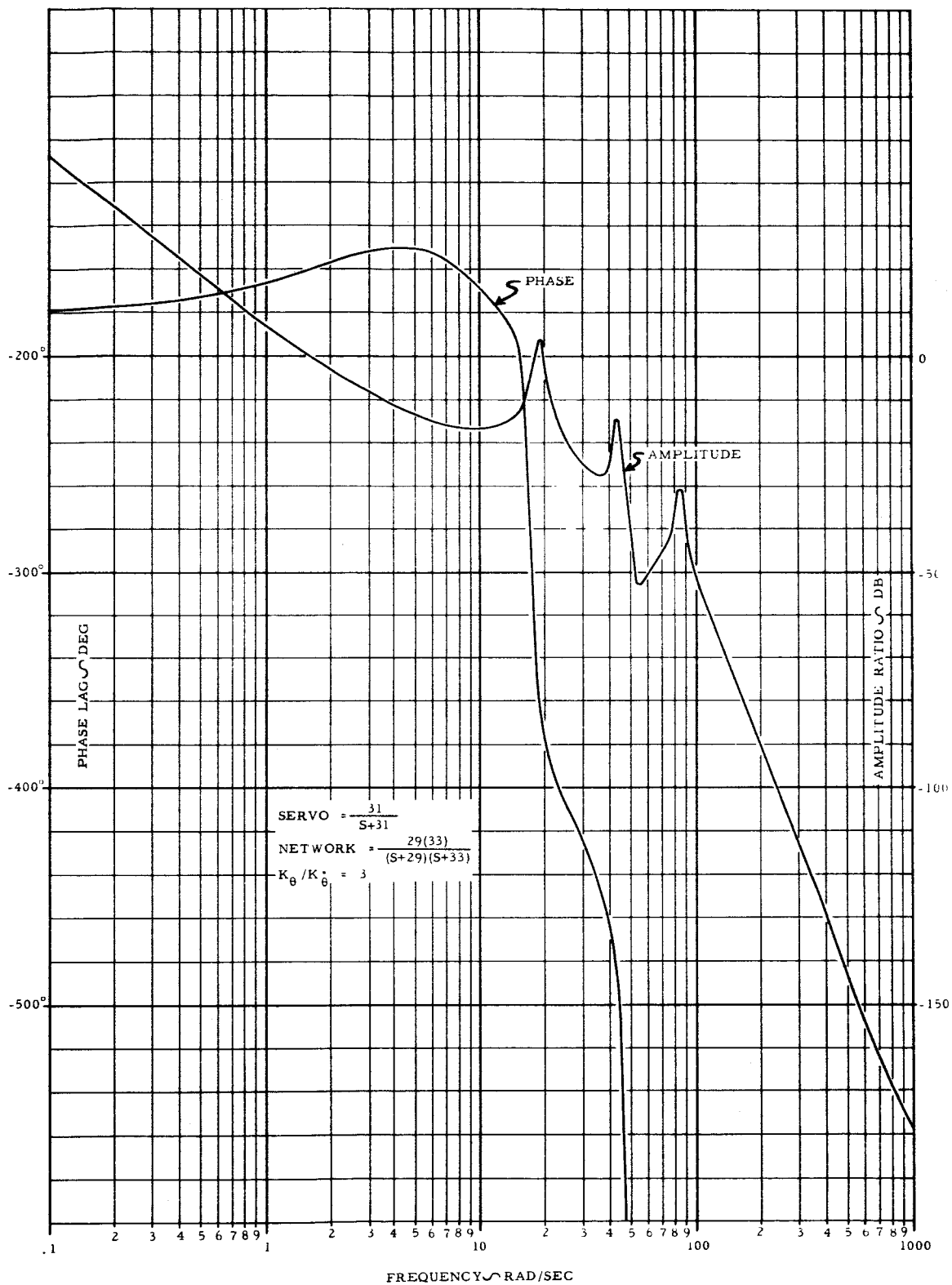
Figure 13 Bode Plot of Nominal First-Stage System at Launch
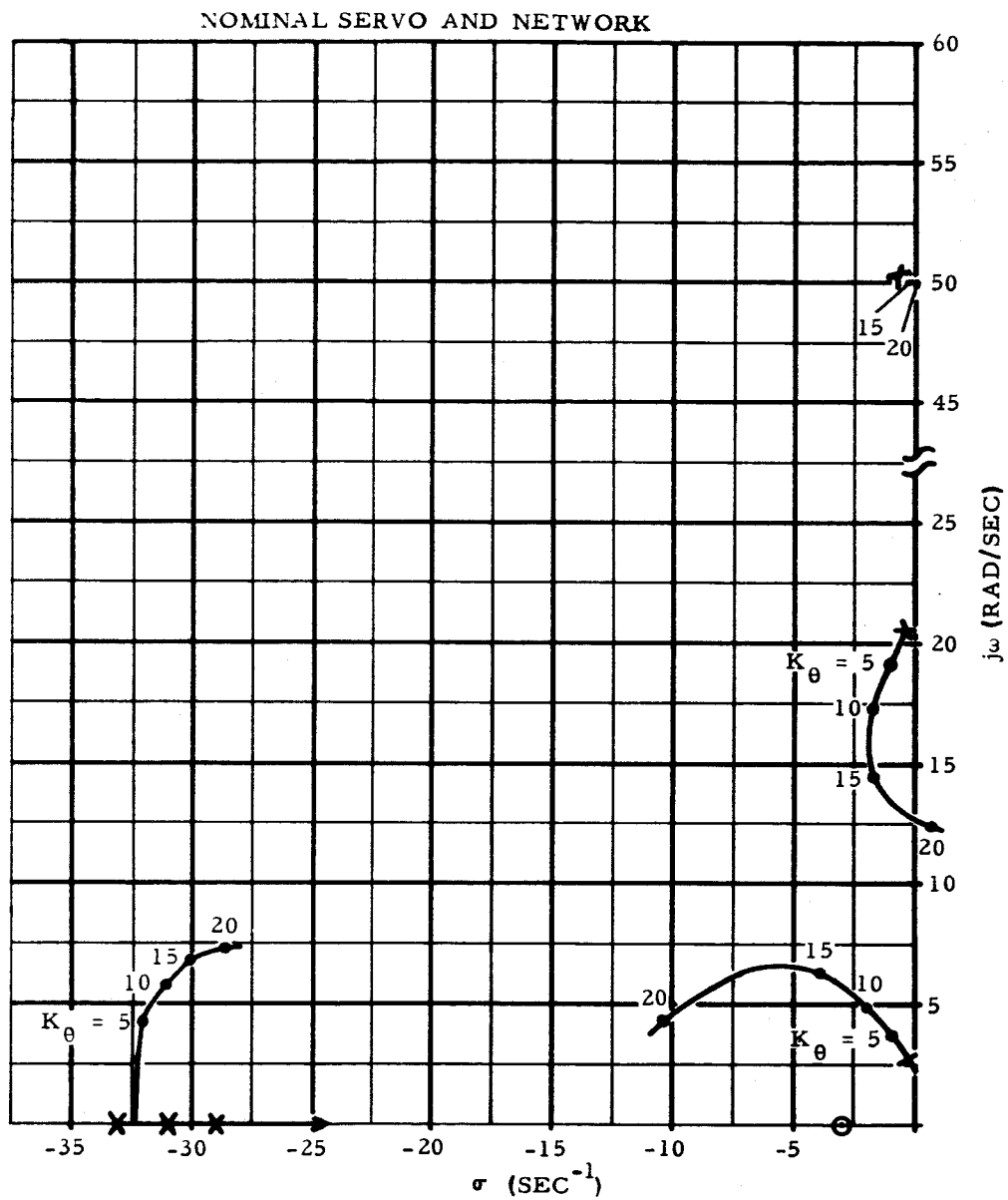
Figure 14 Root Locus Plot of Nominal First-Stage System 17 Seconds after Launch

BURNOUT (FULL THRUST)
NOMINAL SERVO AND NETWORK

Figure 15 Root locus Plot of Nominal First-Stage System at Burnout

SERVO $= \frac{31}{S+31}$

NETWORK $= \frac{29(33)}{(S+29)(S+33)}$

$K_\theta / K_{\dot\theta} = 3$

BURNOUT (FULL THRUST)

AMPLITUDE

PHASE

FREQUENCY ∿ RAD/SEC
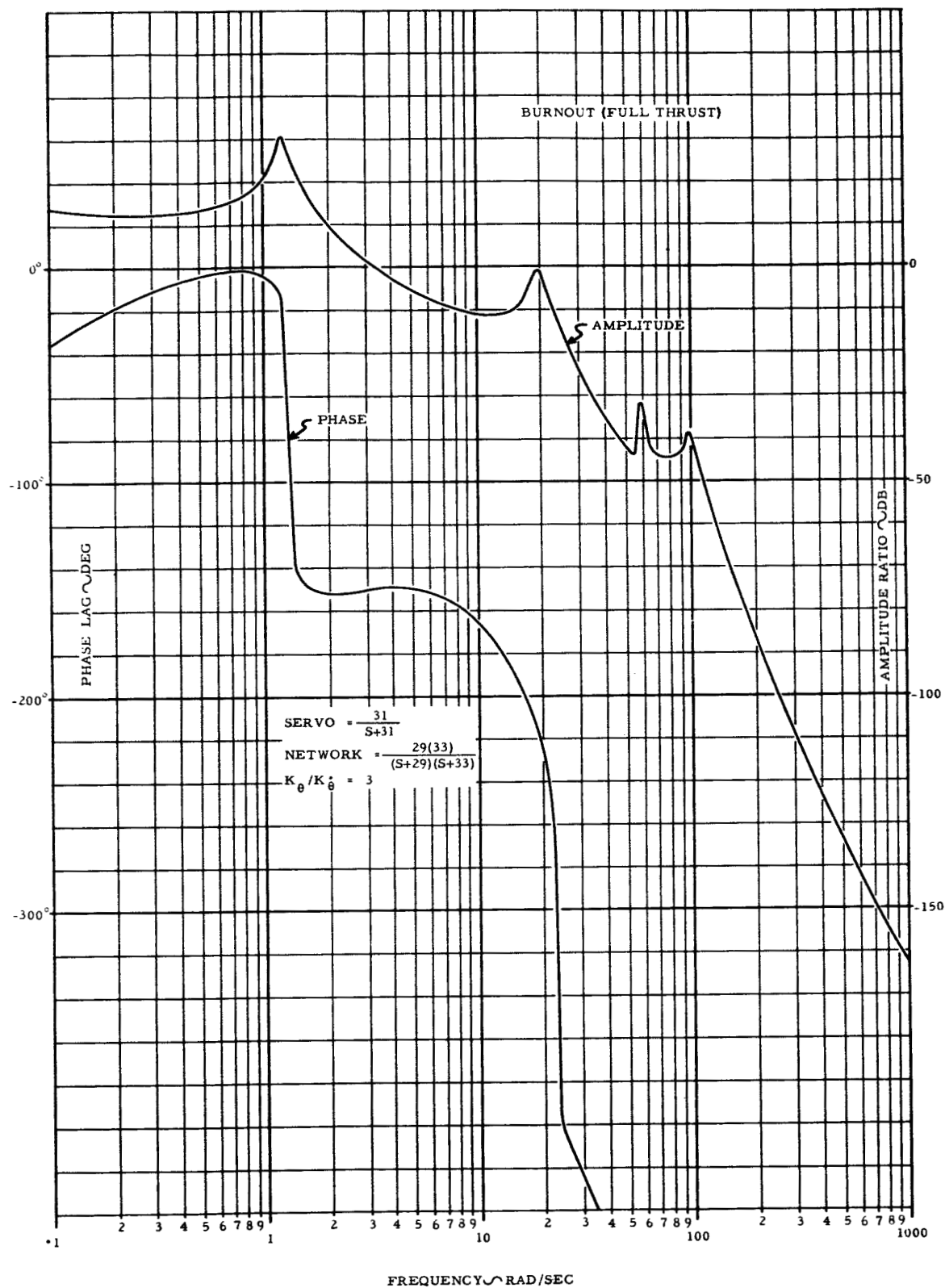
Figure 16 Bode Plot of Nominal First-Stage System at Burnout

- Compensation network response
- Extraneous lags
- Gain ratio

The nominal control gains and transfer function were chosen so that reasonable changes in such quantities as servo response and bending frequency would maintain the gain and phase margin within their proper limits. Tolerances were established for gain, gain ratio, servo response, and the network break frequencies. These tolerances are quite conservative in that the system will perform satisfactorily even if each parameter is in error in its worst direction.

The most difficult requirement to specify, and one which causes the most concern about stability, is the frequency response of the network-servo transfer function. Since this transfer function is composed of three poles, it is unlikely that all of them will either increase or decrease in frequency together. If one pole shifts in the lower frequency direction, the rigid-body damping will be decreased, but the system will become more stable due to the beneficial phase shift at the first mode. This pole can vary by more than a factor of three in frequency and still maintain a six db gain margin. Most variations in the compensating-network component values tend to separate the two break frequencies, a behavior which reduces the effect of the change on the system. Component tolerances are held to within five percent, so that several combined value shifts are needed to significantly alter the response.

Changes in the rate-to-position gain ratio shift the locations of most

of the zeros on the complex plane. Therefore it is difficult to judge beforehand the results of a single gain variation. In general, as can be seen from the plots of "SCOUT System Design Report, Supplement II," increasing the rate gain aids the rigid-body damping but aggravates the bending modes. Gain ratio has been held to a 10 percent tolerance because of its far reaching effects.

The behavior of the control system after first-stage burnout degrades rapidly as the sensible atmosphere is left behind. Figure 17 shows the Bode plot of the nominal system just after burnout (with zero jet vane lift). As can be seen from the rigid-body portion of the amplitude response, the damping has deteriorated even at this relatively high q condition. In the coasting period before second-stage ignition, the system damping will be reduced to only a few percent of critical, and angular momentum still present will result in continued attitude oscillations. Moreover, as M_α decreased due to the decreasing q, the frequency of oscillation is reduced, causing the amplitude to become greater. Part of this effect could be compensated by switching to a higher loop gain soon after burnout, thus helping to damp any transients applied at that time (such as sudden removal of thrust misalignment) before the controls become too ineffective.

Gain switching after burnout, however, was not considered to offer sufficient improvement in performance to justify the complexity (at least for the early flights). A means of accomplishing this switching is incorporated in the SCOUT electronics package in case it is deemed advisable in the future. Even increased loop gain does

SERVO $= \dfrac{31}{S + 31}$

NETWORK $= \dfrac{29(33)}{(S + 29)\ (S + 33)}$

$K_\theta / K_{\dot\theta} = 3$

BURNOUT (NO THRUST)

AMPLITUDE

PHASE

PHASE LAG $\sim$ DEG

AMPLITUDE RATIO $\sim$ DB

FREQUENCY $\sim$ RAD/SEC
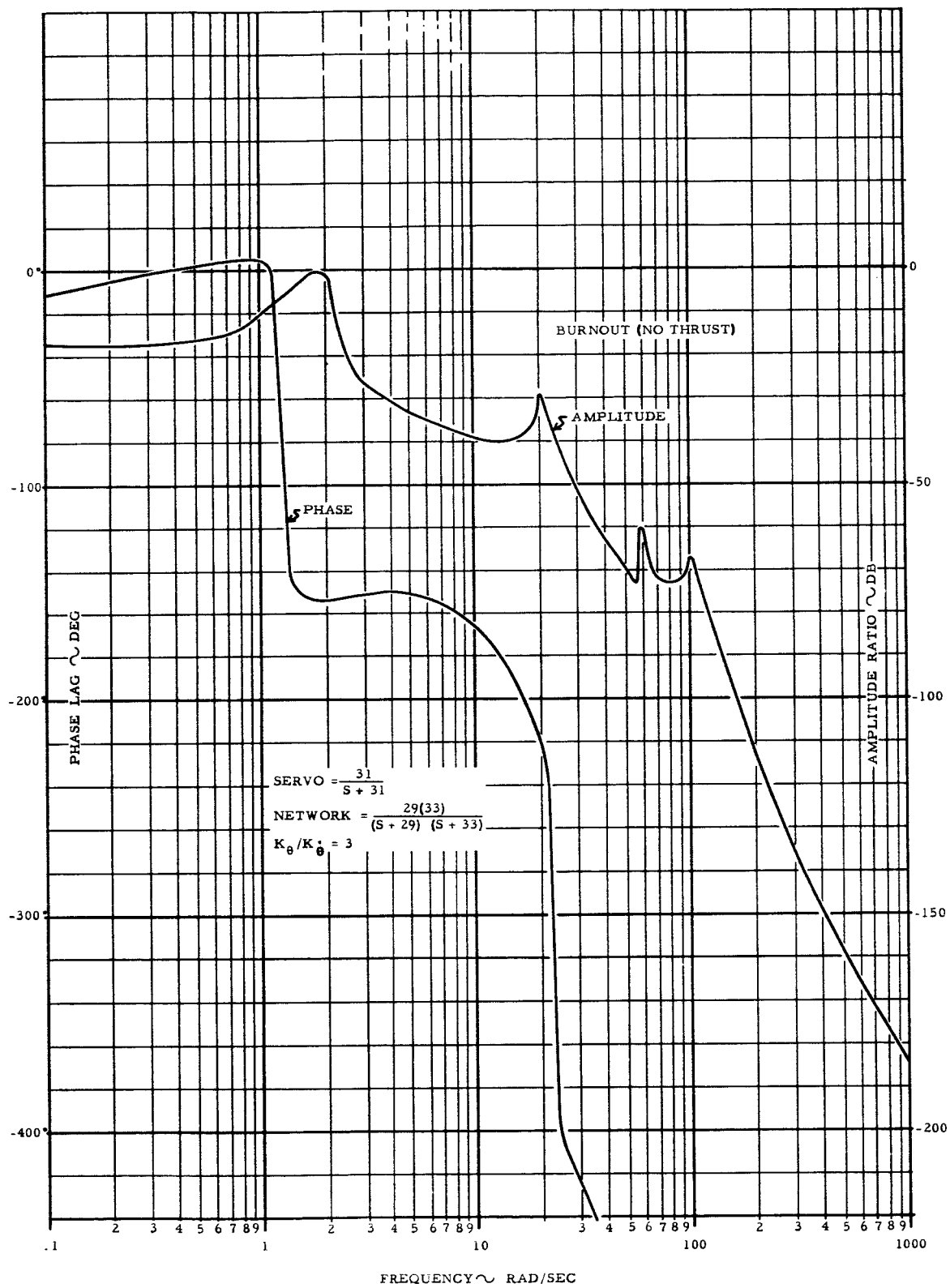
Figure 17 Bode Plot of Nominal First-Stage System after Burnout

not completely solve the oscillation problem, because as the air becomes tenuous in ascending to high altitudes, larger and larger control surface deflections are required. Finally, mechanical stops will prohibit farther increase in control surface deflections, at which time the controls operate in an on/off manner, so that only by increasing rate gain can further damping of the system be accomplished. The reason why such an underdamped system is tolerable is that burnout transients are controlled well enough before q becomes too low, and because low air density deteriorates wind or gust disturbances. The final, nominal pitch and yaw control system parameters for first-stage operation are as follows:

Rate gain (surface deflection per unit rate error)	$1.67 \pm 10\%$
Position gain (surface deflection per unit error)	$5.0 \pm 10\%$
Rate to position gain ratio	$.33$ sec $\pm 10\%$
Servo transfer function	$\dfrac{1}{31S+1}$

(see figure 18 for frequency response tolerance bands)

Compensating network transfer function	$\dfrac{1}{(29S+1)(33S+1)}$

(see figure 19 for frequency tolerances of servo and network combination)

Maximum yaw error signal	3.5 degrees $+ 0, - 10\%$

Along with the above specifications, of course, there is the restriction that no extraneous dynamic terms of significance exist anywhere in the system other than those which have been accounted for in the design.
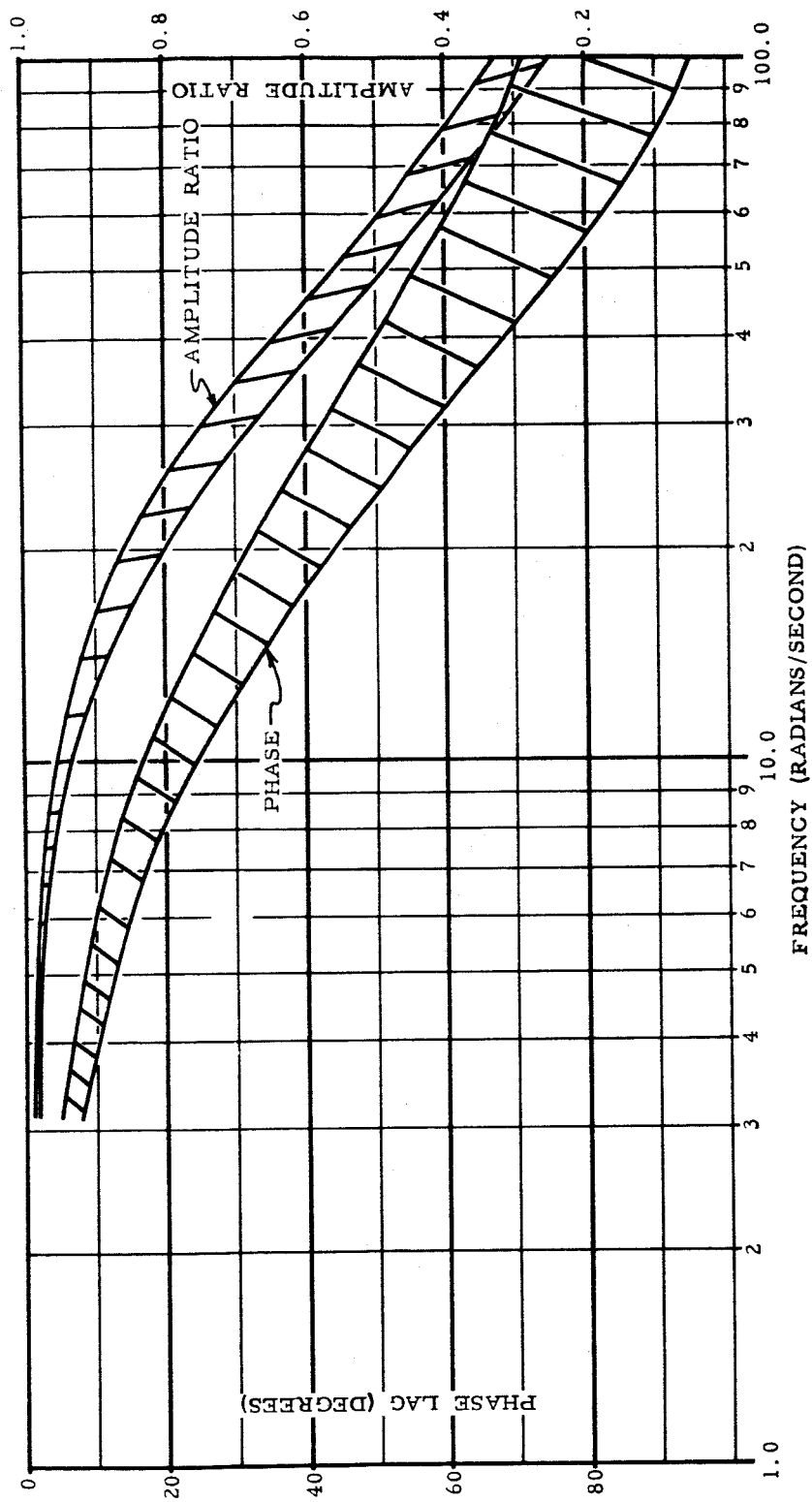
Figure 18 First-Stage Hydraulic Servo Frequency Response Tolerance
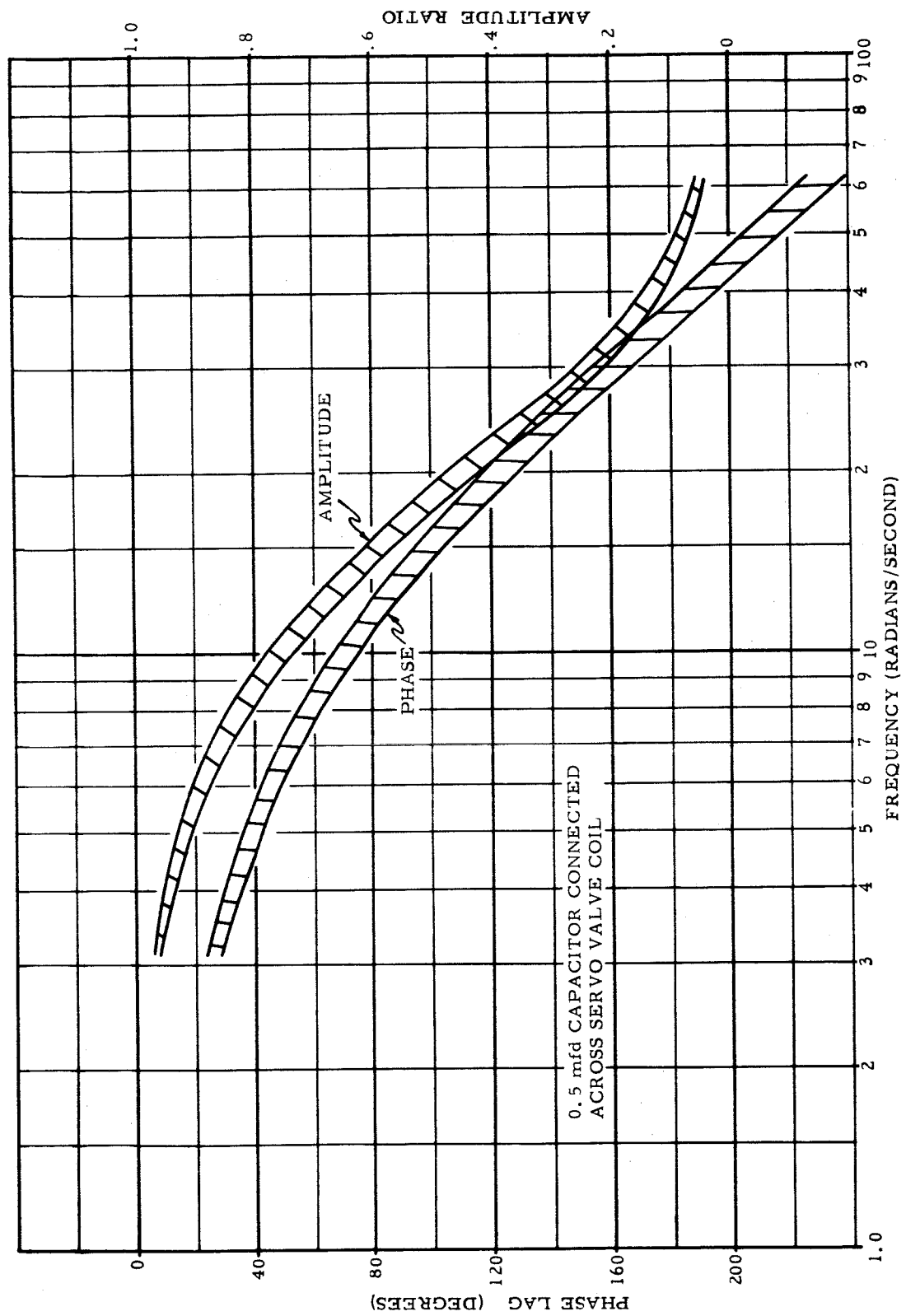
Figure 19 First-Stage Servo and Network Frequency Response Tolerance

Thus components such as ripple filters and transformers must be checked to ensure that their pass bands are compatible with the design dynamics.

The servo transfer function, during design taken to be $\frac{1}{31S+1}$, was specified in terms of its frequency response. Servo response specifications were required to be met twice; once in a preliminary component check to be certain that a particular valve-actuator combination was capable of responding as a first-order device, and again in a more complete test in which the servo and network responses were measured together. In the first instance faulty valves and actuators were to be detected by the presence of high-frequency lags or nonlinear operation. Accordingly, frequency response tolerance bands were established to exclude the possibility of significant changes in curve shape, although they were not adequate to specify break frequency. The frequency-response tolerance bands used to check actuators and valves are shown in figure 18.

These bands were generated by taking as the upper limit the response of a first-order system having a break frequency 10 percent higher than that desired for the servo, while the lower limit was established by the response of a second-order system with one break frequency 10 percent lower than the servo nominal and the other break frequency at 150 rad/sec. Because later servos in good condition do not exhibit high-frequency lags below 300 rad/sec, the lower tolerance limit should be tightened somewhat.

The servo consisting of the valve and actuator to be tested and a

typical amplifier and feedback element, was to be adjusted by varying
its loop gain until the correct response was achieved. Having met the
specifications defined in figure 18 the servo components were to be
incorporated in the flight system and the loop gain set to meet the
overall requirements with the compensating network included. By
adjusting the servo response until overall requirements are met, slight
deviations of the network transfer function from nominal can be compensated.
Since the servo is known to have the desired type of behavior, i. e.,
nearly that of a first-order system, the tolerance bands on overall
frequency response need not be narrow. Because the control system
can function properly if the poles of the network or servo transfer
function differ by 10 percent each from their nominal values, the
tolerance bands for the network and servo together were formed by
allowing high and low variations of all three poles. The resulting
response tolerance, to which the system is tested in the field, is
shown in figure 19.

To insure that the first-stage control system as defined above would
perform in a satisfactory manner with real components, an analog
computer simulation was made including as many of the SCOUT
amplifiers, demodulators, etc., as was possible. The computer
simulated the airframe behavior including the first three bending
modes (and later, the first torsion mode and the roll dynamics).
Rate and position gyros were also simulated on the computer. The
gyro outputs, which suppressed-carrier modulated a 400-cps wave,
were connected to the flight equipment at the "poppet valve electronics"
module. From there the signals progressed as they would during
actual operation through the demodulator and ripple filter, several

stages of amplification, the compensation network, and finally, the
hydraulic servo. The servo shaft position, corresponding to jet
vane and tip deflection, was sensed by a dc potentiometer and the
resulting signal returned to the computer where it completed the
control loop. The time and frequency responses of the entire system
could then be measured and compared with those predicted by the more
exact, but less complete, digital analysis. Phase and gain margins
obtained in this way agreed with predicted values very closely (within
1/4 db in gain). The effect of several anomalies in control components
was measured with analog simulation that would have been impossible
to determine by solving the linearized system equations. First, the
control behavior was checked with the servo loaded with springs,
corresponding to hinge moment loading expected in flight. The spring
rate was made both positive and negative and, in addition, a large
steady (invariant with deflection) moment was applied. The vehicle
response variations could be observed but they were negligibly small.
The effect of connecting a 0.5-mfd capacitor across the servo valve
coil was also considered, because field operation had shown that
electrical noise imposed on the long signal wires connecting the first
and third stages had caused the servo to chatter. Filtering, most
conveniently accomplished at a dc point, could eliminate the chatter,
and tests showed that a capacitor connected across the valve coil
would suffice. The addition of the capacitor, however, caused a
nonlinear performance of the servo amplifier, which altered the servo
response in a manner not easily described in terms of transfer-function
poles and zeros. Time responses of the airframe were determined
by applying either simulated wind gusts (instantaneous changes in
angle of attack) or attitude commands.

Responses of the nominal system (all simulated components) for conditions of launch, maximum q, and burnout are shown in figures 20 through 22. The effect of using actual hardware (which differs somewhat from nominal response but is within tolerance) can be seen by comparing figures 21 and 23. More time responses showing the vehicle behavior with various control gains, servo dynamics, etc., may be found in Supplement II.

Roll Axis

Airframe Description: The SCOUT airframe is easily described in roll. Because of its torsional stiffness it behaves very nearly as a body restrained only by inertia and by an aerodynamic moment proportional to rolling rate, but in a control application, it is prudent to include the effects of flexibility. Data giving the torsional mode shapes and frequencies were available only at the launch condition, but this was considered adequate provided that the analysis showed that large variations in frequency and mode shape could be tolerated.

The torsion modes are given in Supplement I. The airframe roll description used in the analysis is shown below in matrix form.

$$
\begin{bmatrix}
S + \dfrac{lp}{I} & R_1\dot{r}_1 S + R_1 r_1 & R_2\dot{r}_2 S + R_2 r_2 \\[2ex]
R_{1\dot{\phi}} & S^2 + 2\zeta\omega_1 S + \omega_1^2 & R_1\dot{r}_2 S + R_1 r_2 \\[2ex]
R_{2\dot{\phi}} & R_2\dot{r}_1 S + R_2 r_1 & S^2 + 2\zeta\omega_2 S + \omega_2^2
\end{bmatrix}
\begin{bmatrix}
\dot{\phi} \\[2ex]
r_1 \\[2ex]
r_2
\end{bmatrix}
= \delta
\begin{bmatrix}
L_{\delta}/I \\[2ex]
R_{1\delta} \\[2ex]
R_{2\delta}
\end{bmatrix}
$$

$$K_\theta = 5$$

ANGLE OF ATTACK

+5°
0
-5°

NOMINAL SYSTEM,
SIMULATED COMPONENTS

PITCH ANGLE

-5°
0
+5°

SURFACE DEFLECTION

+25°
0
-25°

FIRST BENDING NORMALIZED DEFLECTION

+5 FT.
0
-5 FT.

SECOND BENDING NORMALIZED DEFLECTION

+0.5 FT.
0
-0.5 FT.

THIRD BENDING NORMALIZED DEFLECTION

+0.4 FT.
0
-0.4 FT.

→| |←1 SEC.
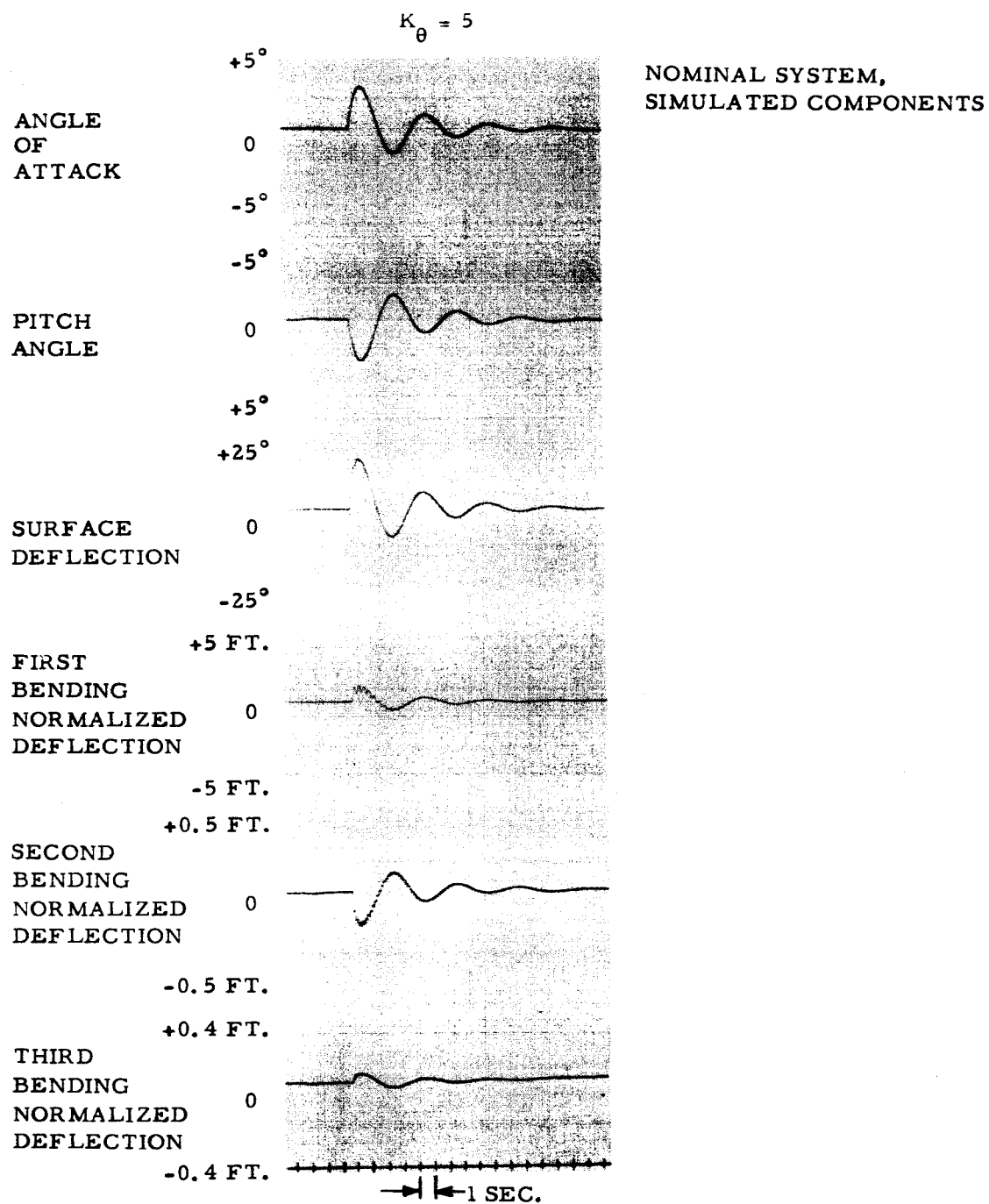
Figure 20 First-Stage Pitch Time Response at Launch

$K_\theta = 5$

NOMINAL SYSTEM,
SIMULATED COMPONENTS

ANGLE
OF
ATTACK

+5°

0

-5°

-5°

PITCH
ANGLE

0

+5°

+25°

SURFACE
DEFLECTION

0

-25°

+5 FT.

FIRST
BENDING
NORMALIZED
DEFLECTION

0

-5 FT.

+0.5 FT.

SECOND
BENDING
NORMALIZED
DEFLECTION

0

-0.5 FT.

+0.4 FT.

THIRD
BENDING
NORMALIZED
DEFLECTION

0

-0.4 FT.

1 SEC
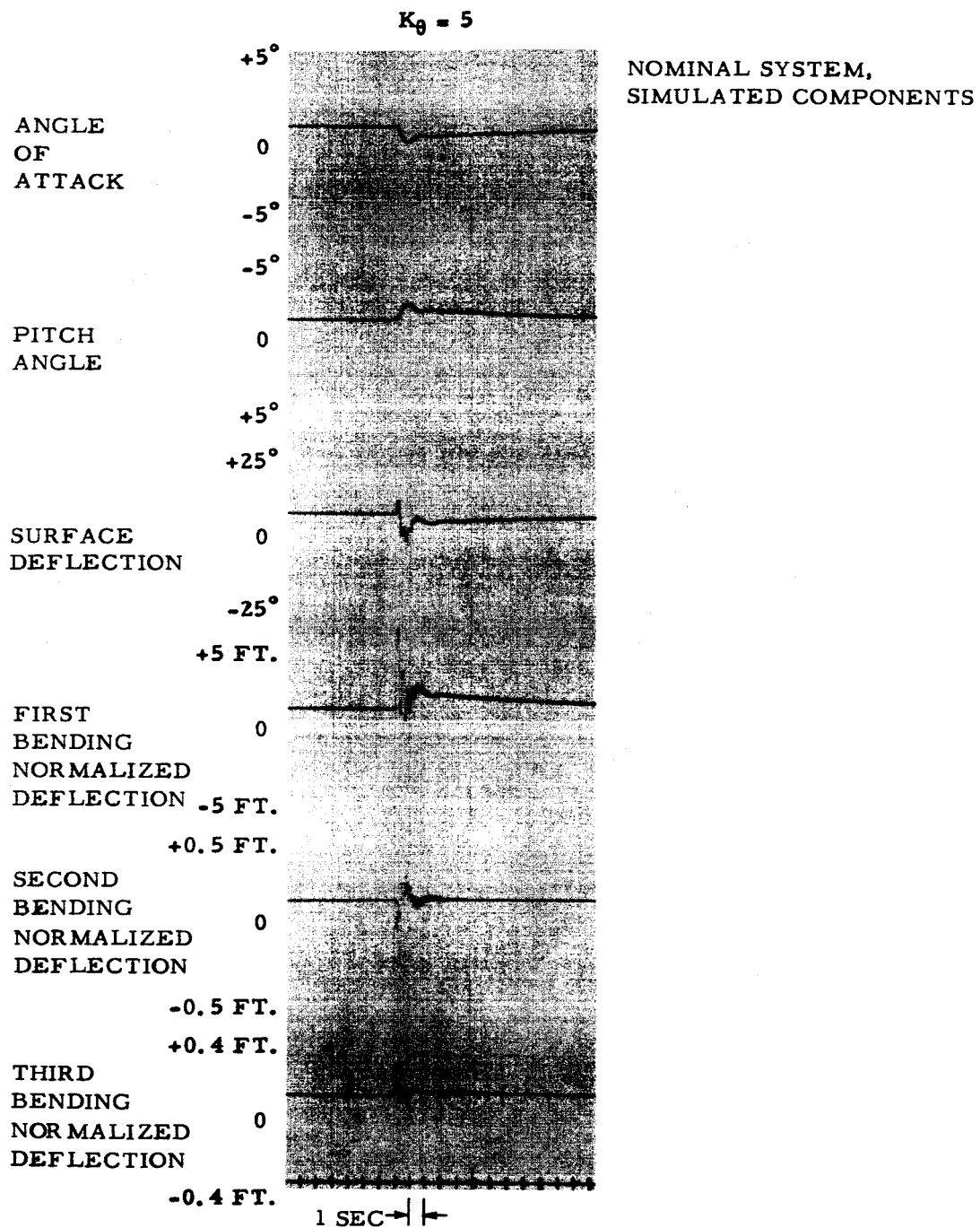
Figure 21 First-Stage Pitch Time Response at Maximum q Condition
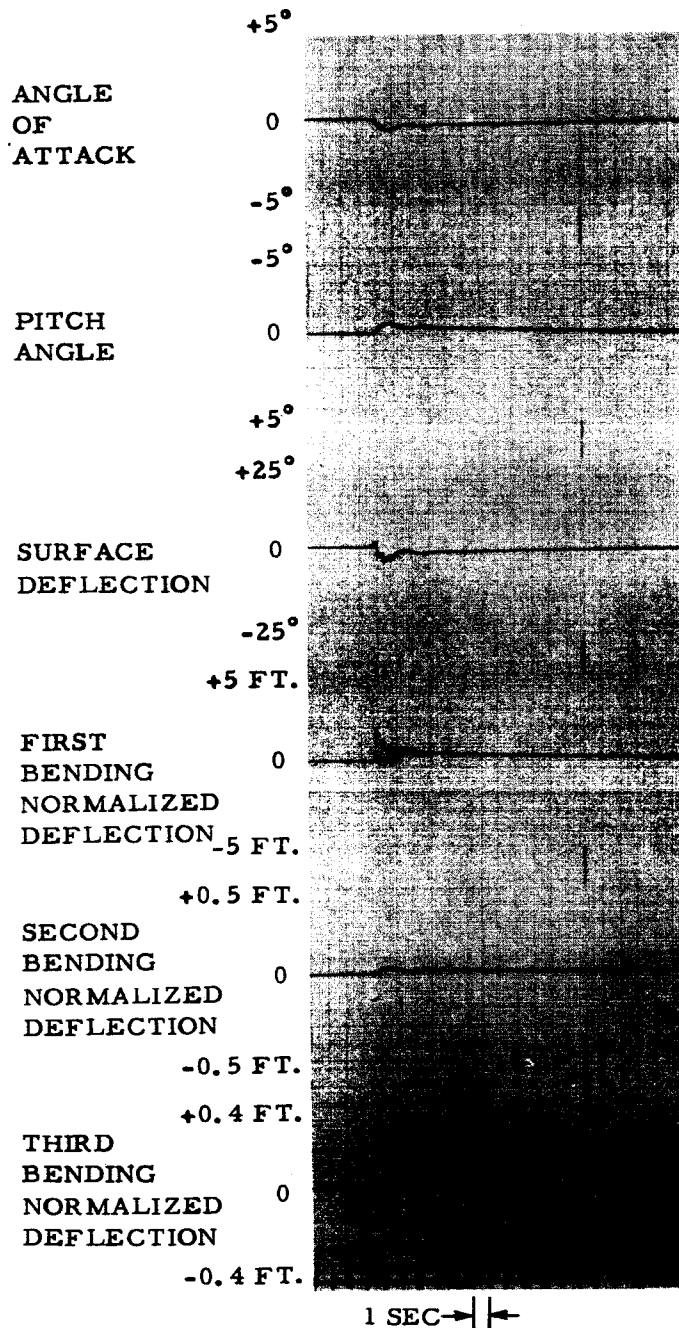
Figure 22 First-Stage Pitch Time Response at Burnout

MAXIMUM DYNAMIC
PRESSURE CONDITION

NOMINAL SYSTEM WITH
ACTUAL NETWORK, ELECTRONIC,
AND SERVO HARDWARE.

ANGLE
OF
ATTACK

PITCH
ATTITUDE
ANGLE

CONTROL
SURFACE
DEFLECTION

FIRST
BENDING
NORMALIZED
DEFLECTION

SECOND
BENDING
NORMALIZED
DEFLECTION

THIRD
BENDING
NORMALIZED
DEFLECTION
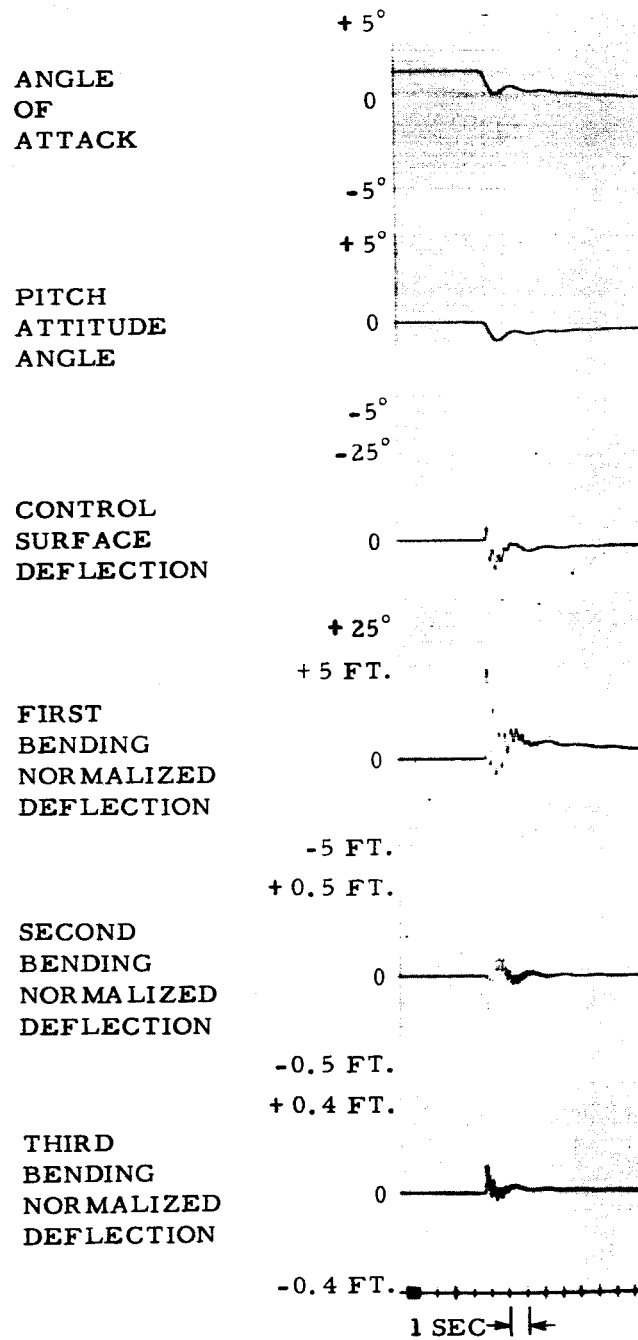
Figure 23 First-Stage Time Response of System with Actual Hardware

R-ED 11117

- 49 -

There is essentially no coupling among the torsional modes of vibration and the rigid-body since all the aerodynamic terms are very small, so that in practice, the above matrix is degenerate and can be written with only its diagonal terms. The moments applied to the body which excite the "rigid" or flexible modes are functions only of the control surface deflection. The coefficient $\frac{L_\delta}{I}$ is obviously the roll moment per unit differential deflection of the two surfaces divided by the roll moment of inertia. $R_{1\delta}$ and $R_{2\delta}$ are given by the relation

$$R_{i\delta} = \frac{\lambda_{i\delta} L_\delta}{I_i}$$

where $R_{i\delta}$ = Angular acceleration of the ith torsion mode due to a unit control deflection

$\lambda_{i\delta}$ = Torsion mode shape of the ith mode at the control surface station

L_δ = moment due to a unit control deflection

I_i = characteristic inertia of the ith mode

The first two torsion modes were considered adequate to describe the airframe for the control analysis; the natural frequencies of the first and second modes are 22 and 37 cps, respectively.

Control System Design: Because first-stage roll control appeared at the outset to be a relatively small problem, the first-stage electronics were designed with no provision for roll compensation. Moreover, the servos driving the roll control members were the same as those used in yaw, and their response had been set to meet the requirements of the latter system. The only latitude left the

designer was the selection of roll control gains. This was done by analyzing the system using the root-locus technique to solve the total loop equations of motion shown in the zero matrix of figure 24. The roll rate and position gyros are separated just as are those of the pitch and yaw channels, so that different combinations of rigid and flexible body motion are sensed by each. The rate gyro senses

$$\dot{\phi}_{RG_{in}} = \dot{\phi} + \left(\lambda_{1RG}\right)\left(\dot{r}_1\right) + \left(\lambda_{2RG}\right)\left(\dot{r}_2\right)$$

while the position gyro registers

$$\phi_{G_{in}} = \phi + \lambda_{1G}r_1 + \lambda_{2G}r_2$$

The position-gyro dynamics are negligible, while those of the rate gyro are second order with a nominal natural frequency and damping ratio of 33 cps and 0.5, respectively.

The roll control system was analyzed at two flight conditions: at launch where the loop gain is low and the damping could be expected to be poor, and at a time when the combination of dynamic pressure, vehicle inertia, and control surface effectiveness produced the highest loop gain. The two sets of coefficients used were:

	LAUNCH	PEAK GAIN
L_δ/I	2.325 deg/sec^2/deg	12.83 deg/sec^2/deg
$R_{1\delta}$	-3370 deg/sec^2/deg	-11670 deg/sec^2/deg
$R_{2\delta}$	6740 deg/sec^2/deg	23340 deg/sec^2/deg

The roll control system must maintain the vehicle attitude within specified limits in the presence of external disturbance moments. Disturbances in roll can occur in a number of ways, but the more

	$\dot{\phi}$	r_1	r_2	δ_ϕ	$\delta_{\phi c}$	ϕ_{GYRO}	$[\dot{\phi}_{RG}]_{IN}$	$[\dot{\phi}_{RG}]_{OUT}$
ROLL MOMENT EQUATION	S	0	0	$\dfrac{L_\delta}{-I}$	0	0	0	0
FIRST TORSION	0	$S^2+2\zeta_{T1}S+\omega^2_{T1}$	0	$-R_{1\delta}$	0	0	0	0
SECOND TORSION	0	0	$S^2+2\zeta_{T2}S+\omega^2_{T2}$	$-R_{2\delta}$	0	0	0	0
SERVO TRANSFER FUNCTION	0	0	0	$S+\dfrac{1}{\tau_s}$	$-\dfrac{1}{\tau_s}$	0	0	0
RATE GYRO TRANSFER FUNCTION	0	0	0	0	0	0	$-\omega^2_{RG}$	$S^2+2\zeta_{RG}S+\omega^2_{RG}$
RATE GYRO INPUT	1	$\lambda_{1RG}S$	$\lambda_{2RG}S$	0	0	0	-1	0
ATTITUDE GYRO INPUT	1	$\lambda_{1G}S$	$\lambda_{2G}S$	0	0	$-S$	0	0
CONTROL EQUATION	0	0	0	0	1	K_ϕ	0	$K_{\dot\phi}$

Figure 24 Matrix of Roll Airframe and Control Equations for First Stage

severe disturbances are caused by fin misalignment, control-surface offset, and by aerodynamic coupling of yaw and pitch angles of attack through the $C_{1\beta}$ term. The largest moments are produced by fin misalignment, and can exceed 1000 ft-lbs.

The change in control system response with flight condition is very nearly that caused by a loop gain change, a fact which makes it easy to select approximate control parameters without solving an additional set of equations.

Root-locus plots were made of the roll system using the two torsion modes, gyro dynamics, and a servo transfer function of $\frac{1}{31S + 1}$. Different gain ratios were tried and it was determined that large deviations were tolerable without sacrificing good damping and stability margins. Figures 25 and 26 are root-locus plots of the system selected as nominal at launch and at 32 seconds after launch. The damping ratio is 0.5 at these extremes if the control gain is set at 4.0, and is even greater (sometimes greater than unity) at other flight conditions. The ratio of rate-to-position gain was set at 0.4 sec since it gave satisfactory operation and at the same time was compatible with the upper stage systems. This gain setting also eliminated the need for one gain switch.

In summary, the roll control parameters are:

Attitude gain (differential deflection per unit roll error) 4.0 ± 15%

Rate gain (differential deflection per unit roll rate) 1.6 ± 15%

Rate to position gain ratio (sec) 0.4 ± 10%

Servo dynamics (transfer function) $\frac{1}{31S + 1}$

(same tolerance as yaw servo)

R-ED 11117

$$\frac{K_\phi}{K_{\dot\phi}} = 2.5$$
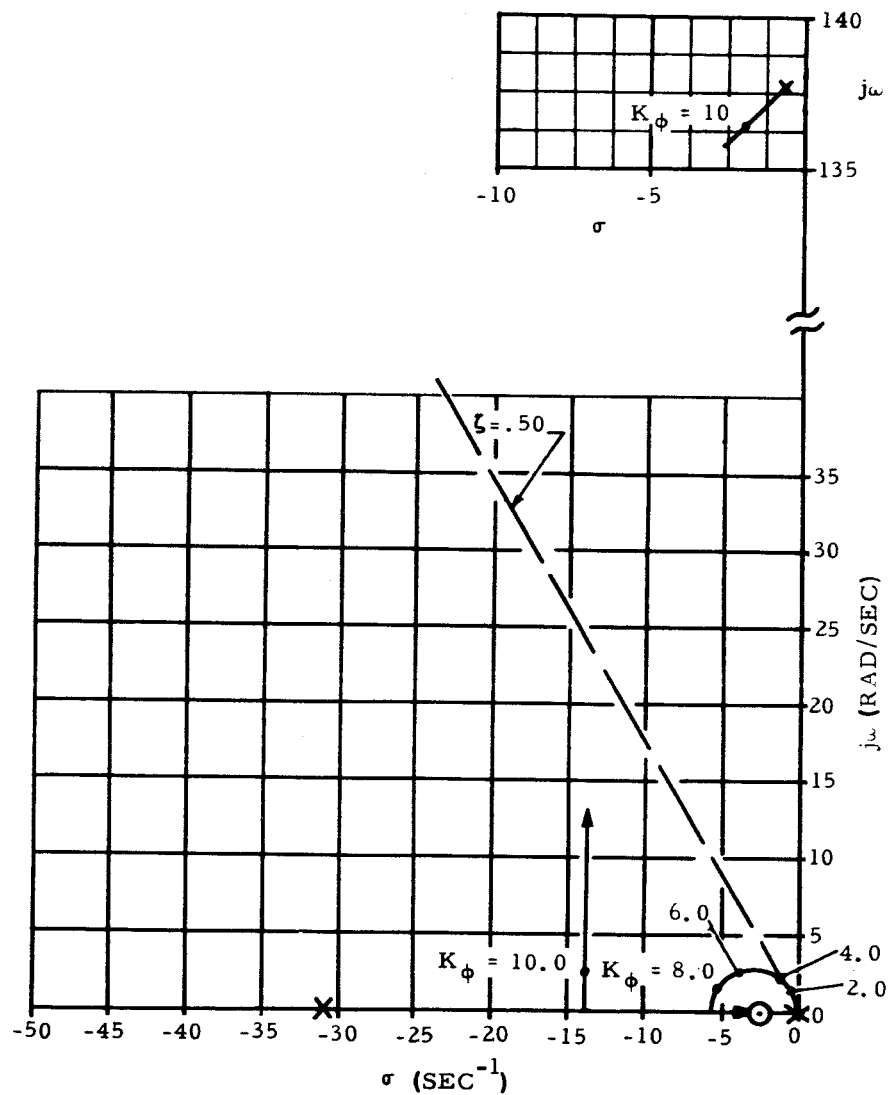
Figure 25 Root Locus Plot of Nominal First-Stage Roll System at Launch

$$\frac{K_{\dot\phi}}{K_\phi} = 2.5$$
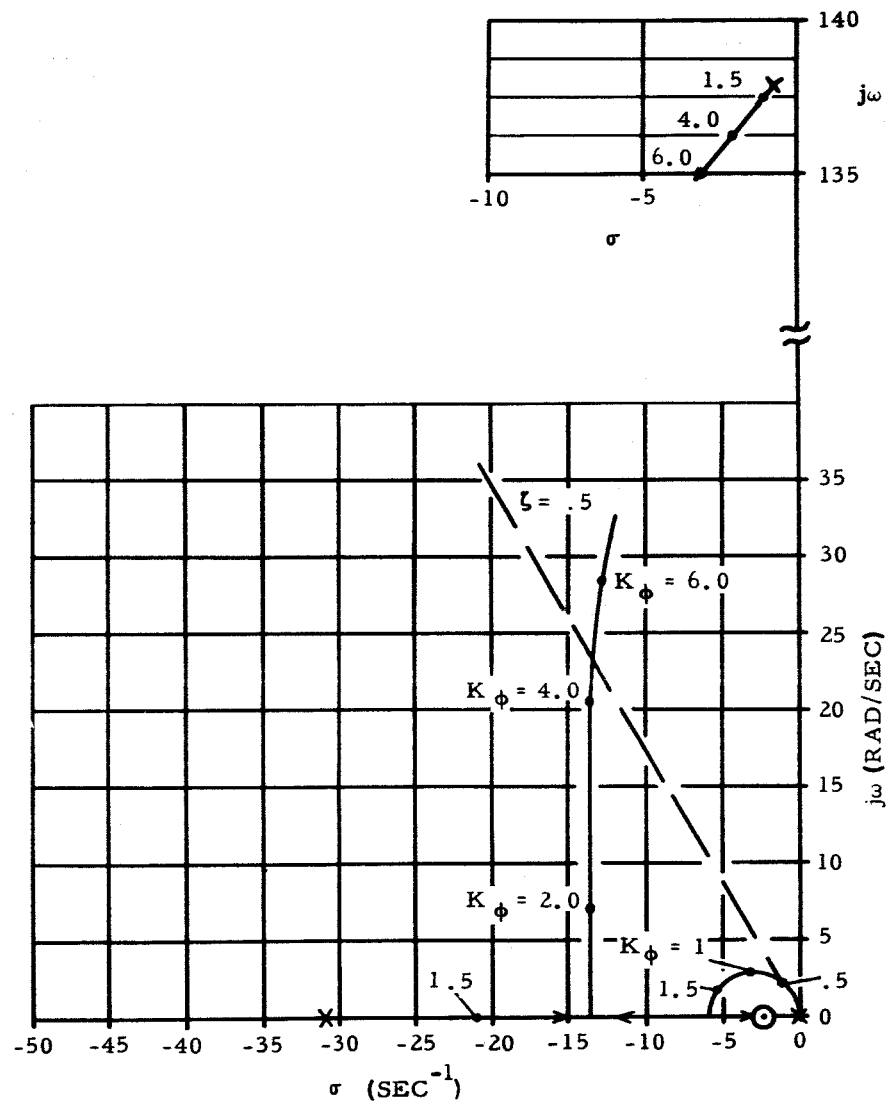
Figure 26 Root Locus Plot of Nominal First-Stage Roll System at Maximum q Condition

These control gains are sufficient to prevent serious roll errors in the presence of the largest expected disturbance moment.

Roll-Yaw Coupling: In practice it is not possible to consider the control system of each axis separately because there is coupling among axes from a variety of sources. Coupling can occur through aerodynamic, structural, or control terms in the equations of motion of the otherwise separate systems. The roll and yaw control loops exhibit the only significant coupling problem on SCOUT, and their interaction was, accordingly, studied to determine the effect on performance and stability.

Roll and yaw axes are naturally subject to interaction because the same control members are used in both axes. In addition, an aerodynamic moment is introduced to roll (through the $C_{l\beta}$ term) whenever a pitch and yaw angle of attack occur simultaneously. Because an unbalance in the roll control signal to the jet vane and tip servos can cause a residual yawing moment, and since vehicle yaw can induce an aerodynamic rolling moment, a closed loop can be formed including the roll and yaw control channels.

The roll and yaw interaction can have either a stabilizing or destabilizing effect upon either control loop, depending upon the direction of roll signal or servo unbalance. There is further coupling possible, however, through gain unbalance between the two yaw-roll servos, which is always of a destabilizing nature. Suppose, for example, that the upper control surface servo has 10 percent more closed-loop gain than does the lower one. In applying a negative yaw

moment through deflection of the top and bottom surfaces, a positive yaw error will induce an extraneous positive roll moment. On the other hand, a positive roll moment soon produces a positive error, and the control system attempts to deflect the surfaces to generate a negative roll moment. Since the upper surface deflects farther, however, a net positive yaw moment results which closes the loop and tends to continue the process. The amount of equivalent deflection coupled into yaw from the roll channel is $(K-1) K_\phi \phi_\varepsilon$ and into roll from the yaw channel is $(K-1)(K_\psi \psi_\varepsilon)$, where K_ϕ, K_ψ are the roll and yaw position control gains, ϕ_ε and ψ_ε are the roll and yaw errors, and K is the ratio of upper to lower static servo gain. Note that, in order to complete the coupling loop, the interaction gain (K-1) must be used twice, making the total coupling proportional to $(K-1)^2$.

The effect of roll-yaw interaction was investigated considering that one servo had a gain 10 percent high and the other 10 percent low. The investigation also included the contribution of the $C_{l\beta}$ term. The $C_{l\beta}$ value used was +.0143 deg^{-1} (based on a reference area and length of 8.72 ft^2 and 3.33 ft), assuming that the vehicle is operating at four degrees pitch angle of attack. This term was always introduced with such a sign that it aided the effect of servo unbalance. The vehicle behavior in the presence of interaction was determined in two ways: by solving the total equation of motion (simplified) and by simulating the problem on the analog computer.

In simplifying the system equations to facilitate analysis, it was decided to dispense with the dynamics of the position and rate gyros.

This eliminates four relations which do not influence the control greatly, and in any event, are not required to compare the performances of the vehicle with and without coupling of axes. The second torsional mode was also eliminated since it does not contribute greatly to the problem, but the third bending and first torsion modes were retained.

The matrix of equations used is given in figure 27.

In this set of equations, the fraction of surface deflection in one channel that is added into the other is contained in the terms $\frac{Z_{\delta\phi}}{V}$, $N_{\delta\phi}$, $Z_{1\delta\phi}$, $Z_{2\delta\phi}$, $Z_{3\delta\phi}$, $L_{\delta\psi}$, and $R_{1\delta\psi}$. Solutions of the system equations were obtained under various conditions of roll and yaw gain, degree of control coupling, and $C_{l\beta}$. A root-locus plot of the singularities of the complete equation with varying yaw gain and with roll gain fixed at its nominal value (4.0 degrees differential deflection per degree roll error), is shown in figure 28. Here the coupling is due to the combined effects of the aerodynamic term $C_{l\beta}$ and two servos, one of which was 10 percent high in gain and the other 10 percent low. It can be seen that the change in response, although noticeable, is not serious. Only a maximum q condition was studied, since at this condition the controls are very effective and $C_{l\beta}$ is large. The analog computer with simulated control components was used to check the results obtained by solution of the simplified equations and to measure the effect of the interaction upon time response. The same coupling terms and flight condition were used but the rate gyro dynamics were included in the simulation. Figure 29 shows the transient response of the airframe in roll and yaw.

	β	$\dot\psi$	z_1	z_2	z_3	$\delta\psi$	NETWORK OUTPUT	$\dot\phi$	r_1	$\delta\phi$	$\delta\phi c$	$\delta\psi c$
FORCE EQUATION	$-S+\frac{Z_\beta}{V}$	1	$\frac{Z_{\dot z_1}S}{V}+\frac{Z_{z_1}}{V}$	$\frac{Z_{\dot z_2}S}{V}+\frac{Z_{z_2}}{V}$	$\frac{Z_{\dot z_3}S}{V}+\frac{Z_{z_3}}{V}$	$\frac{Z_\delta}{V}$	0	0	0	$\frac{Z_{\delta\phi}}{V}$	0	0
YAW MOMENT EQUATION	N_β	$-S+N_{\dot\psi}$	$N_{\dot z_1}S+N_{z_1}$	$N_{\dot z_2}S+N_{z_2}$	$N_{\dot z_3}S+N_{z_3}$	N_δ	0	0	0	$N_{\delta\phi}$	0	0
FIRST BENDING MODE	$Z_{1\beta}$	$Z_1\dot\psi$	$-S^2+Z_{1\dot z_1}S+Z_{1z_1}$	$Z_{1\dot z_2}S+Z_{1z_2}$	$Z_{1\dot z_3}S+Z_{1z_3}$	$Z_{1\delta}$	0	0	0	$Z_{1\delta\phi}$	0	0
SECOND BENDING MODE	$Z_{2\beta}$	$Z_2\dot\psi$	$Z_{2\dot z_1}S+Z_{2z_1}$	$-S^2+Z_{2\dot z_2}S+Z_{2z_2}$	$Z_{2\dot z_3}S+Z_{2z_3}$	$Z_{2\delta}$	0	0	0	$Z_{2\delta\phi}$	0	0
THIRD BENDING MODE	$Z_{3\beta}$	$Z_3\dot\psi$	$Z_{3\dot z_1}S+Z_{3z_1}$	$Z_{3\dot z_2}S+Z_{3z_2}$	$-S^2+Z_{3\dot z_3}S+Z_{3z_3}$	$Z_{3\delta}$	0	0	0	$Z_{3\delta\phi}$	0	0
YAW SERVO TRANSFER FUNCTION	0	0	0	0	0	$S+\frac{1}{\tau_s}$	$-\frac{1}{\tau_s}$	0	0	0	0	0
NETWORK TRANSFER FUNCTION	0	0	0	0	0	0	$S^2+2\zeta\omega_p S+\omega_p^2$	0	0	0	0	$-\omega_p^2$
ROLL MOMENT EQUATION	L_β	0	0	0	0	$L_{\delta\psi}$	0	S	0	$-\frac{L_\delta}{1}$	0	0
FIRST TORSION MODE	R_β	0	0	0	0	$R_{1\delta\psi}$	0	0	$S^2+2\zeta\omega_{T1}S+\omega_{T1}^2$	$-R_{1o}$	0	0
ROLL SERVO TRANSFER FUNCTION	0	0	0	0	0	0	0	0	0	$S+\frac{1}{\tau_s}$	$-\frac{1}{\tau_s}$	0
ROLL CONTROL EQUATION	0	0	0	0	0	0	0	$K_\phi S+K_\phi$	$\lambda_{1RG}K_\phi S^2+\lambda_{1G}K_\phi S$	0	S	0
YAW CONTROL EQUATION	0	$K_\psi S+K_\psi$	$\lambda_{1RG}K_\psi S^2+\lambda_{1G}K_\psi S$	$\lambda_{2RG}K_\psi S^2+\lambda_{2G}K_\psi S$	$\lambda_{3RG}K_\psi S^2+\lambda_{3G}K_\psi S$	0	0	0	0	0	0	$-S$

Figure 27   Matrix of Coupled Roll-Yaw Airframe and Control Equations for First-Stage

R-ED 11117
- 59 -

YAW AND ROLL CONTROLS COUPLED BY
20 PERCENT DIFFERENTIAL SERVO GAIN
AND MAXIMUM AERODYNAMIC EFFECT
THROUGH C_{l_β}

MAXIMUM q CONDITION
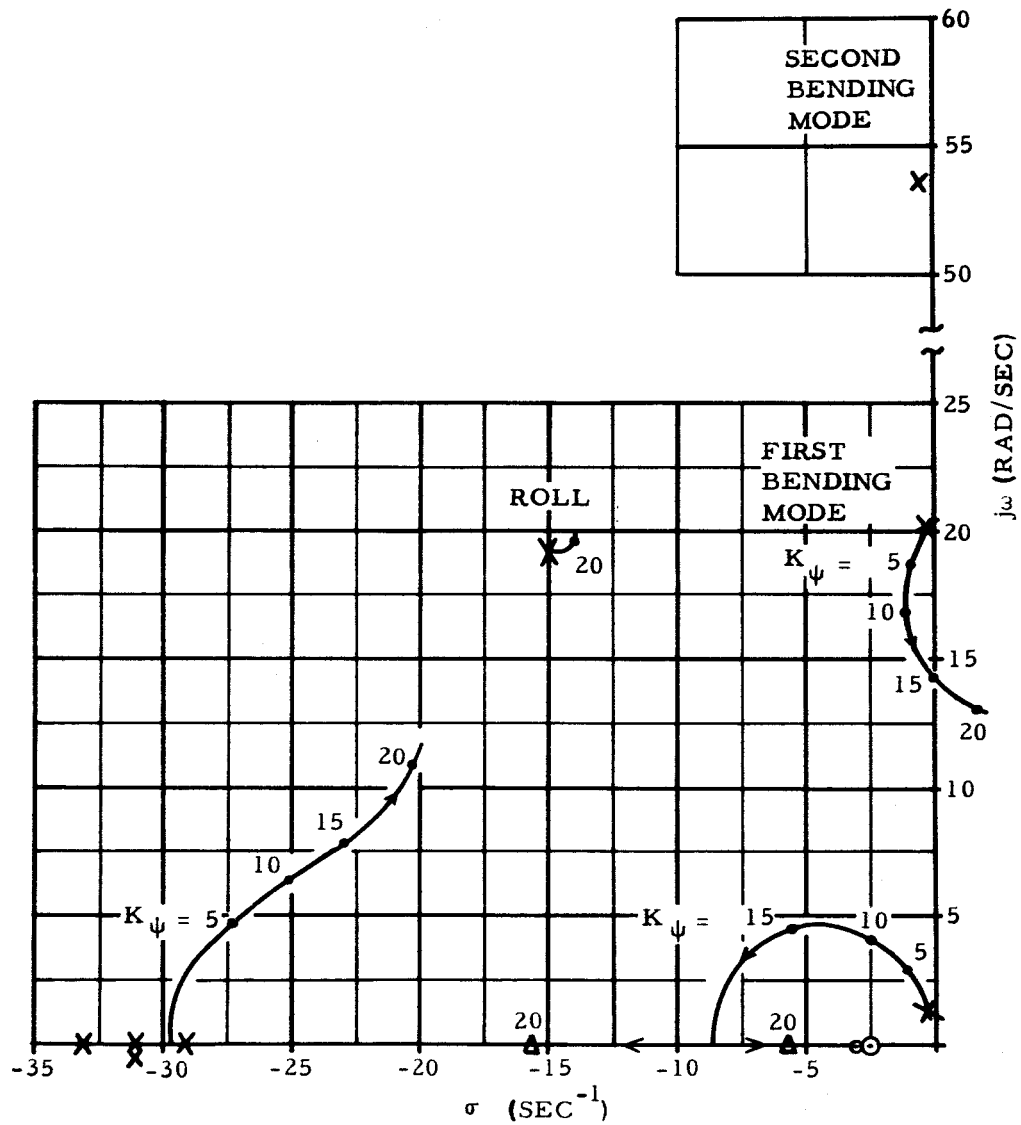
Figure 28 Root Locus Plot of the First-Stage Coupled Roll-Yaw System

MAXIMUM q CONDITION

$\delta_{et} = \delta_e + .2\,\delta_a$ $\beta_o = 2°$ $\delta_{et} = \delta_e - .2\,\delta_a$

$\delta_{at} = \delta_a + .2\,\delta_e$ $\psi_o = 5°$ $\delta_{at} = \delta_a - .2\,\delta_e$

SIDE SLIP ANGLE

YAW ANGLE

YAW CONTROL SURFACE DEFLECTION

FIRST BENDING NORMALIZED DEFLECTION

ROLL ANGLE

ROLL CONTROL SURFACE DEFLECTION

1 SEC

Figure 29 First-Stage Time Response with Roll-Yaw Coupling

More plots of coupled responses may be found in Supplement II. The degree of interaction used in the analysis was considerably greater than that to be expected in practice. Servo specifications were written so that the roll-yaw servos would not differ in gain by more than 10 percent, thus reducing the loop coupling coefficient by a factor of four. The pitch servos are subject to the same specification for they could otherwise introduce disturbance moments into the roll axis. A pitch-roll loop, however, cannot be formed.

There is a difficulty connected with sharing control surfaces which is not evident from a linear analysis. If no measures are taken to prevent it, a large error in one channel could drive the surfaces to their stops, leaving no control for the other axis. On SCOUT this possibil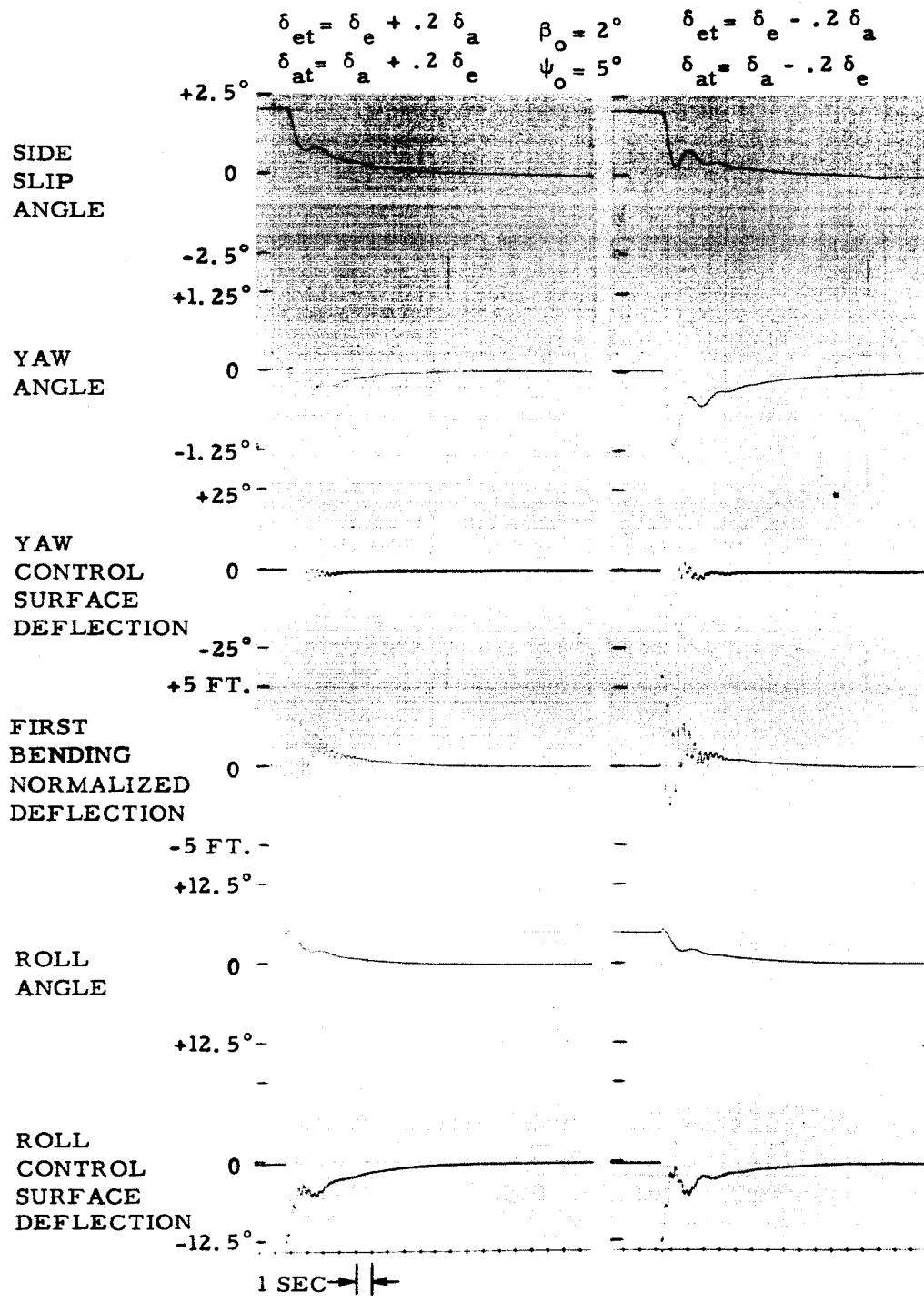ity has been partially eliminated by limiting the magnitude of the yaw error signal before it is mixed with roll error and applied to the servo. With this limiting, a maximum yaw signal will produce no greater than a ± 17.5 degree surface deflection. Thus a maximum of two degrees of deflection remains before a mechanical stop is encountered. If a maximum yaw signal has been commanded and a roll deflection of greater than two degrees is required immediately thereafter, only one surface will be free to deflect the required amount. Deflection of the other surface will be restricted by the proximity of a mechanical stop. Yaw limiting is not abrupt; the error signal is linear only up to 2.5 degrees, beyond which it asymptotically approaches a maximum of 3.5 degrees. There is no limiting in the roll channel.

SECTION II

SCOUT SECOND AND THIRD-STAGE CONTROL SYSTEMS

REACTION-JET CONTROL SYSTEMS

The second and third stages of the SCOUT vehicle are controlled by a system of eighteen hydrogen-peroxide reaction jets. These jets are arranged to provide moments about the pitch, yaw, and roll axes in response to commands from the control system. They are operated in an on/off manner; the appropriate jet is turned on whenever a combination of attitude error and rate signals exceeds a certain value called the "deadband".

A characteristic of this type of control system is that it oscillates about the proper attitude within the deadband when no disturbances are applied, and that when an external disturbing moment is introduced, it oscillates about the edge of the deadband. The arrangement of components in the control loop is depicted in figure 30.

Of the total number of jets, eight are used on the second stage and ten are used on the third stage. The jets are placed about the periphery of the body as shown in figure 31. Each jet is composed of a nozzle, a catalyst bed and decomposition chamber, and a fast-acting poppet valve. Hydrogen peroxide (90 percent) is supplied to each valve from a manifold which is connected to the storage tanks. The peroxide is stored within plastic bladders which are suspended within tanks constructed of aluminum or stainless steel. Separate tanks of nitrogen are used to pressurize the peroxide tanks via a regulator.
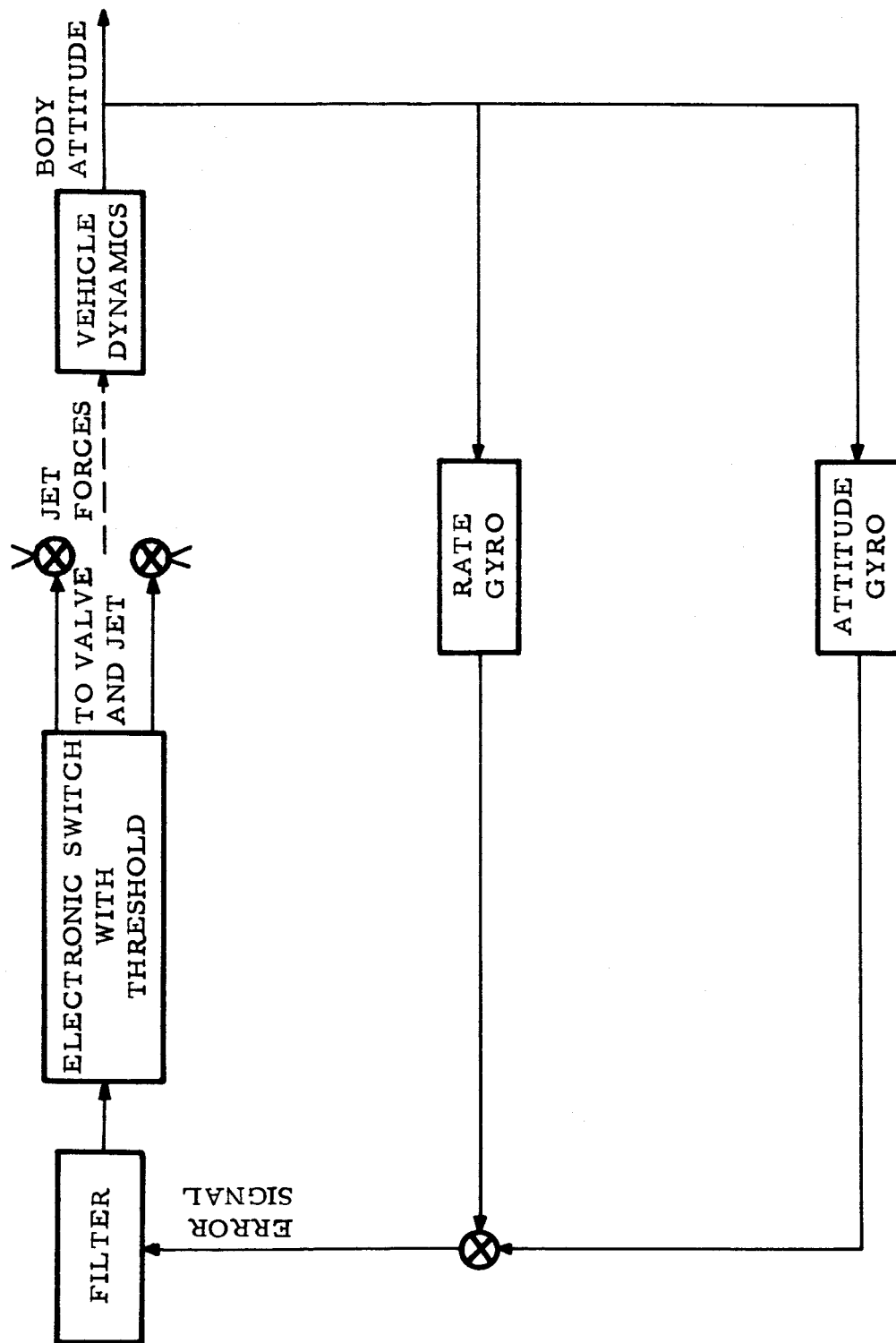
Figure 30 Block Diagram of the Second and Third-Stage Reaction-Jet Control System
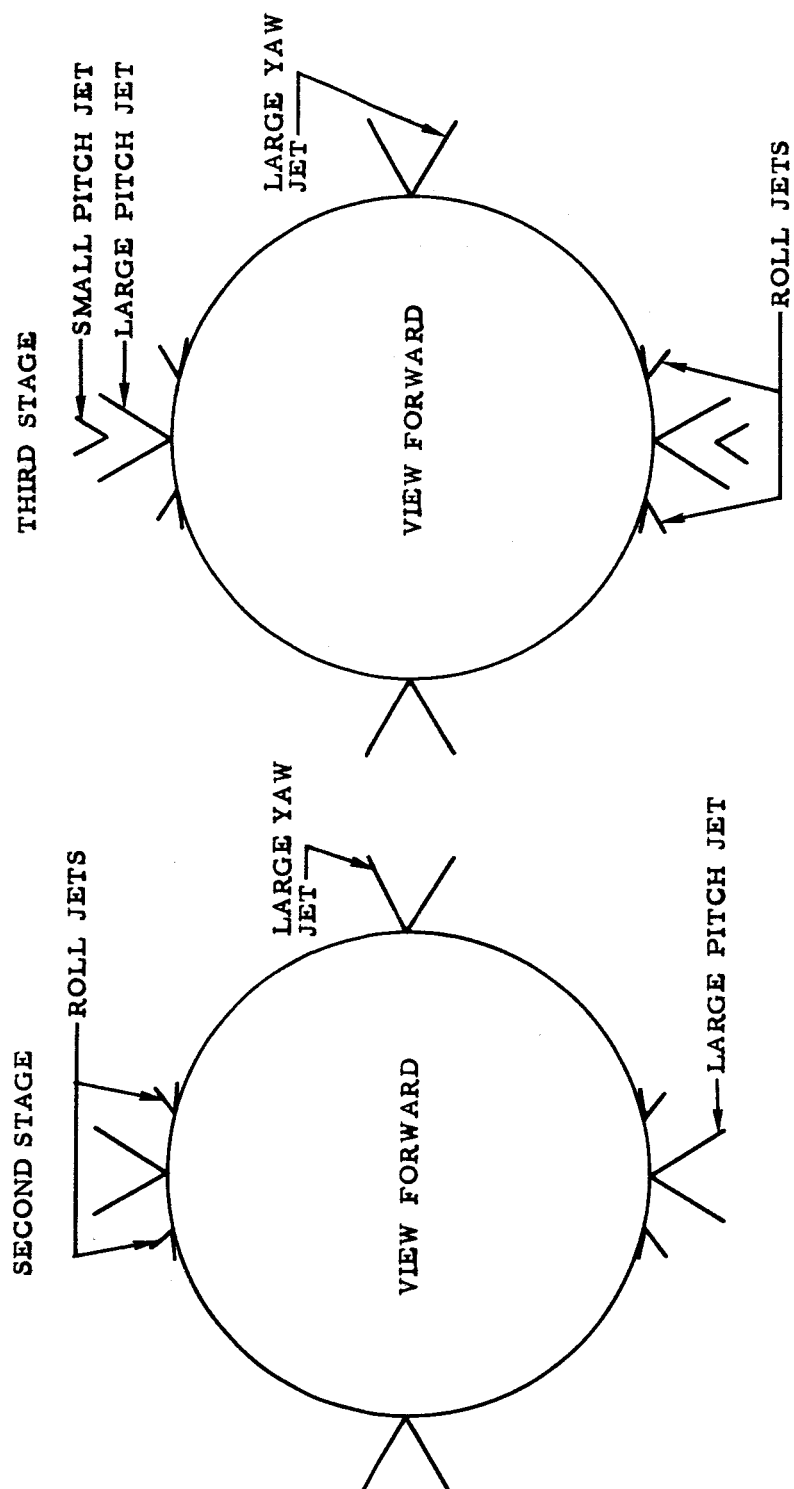
Figure 31 Second and Third-Stage Diagram of Jet Arrangement

The nitrogen pressure forces the fuel out of the bladders to the valves. The second-stage carries six peroxide and six nitrogen tanks, while the third-stage has only two of each type.

The design of the SCOUT upper-stage control system involved the selection of reaction-jet thrust levels and permissible response times, the deadbands, degree of damping, and other parameters. The system design thus determined was to consume no more than a specified amount of fuel while maintaining the vehicle attitude in each axis within tolerances, counteracting external disturbance moments and holding transient errors to a minimum. The requirements of precise control and low fuel consumption are contradictory objectives, therefore compromises had to be reached which gave satisfactory overall performance. Both stages are subject to disturbances due to engine thrust misalignment during boost periods, and to the additional influences of initial angular rates and attitude errors at ignition.

Moreover the second-stage, which is ignited at a condition of considerable dynamic pressure, is aerodynamically unstable and can be expected to produce a disturbing moment. It was decided that each stage system must be capable of restricting the ignition transient errors to less than eight degrees (less than the narrowest of the gyro limits) under the simultaneous action of the maximum thrust misalignment, three degrees of initial attitude error, and three degrees per second of angular rate. All these disturbances were to be combined in the most adverse manner. The maximum engine thrust misalignment was specified to be 0.25 degree for the second-stage and 0.10 degree for the third-stage. For purposes of analysis, this thrust misalignment

was assumed to act at the station of the nozzle throat. The dynamic pressure at which the second-stage could be safely ignited was to be determined. Until second-stage ignition, overall stability would be maintained by retaining the burned out first-stage (with its controls still operative).

The second and third-stages carry 16.6 and 1.66 gallons of hydrogen peroxide, respectively. Accordingly, allowing for expulsion efficiency and a reasonable specific impulse, the total control impulse had to be restricted to less than 25,560 lb-sec on the second-stage and 2556 lb-sec on the third-stage. The second-stage operating time was to be 45 seconds, about forty seconds of which is spent during engine thrust and the remaining time during coasting.

The short coast period between expected second-stage burnout and third-stage ignition was incorporated to reduce the possibility of a slow-burning second-stage having sufficient thrust left to overtake and ram the third-stage after separation. The third-stage burns for approximately 40 seconds and then coasts under control for a maximum of 600 seconds.

Because of the very different requirements of counteracting large disturbing moments during boost and conserving fuel for a prolonged coast, different sets of reaction jets are used for boost and coast operation on the third-stage. At the end of the third-stage coast period, the control system is turned off and the ignition signal is sent to the fourth-stage. The fourth-stage, which is mounted on a spin bearing at the upper end of the third-stage, is given a roll

angular velocity by three small spin-up rockets, and is then ignited. Compromises were continually required in the selection of control system parameters such as reaction jet thrust, jet response time, and deadband. At first, jet response time was assumed to be rather large, but as later information became available from tests, the estimate was revised, and eventually specifications were written defining the maximum tolerable time delays from valve signal to the different portions of full thrust. In general the responses are characterized by a certain deadtime after the valve command during which no thrust occurs, and then a risetime during which the thrust rises from zero to full value. When the jet is turned off, a similar sequence occurs. Frequently for convenience, the terms turn-on or turn-off time are used to mean deadtimes equivalent to the actual response. Once jet response specifications were written, system performance was calculated using the specified values. Since it was recognized that tolerances would be applied to each parameter value selected, performance calculations were always made with jet thrusts, deadbands, etc., differing from nominal by the expected tolerance and in the most detrimental direction.

In the interest of improving the performance and reliability of the SCOUT system, and for the purpose of correcting unavoidable or unsuspected conditions, several changes were made in the control systems of the later vehicles. Accordingly, the design described here is different for each of the first three SCOUTS, and each has been considered separately. The fourth vehicle has not been launched at the time of this writing, so that only estimated final data can be given.

SECOND STAGE CONTROL SYSTEM

Airframe Description

The second SCOUT step is composed of the Castor, Antares, and Altair rocket motors and associated equipment. Dynamically it behaves as a free body exhibiting inertia effects and an aerodynamic moment due to angle of attack. In addition, the structure itself is flexible, and if desired, the effects of body bending and torsion can be taken into account. Except for certain specific tests, body flexibility has been ignored in the design of SCOUT upper-stage systems.

In pitch and yaw during burning the second-stage is characterized by a moment of inertia varying between 35,952 and 24,026 slug-ft^2 about a center of mass moving from body station 298.1 to 236.2. In roll, the moment of inertia about the vehicle centerline decreases from 370.2 slug-ft^2 at second-stage ignition to 185.3 slug-ft^2 at burnout. The reaction jets were specifically placed to provide the largest practical moment arm for control. The pitch and yaw jets act at body station 467.68, and the roll-jet effective distance from the vehicle centerline is 16.02 inches. The aerodynamic center of pressure near ignition is taken to be at station 220 and the lift coefficient is 0.072 degree^{-1} based on a 5.25-ft^2 reference area.

Selection of Pitch and Yaw Control Parameters for First Two Vehicles

When the second-stage is ignited, the pitch and yaw control system can be subjected to disturbances due to engine thrust misalignment,

initial attitudes and rates, and to angles of attack. These disturbances must be sufficiently counteracted by the control jets to insure that the initial transient error does not exceed eight degrees. The reaction-jet thrust level necessary to restrict the error to eight degrees was determined by simulating the entire dynamic situation on an analog computer and varying the pertinent parameters.

The magnitude of the initial transient error depends upon the jet response time as well as upon the thrust, as is also affected by the deadband and the degree of damping. The response of peroxide jets and valves capable of delivering more than 500 pounds of thrust was at first found to be of the order of 100 ms turn-on and turn-off time. Accordingly, the jet response times used in the analysis of the first systems and specified as a requirement to the jet supplier were 110 ms deadtime and a total of 130 ms for thrust to reach 90 percent of final value for both turn-on and turn-off. With this response, and with values of deadband and rate gain which would give reasonable accuracy, the minimum allowable reaction jet thrust was determined to be just over 500 pounds. It was found, however, that when the system of pitch, yaw, and roll jets were plumbed, some supply pressure interaction existed and that any single jet thrust was lower if other jets were turned on. It is possible for the afore-mentioned disturbances to occur at ignition in all axes. Such a condition could require many jets to fire simultaneously and thus momentarily reduce the thrust capability of individual jets. Under these conditions, it was determined that the thrust level of each jet was to be at least 510 pounds and that the thrust level of a jet acting individually was to be 570 pounds.

The dynamic pressure under consideration at this time was equivalent to an ignition altitude between 100,000 and 130,000 feet. Since the trajectory information for different launch angles indicated that the dynamic pressure sometimes remained constant or even increased slightly after ignition at the proposed altitudes, the dynamic pressure, q, was held constant in the analog simulation for 10 seconds after ignition. It was found that a q of 40 psf could be allowed at ignition.

Once the jet size was determined, the combined pitch and yaw fuel consumption was considered. With proper choice of deadband and rate gain, the fuel consumption during burning could be made dependent only upon the disturbance moment, thus minimizing the required impulse. During the period after the engine thrust has decayed to a low value (8 to 10 seconds), the fuel consumption rate depends upon many things, chief among which are the jet thrust and time response. It was found that unless the system deadband was increased to an undesirably large value, the jets selected to properly control the initial transient consumed more fuel during the short coast period than could be allowed. The amount of rate gain employed, the hysteresis in the switching circuit, and the various lags associated with the gyros and electronics also contributed to the impulse consumption rate.

The conflict in requirements for the initial "capture" and for economy in fuel made it necessary to consider changing the system thrust levels between ignition and the coast period. The solution finally employed was to use high jet thrust for a few seconds after ignition

to minimize initial transient errors and then to reduce the thrust for the remainder of the second-stage operation. The change in thrust level was accomplished by using two nitrogen pressure regulators set at different levels so that each would force hydrogen peroxide to the jets at a different rate. The higher pressure device was connected to a very small nitrogen tank which would be depleted rapidly. Because of its shape, this tank is called a "toroid". When the toroid tank is charged, the peroxide tanks are pressurized to the control level of its regulator because it has the highest setting. In this condition the second regulator, which is connected to the normal large nitrogen tanks, acts as a check valve and does not supply gas. When the toroid pressure decays to a level which would cause the output of its regulator to fall below the pressure setting of the other regulator, gas is supplied from the main tanks at the lower pressure. The toroid with a normal charge expels an amount of fuel equivalent to 3080 lb-sec of impulse. The advantage of this scheme (first suggested by NASA personnel) is that it is passive and no switching is necessary.

This scheme provided two single jet thrust levels of 570 pounds minimum and 475 pounds nominal. In conjunction with pitch and yaw deadbands of 14 mr, position-to-rate gain ratio of 2.5, and a lag network, the transient behavior and fuel consumption were satisfactory. The position-to-rate gain ratio is often referred to as the "switching line slope", because of its significance when the control performance is analyzed on the phase plane. The lag network mentioned was incorporated just prior to launching the first vehicle. The network was not intended to improve the control system (in fact it had a dele-terious effect), but it was required to reduce the expected effect of

harmful noise pickup in the rate gyro channel during third-stage burning.

On the first flight, this lag, a simple time constant of 17 ms, was present during second-stage operation; on later flights it was switched into the circuit at third-stage ignition.

The calculated behavior of the second-stage pitch and yaw control system used on the first SCOUT flight can be seen from the time response and fuel consumption shown in figures 32 and 33. The second SCOUT flight differed somewhat in that it had no lag network and slightly faster jet responses, so that its performance was better than that shown. The pertinent conditions are marked on the graphs. Note that for attitude time responses in which the initial transient is of primary importance, the system deadband is made 10 percent greater than nominal and the reaction jet thrust used is the minimum value allowed by the specifications. When fuel consumption is calculated, the deadband is made 10 percent too narrow and the thrust is increased to the high side of the tolerance. Also q is removed very soon after ignition because it tends to decrease fuel consumption. Note that in both figures the jets begin steadily pulsing immediately after engine burnout occurs. This situation is not intended to be typical of the behavior in actual flight, but rather it represents the most severe condition possible. In figure 33 three curves have been plotted, one each for conditions of full engine thrust misalignment, for $1/2 \ \sqrt{2}$ times maximum thrust misalignment, and for no misalignment. The reason for making three curves is that maximum total pitch and yaw impulse can be shown to be either the sum of the
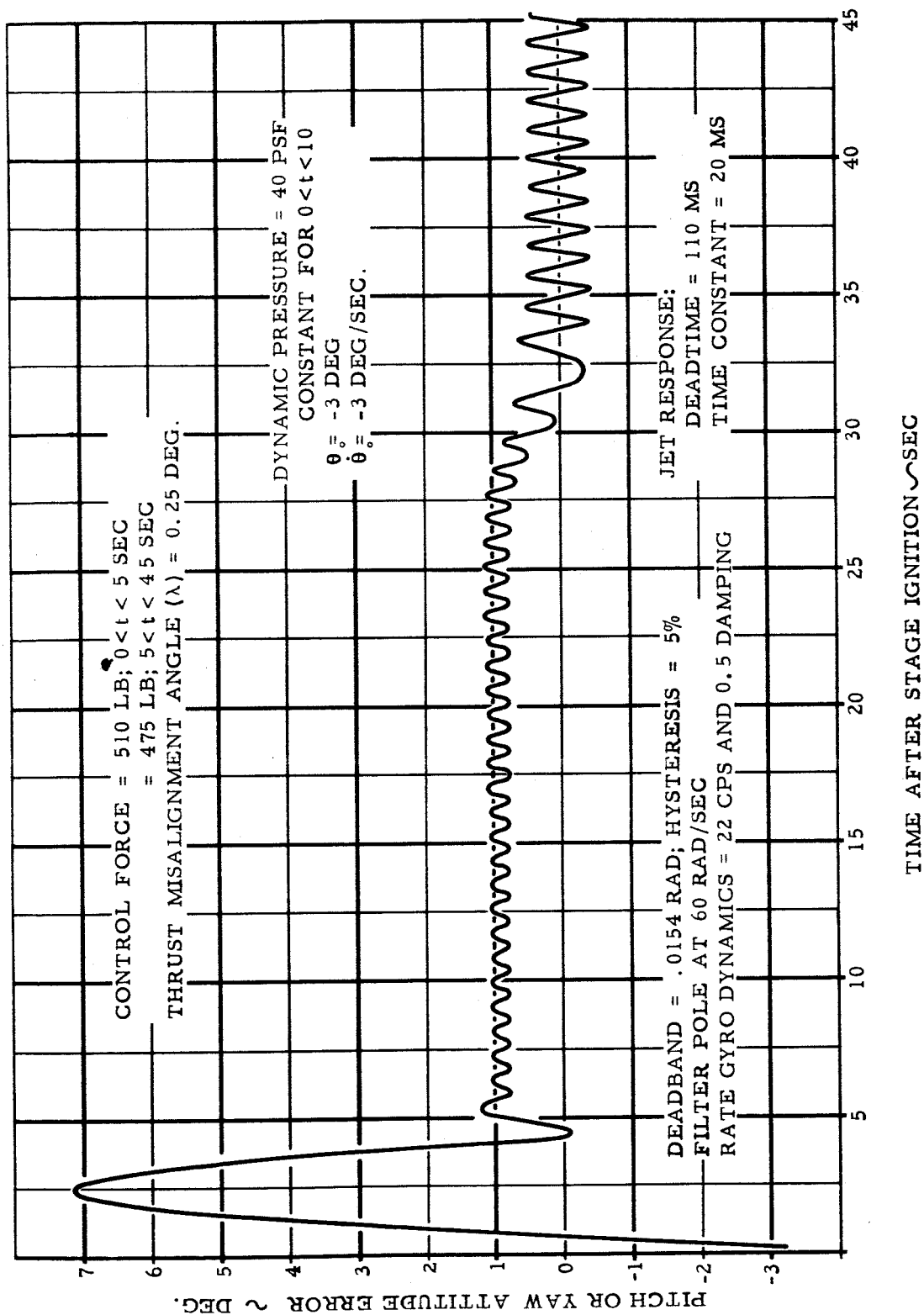
Figure 32 Second-Stage Pitch Time Response with Dual Thrust Levels

CONTROL FORCE = 696 LB; $0 < t < 3$ SEC AND 525 LB FOR $t > 3$ SEC
THRUST MISALIGNMENT ANGLE ($\land$) = 0.25 DEG.
DEADBAND = .0126 RAD
HYSTERESIS = 5%

JET RESPONSE:
DEADTIME = 110 MS
TIME CONSTANT = 20 MS

FILTER POLE AT 60 RAD/SEC
RATE GYRO DYNAMICS = 22 CPS AND 0.5 DAMPING
DYNAMIC PRESSURE = 40 PSF; $0 < t < 4$ SEC
$\theta_o^. = -3$ DEG; $\dot\theta_o = -3$ DEG/SEC
$\theta_o^. = -3$ DEG; $\dot\theta_o = -3$ DEG/SEC

MAX. IMPULSE = $\land$ SIN 90° + $\land$ SIN 0° = 24,700 LB - SEC
MAX IMPULSE WHEN FILTER POLE IS AT 670 RAD/SEC = 21,600 LB-SEC

$\land$ SIN 0°
$\land$ SIN 45°
$\land$ SIN 90°
$\land$ SIN γ

TIME AFTER STAGE IGNITION (SEC)

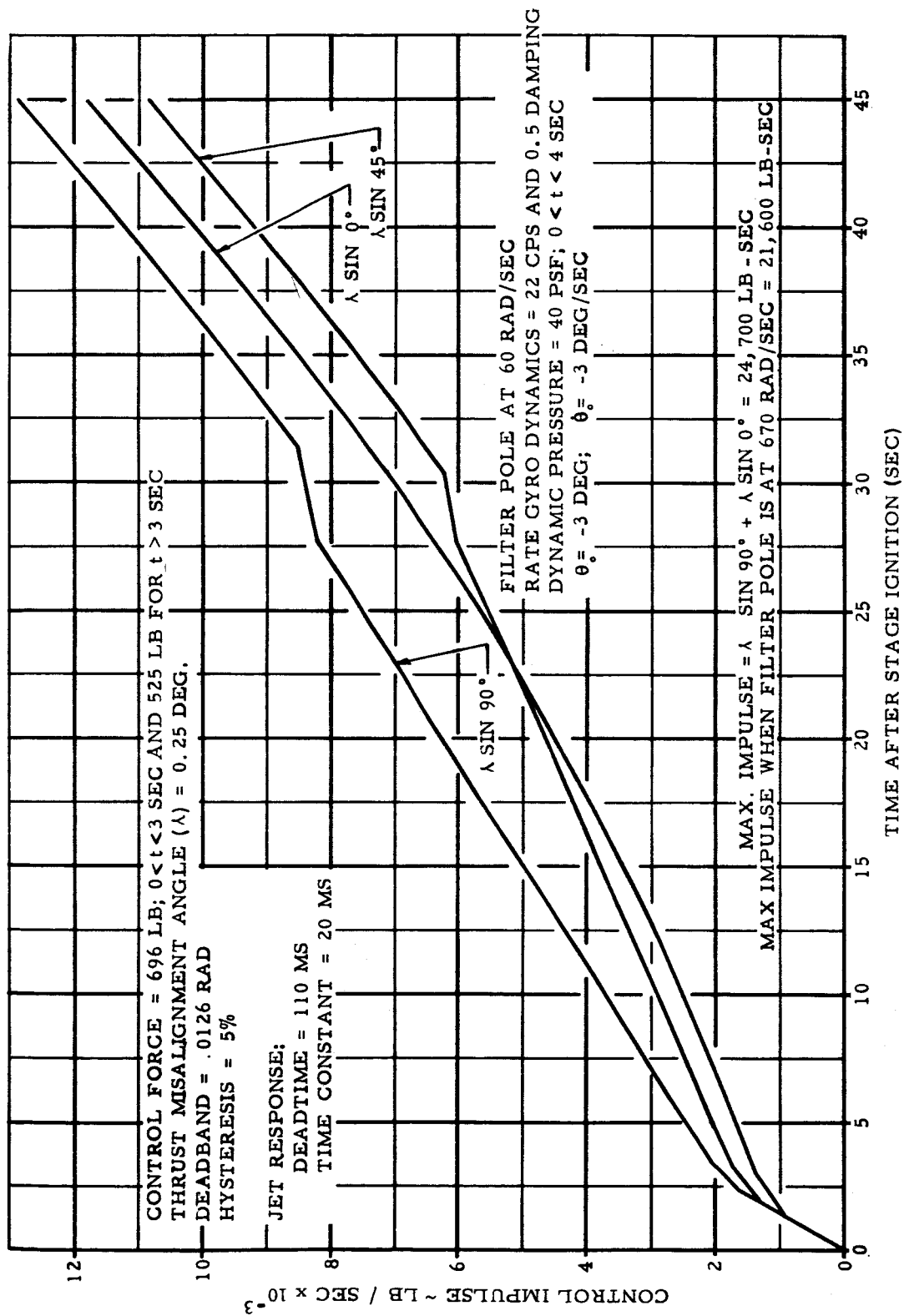CONTROL IMPULSE ~ LB / SEC $\times 10^{-3}$

Figure 33 Second-Stage Pitch and Yaw Fuel Consumption with Dual Thrust Level

maximum and the zero misalignment curves or double the 1/2 $\sqrt{2}$ misalignment curve. The amount of impulse required to overcome the initial transient is that of the steep part of the curves. As the engine thrust (and, hence, misalignment magnitude) decreases near burnout, the impulse rate is attenuated slightly and then continues at a new rate determined by the control parameters above. The system is conservative if the maximum impulse consumed is double that given by the 1/2 $\sqrt{2}$ misalignment curve. The reasoning is that the most severe disturbing effects occur when the engine thrust misalignment is maximum and lies directed half way between the pitch and yaw planes. In this condition each jet must produce 1/2 $\sqrt{2}$ times as much impulse as does the disturbance. If the case of full misalignment in one plane and zero in the other used the greater quantity of fuel it would indicate that the deadband had been set too narrow. The simulations which generated these curves included the effect of gyro dynamics, electronic lags, and switching hysteresis equal to five percent of the deadband.

Although it was appreciated that structural flexibility would not present a stability problem on the upper stages as it had on the first, its effects on fuel consumption were considered briefly. When a large pitch or yaw jet is fired, the body bending mode is excited which transmits a high frequency series of local attitude changes to the gyros. If the system is close to the edge of the deadband (as it always is when a jet is fired), the resulting gyro pickup may suffice to keep the jet turned on for a short additional time or may turn it off. In some cases the feedback from flexible motion causes the opposing jet to be turned on briefly. Such effects do not significantly alter the normal fuel

consumption calculations.

Selection of Roll Control Parameters for First Two Vehicles

The second-stage roll control system was the same for the first two flights. The roll axis poses much less a design problem than do the other two because the jets can be made small enough to render fuel consumption almost negligible. The only significant roll disturbances are those caused by misalignment of the larger pitch and yaw jets. These disturbances can introduce a roll moment if their line of action does not pass through the vehicle center of mass. The location of the center of mass was assumed to be at most 0.25 inch from the centerline. The pitch and yaw jet placement tolerances considered to be compatible with the center of mass uncertainty were taken to be 0.125 inch. Each jet was to be positioned so that its line of action lay within 0.125 inch of the vehicle centerline, and in addition, a 0.10-degree angular tolerance was allowed. Since at most one yaw and one pitch jet can fire at one time, the maximum rolling moment induced was calculated by considering that both of these jets were firing and that the center of mass lay 0.25 inches from the centerline in a direction half way between the pitch and yaw planes. This gave each jet an effective moment arm of 0.330 inch, and considering that their thrust was 10 percent greater than nominal, the maximum roll moment was determined to be 38.3 ft-lbs. The reaction-jet thrust necessary to overcome this moment and hold the transient error within limits was found to be 24 pounds if a 14 mr deadband was used. The time responses for these smaller jets were considerably less than those for the pitch and yaw motors. The equivalent turn-on and

turn-off times were taken to be 70 ms. These times were later incorporated in specifications, which allowed 45 ms deadtime and 45 ms additional risetime to reach 90 percent of full thrust.

The roll system time response at ignition is shown in figure 34. The fuel consumption curve is not shown, but the total roll impulse at the end of 45 seconds of second-stage operation is calculated to be no more than 650 lb-sec. This figure is based upon the roll system oscillating freely with no disturbances and with a duty cycle of 30 percent. If the maximum disturbance moment were applied for half the time (a 50 percent duty cycle for the entire operating period), a 640 lb-sec impulse would be required.

First and Second Vehicle System Design Summary

The total impulse required for second-stage operation in pitch, yaw, and roll on the first flight under the most adverse circumstances is seen to be 25350 lb-sec. Some margin was to be allowed to account for the suspected reduction in peroxide specific impulse when the jets are operated at a low duty cycle. This reduction was subsequently measured and found to be small enough to be disregarded.

In summary, the parameters used for the design and flight of the first and second SCOUT second-stage systems are given in table 2.
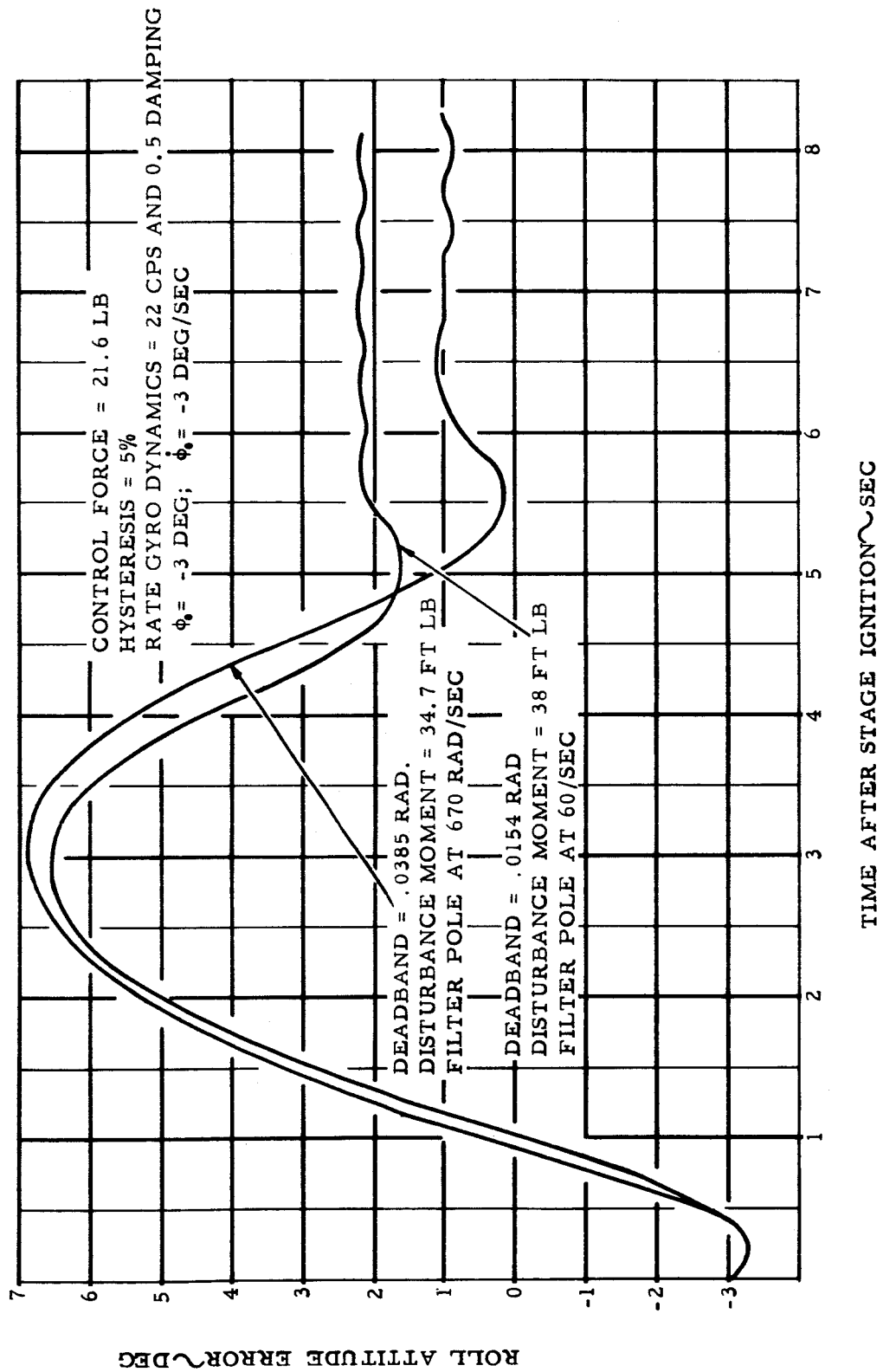
TIME AFTER STAGE IGNITION∿SEC

Figure 34 Second-Stage Roll Time Response

| | FLIGHTS | |
	NUMBER 1	NUMBER 2
DEADBANDS:		
Pitch	.014 rad ± 10%	same
Yaw	.014 rad ± 10%	same
Roll	.015 rad ± 10%	same
RATE-TO-POSITION GAIN RATIO:		
Pitch, Yaw, Roll	0.4 ± 10%	same
DUAL-LEVEL REACTION JET THRUST:		
Initial: Pitch and Yaw	510 to 696 lbs	same
Roll	19.3 to 26.4 lbs	same
Second Level: Pitch and Yaw	475 lb ± 10%	same
Roll	18 lbs ± 10%	same
REACTION JET RESPONSE:		
Turn-on time: Pitch and Yaw	0.13 sec	same
Roll	0.07 sec	same
Turn-off time: Pitch and Yaw	0.13 sec	same
Roll	0.07 sec	same
CONTROL-LOOP FILTER TIME CONSTANT (LAG)	.0145 to .0195 sec	.0015 sec
ALLOWABLE DYNAMIC PRESSURE AT IGNITION	40 psf	same
TOTAL REACTION CONTROL IMPULSE AVAILABLE	25,560 lb-sec	same
CALCULATED MAXIMUM CONTROL IMPULSE REQUIRED	25,350 lb-sec	22,200 lb-sec
CALCULATED INITIAL TRANSIENT ERROR, STANDARD CONDITIONS		
Pitch or Yaw	7.1 deg	7.1 deg
Roll	6.6 deg	6.9 deg

Table 2   Second-Stage Control Parameters for Vehicle One and Two

Selection of Control Parameters for Third and Fourth Vehicles

Some time before the third system was constructed, it became apparent that a faster time response was highly desirable for the pitch and yaw jets. It was determined that, if the equivalent turn-off times could be reduced to 90 ms, the toroidal tank and the dual thrust-level system could be eliminated. Much of the deadtime was traceable to the poppet valve, which was a two-stage device using a solenoid operated pneumatic valve to actuate the poppet valve proper. This valve was improved until its response was of the desired order, but it was finally replaced with an equally fast single-stage solenoid valve. Specifications were rewritten establishing the equivalent turn-off time at 90 ms, and new response and fuel consumption curves were plotted. The second stage, thus improved, operated at a single, high, reaction-jet thrust level for the full 45 seconds. Due to the fast jet response and to certain modifications in the way thrust misalignment and dynamic pressure were simulated, the minimum thrust level required was reduced to 470 pounds. The performance of the new system, used on the third and fourth flights, can be seen from the plots of figures 35 and 36. The system deadbands have been changed somewhat from those of the second and third flights for reasons of third stage fuel consumption. The deadbands were made the same between the two stages where possible to avoid the necessity for gain switching. Total fuel consumption for flights three and four was obtained by adding 600 lb-sec to the impulse obtained from figure 36, yielding a maximum impulse of 19100 lb-sec. Roll transient response for the later vehicles is shown in figure 34 for the 38.5 mr deadband. The disturbance moment used here is
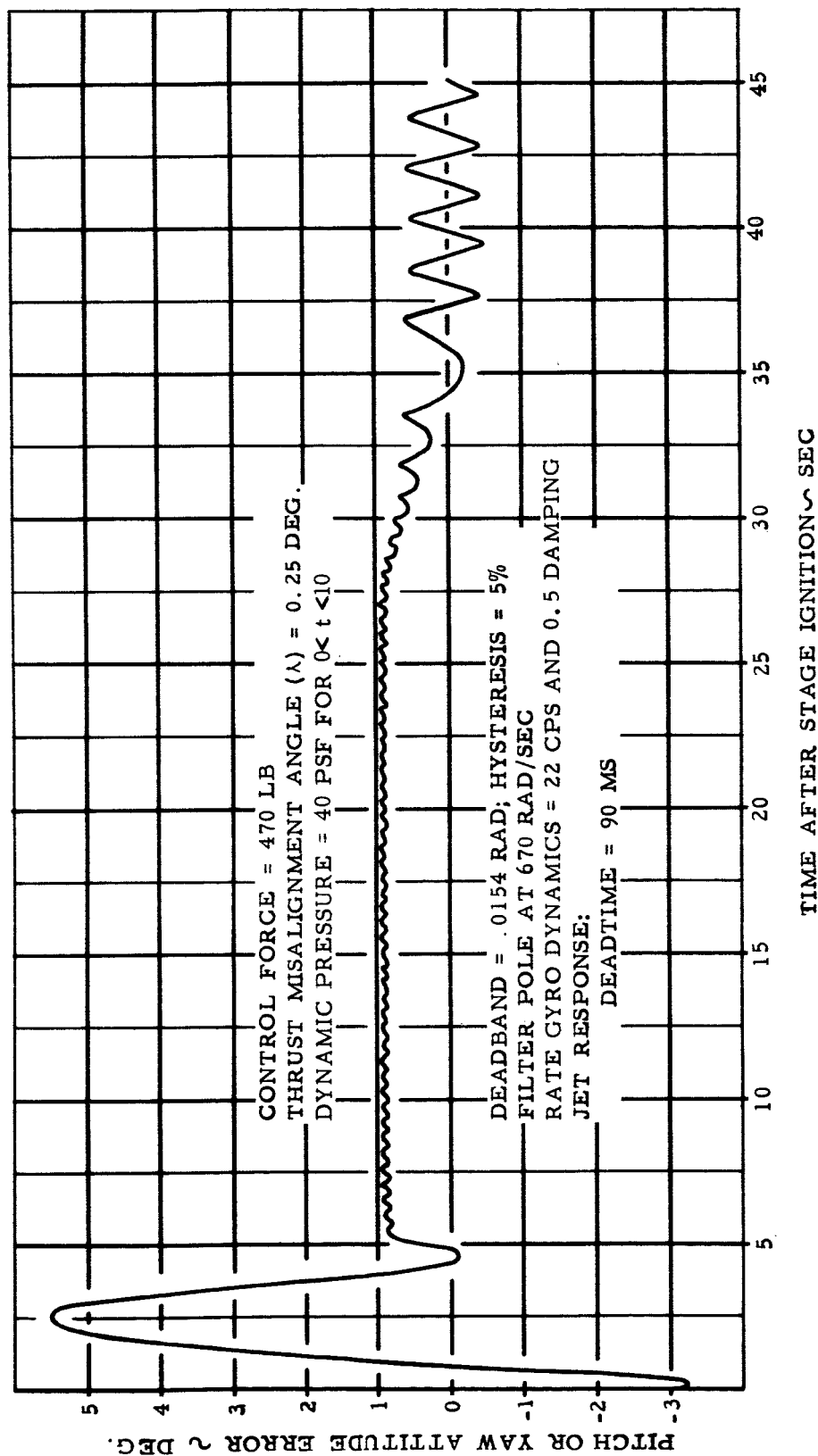
Figure 35 Second-Stage Pitch Time Response with Single Thrust Level

CONTROL FORCE = 636 LB
THRUST MISALIGNMENT ANGLE = 0.25 DEG.
DEADBAND = .0154 RAD
HYSTERESIS = 5%
FILTER POLE AT 670 RAD/SEC
RATE GYRO DYNAMICS = 22 CPS AND 0.5 DAMPING

JET RESPONSE:
DEADTIME = 90 MS

DYNAMIC PRESSURE = 40 PSF; $0 < t < 4$ SEC
$\bar{\theta}_o = -3$ DEG; $\dot{\theta}_o = -3$ DEG/SEC

MAX IMPULSE AT λ SIN 90° + λ SIN 0° = 18,700 LB - SEC.

TIME AFTER STAGE IGNITION (SEC)

CONTROL IMPULSE $\sim$ LB - SEC X 10^{-3}

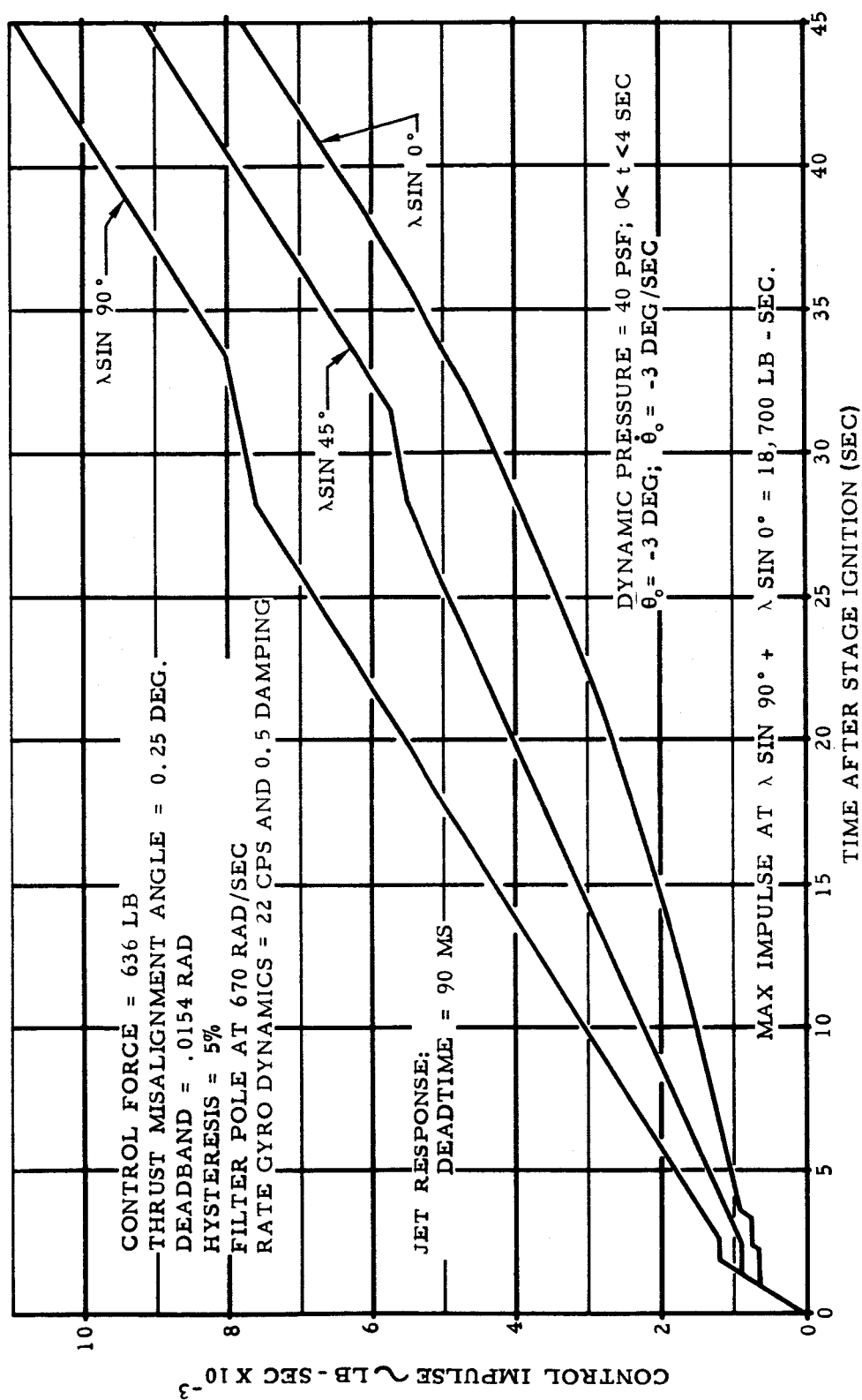λ SIN 90°
λ SIN 45°
λ SIN 0°

Figure 36 Second-Stage Pitch and Yaw Fuel Consumption with Single Thrust Level

34.7 ft-lb, and the 17 ms noise filter lag was not included. A summary of the control parameters for the second stage of flights three and four is given in table 3.

THIRD-STAGE CONTROL SYSTEM

Airframe Description

The third stage (step) of SCOUT is composed of the third and fourth stages. The guidance and control package is located at the head of the Antares motor in Transition Section D. The third-stage vehicle behaves in each axis as a pure inertia since aerodynamic forces are negligible at the operating altitude. The structure is quite rigid making it unnecessary to consider bending effects in the control design. The first vehicle system was designed using specified values for moments of inertia and center of mass which were later found to be considerably different from those of the actual SCOUT. The pitch and yaw inertia values used varied from 1388 to 814 slug-ft^2 during engine burning, while the center of mass changed from body station 137.8 to 105.1. The roll inertia varied from 77 slug-ft^2 at ignition to 27.4 slug-ft^2 at burnout. The actual inertias later proved to be larger than these values, a situation which made the design more conservative since larger inertias reduce both transient errors and fuel consumption. For flights two, three, and four, the roll moment of inertia after burnout was changed to 38 slug-ft^2 at the request of NASA. The reaction jet positions were chosen to give the largest practical control moment arm; the pitch and yaw jets are located at body station 220.68 and the roll jets each have an effective arm of

DEADBANDS: 　Pitch 　Yaw 　Roll	 .014 rad ± 10% .016 rad ± 10% .035 rad ± 10%
RATE-TO-POSITION GAIN RATIO: 　Pitch, Yaw and Roll	 0.4 ± 10%
REACTION JET THRUST (SINGLE LEVEL): 　Pitch and Yaw 　Roll	 470 to 636 lbs 18 to 26.4 lbs
REACTION JET RESPONSE: 　Turn-on time:　Pitch and Yaw 　　　　　　　　Roll 　Turn-off time:　Pitch and Yaw 　　　　　　　　Roll	 0.12 sec 0.07 sec 0.09 sec 0.07 sec
CONTROL-LOOP FILTER LAG TIME CONSTANT:	 .0015 sec
ALLOWABLE DYNAMIC PRESSURE AT IGNITION:	 40 psf
TOTAL REACTION CONTROL IMPULSE AVAILABLE:	 25,560 lb-sec
CALCULATED MAXIMUM CONTROL IMPULSE REQUIRED:	 19,350 lb-sec
CALCULATED INITIAL TRANSIENT ERROR, STANDARD CONDITIONS: 　Pitch or Yaw 　Roll	 5.5 deg 6.9 deg

Table 3　Second-Stage Control Parameters for Vehicles Three
and Four

13.46 inches on the first vehicle. Flights two, three and four have modified roll jets and their arm has been extended to 15.1 inches.

Selection of Control Parameters for First Vehicle

At third-stage ignition, the control system must counteract simultaneous disturbances arising from engine thrust misalignment and initial attitude and rate errors. Reaction jets of the thrust level under consideration (20 to 30 pounds) were known to respond with equivalent turn-on and turn-off times of 60 to 70 ms. Specifications were written requiring each jet to have a deadtime of no more than 45 ms and an additional risetime to reach 90 percent of full thrust of 45 ms, resulting in an equivalent turn-on time of 70 ms. When the jets were turned off, 45 ms was allowed before the thrust decay began and 45 ms more to decay to 10 percent of the full thrust value. The turn-off time, which is far more important than the turn-on time for fuel consumption, was taken as the equivalent of 70 ms deadtime and was simulated using a deadtime of 50 ms and a simple 20 ms time constant. The pitch and yaw reaction-jet thrust which offered the best compromise between fuel consumption and transient errors at ignition for the first flight was found to be 44 pounds. At its minimum value of 39.6 pounds, the worst transient was considerably less than eight degrees, even when the thrust misalignment was assumed (as it was initially) to act at the jet station. At the high tolerance level of 48.4 pounds, fuel consumption was not severe. These jets were, of course, to be used only during the so-called boost phase of third-stage operation. They were to be turned off when the coast period began, at which time pitch and yaw control moments would be

provided by additional smaller jets. The fuel consumption during the boost phase was determined primarily by the value of the engine thrust misalignment if the deadband was made sufficiently large. The deadband for pitch and yaw was set at 14 mr ± 10 percent for the first flight. Plots of pitch time response showing the transient at ignition and pitch-yaw fuel consumption are shown in figures 37 and 38. The fuel consumption plot applies to the second, third, and fourth systems; the first system did not require as much impulse as that shown. Although the ignition transient is small, it was not considered necessary to reduce the jet thrust, as fuel requirements were not thought to be severe. A pitch and yaw jet thrust reduction actually saves very little impulse -- at the most 100 lbs-sec.

Fuel consumption during the boost phase, i.e., the period during which the large jets were used, was first calculated assuming that the jets were turned off immediately after engine burning ceased. This was proper because the change from large to small coast jets on the first flight was made when the vehicle forward acceleration fell to 64 ft/sec^2, as detected by an acceleration switch. For all later flights, the change-over was made on a time basis, 43 seconds after engine ignition. The nominal engine burning time is 39 to 40 seconds, and test data showed that variations of nearly ± 4 seconds were possible. If the engine burns out earlier than the maximum time allowed, the control system must coast for a short time using the large jets. The fuel consumption curve of figure 38 reflects this possibility. (The burnout time is 36 seconds, requiring the system to coast for seven seconds.) The amount of fuel using during this period depends a great deal upon the jet thrust and time response,
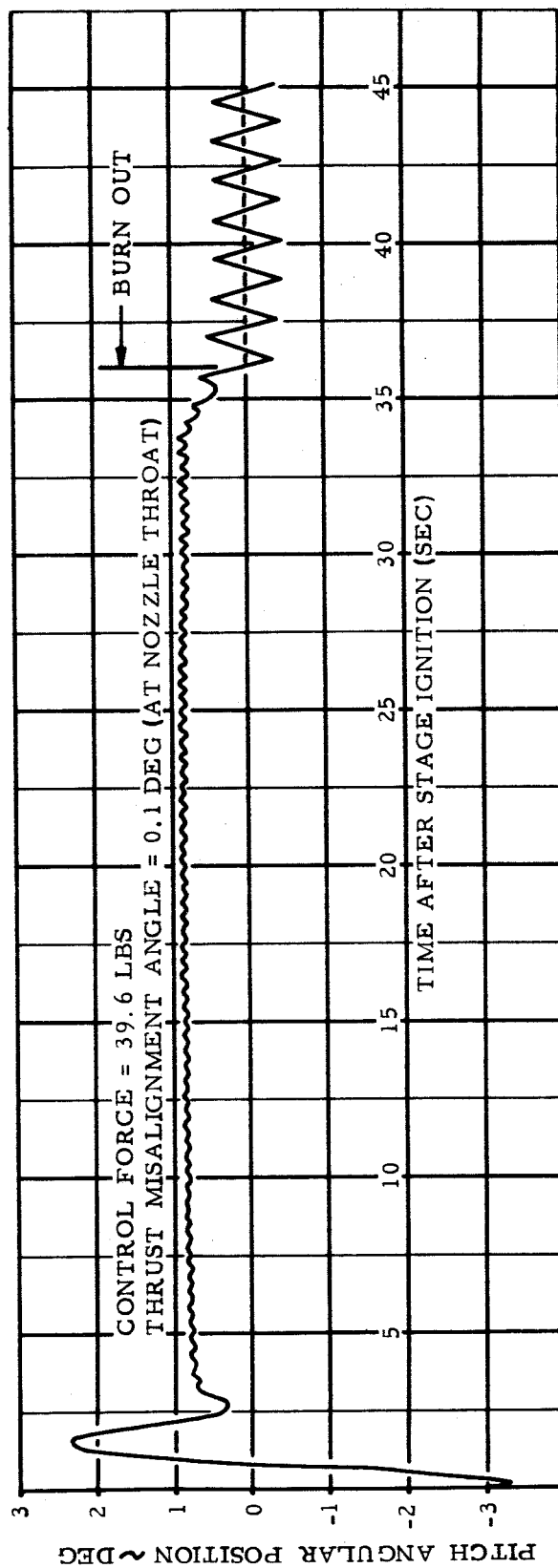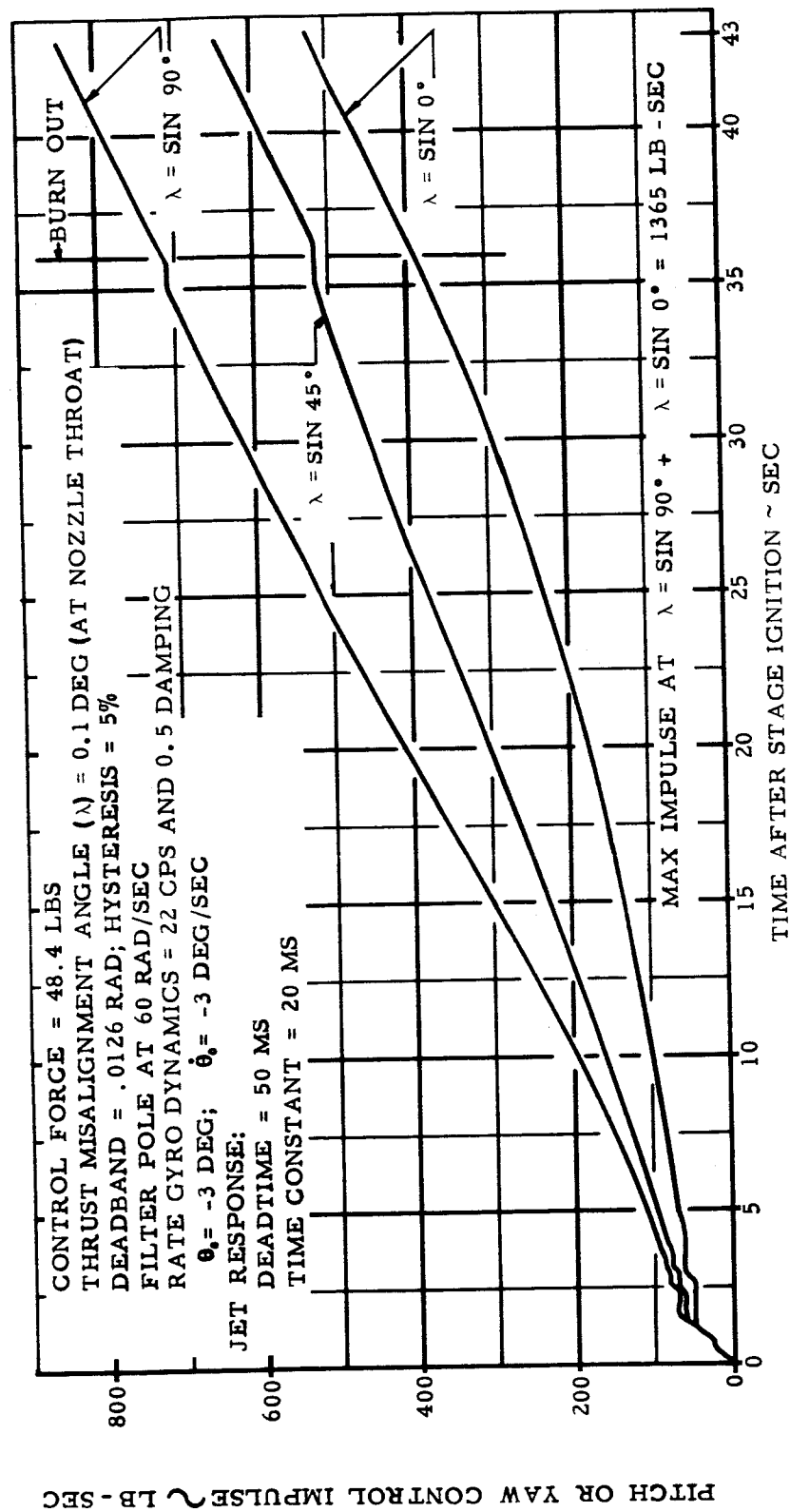
Figure 37 Third-Stage Pitch Time Response

Figure 38 Third-Stage Pitch and Yaw Fuel Consumption

the deadband, the slope of the switching line, and the vehicle moment of inertia.

In figure 38 the zero thrust misalignment curve includes the effect of a noise-filter lag. In the few weeks prior to the first flight, a first-order lag network with a 17 ms time constant was inserted in the forward control loop ahead of the electronic switch. This lag was switched into the circuit at second-stage ignition. On all later flights, it was inserted at third-stage ignition and was removed at the beginning of the coast period. The presence of the lag does not seriously increase the total fuel consumption, but it makes careful consideration of vehicle inertias and jet time responses mandatory because the maximum impulse used with the lag is not solely dependent upon the thrust misalignment.

The purpose of the lag was to filter high-frequency noise or extraneous signals from the control loop. During static firing tests of the ABL X-254 (Antares) engine, it had been found that the rate gyros in their normal mounting were apparently responding to the extremely high level vibration of the rocket. Rate gyro outputs reached levels corresponding to 6 deg/sec at frequencies of 30 and 600 cps. Although the rate-gyro block mounting was stiffened, the gyro outputs were still high. Since the Gnat rate gyros cannot respond to angular rate inputs at 600 cps it was concluded that the pickup occurred through mechanical movement of the gyro signal generator or gimbal due to the extreme vibration level (45 g's rms). Tests showed that the "noise" was extremely detrimental to the third-stage operation; sometimes increasing the apparent switching hysteresis to 100 percent.

It was established that the noise effect could be almost entirely eliminated by attenuating high frequencies in the error signal, which was accomplished by increasing the capacitor value of the normal demodulator ripple filter. The time constant selected was supposed to represent the best compromise between fuel consumption and noise protection. If gyro pickup or noise appears in the frequency range close to the 400-cps carrier or to an integral multiple of it, very little attenuation is provided; the extraneous signal must differ from the carrier frequency by thirty or forty cycles per second if the control system is not to be affected.

The third-stage roll control design proceeded as did that of the second stage. The maximum disturbance moment was 2.6 ft-lb, and jets of 2.2 pounds nominal thrust were found adequate to curb the initial transient, due to its sudden application. The smallest practical thrust level was desirable because the four "roll" jets would be used for both roll and yaw control during the long coast period. The time response associated with reaction jets of this size is somewhat slower than with larger jets because of the difficulty of manufacturing nozzles and decomposition chambers of sufficiently small volume. An equivalent turn-on time of 50 ms and a turn-off time of 90 ms was used in the analysis. Figure 39 shows the ignition transient in roll with jets of this response and with a deadband of 14 mr ± 10 percent. The effect of the noise filter lag is included. The maximum impulse required in roll is quite small - less than 50 lb-sec under the worst conditions of disturbance. The total impulse required in pitch, yaw, and roll for the first-flight boost phase could not exceed 1420 lb-sec, and in practice the third stage would, of course, require much less than
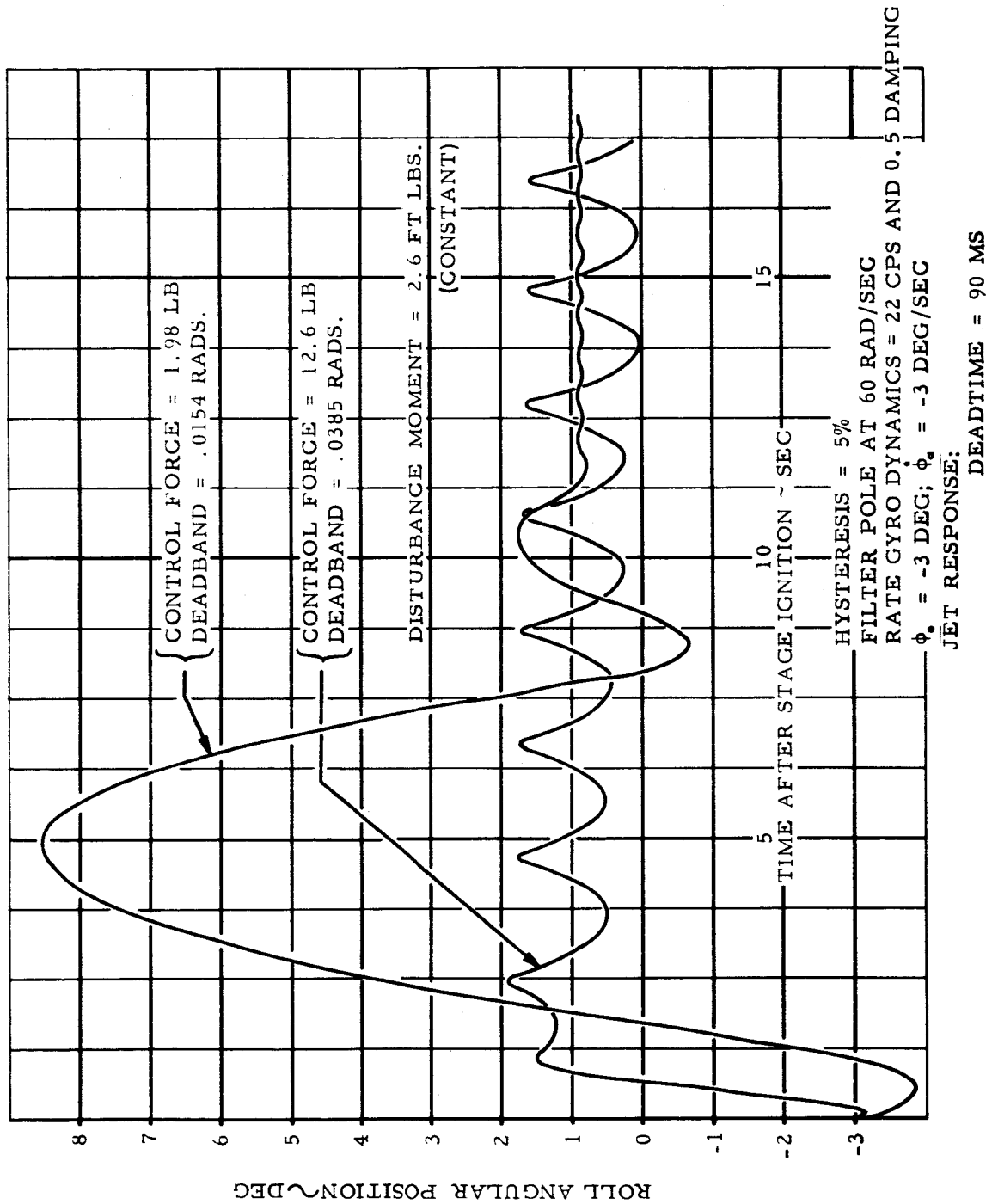
Figure 39   Third-Stage Roll Time Response

this amount. Previous calculations indicating much greater consumption had been made with the assumption that engine thrust misalignment acted further aft than the nozzle throat.

The original design included a provision for turning off the large jets and switching to operation with smaller jets during the long coast period. The two pairs of 2.2 pound "roll" jets were retained for roll control and, in addition, they were used to provide yaw corrections. This was accomplished by mixing the yaw and roll error signals together before they were applied to the electronic switch, so that the diagonally mounted jets would fire when the roll deadband was exceeded and two jets on the right or left side would fire when the yaw error became large enough. The roll moment was thus the same for coast as it was for boost but the yaw moment was reduced to one tenth of its former value. Pitch control during the coast period was provided by a single pair of 2.2 pound jets. At the end of the boost phase, as determined by an acceleration switch on the first flight, the large jets were turned off, the yaw and roll signals were mixed, the small pitch jets were activated, and some of the control deadbands were changed. The deadband changes were made in the interest of accuracy and consisted of reducing the yaw and pitch deadbands to 4.0 mr. With these deadbands, the coast-phase control system was capable of coasting for 600 seconds after burnout.

The level of forward acceleration which would activate the acceleration switch and change the control system to the coast mode of operation was determined by considering the transient disturbance which would be caused if some thrust misalignment still remained when the switch

was activated. The level of two g's was selected as the highest practical value that would not result in a large transient error. Lower level switching was undesirable because the reliability was lower and the switches became more susceptible to vibration.

A summary of the control parameters and tolerances used for the third-stage first flight is given in table 4.

Selection of Control Parameters for Second, Third, and Fourth Vehicles

The first SCOUT firing, performed on 1 July 1960, revealed several unsuspected facets of the overall operation. Telemetered data showed that the acceleration switch behaved poorly in the high acceleration and vibration environment and caused intermittent operation of the large control jets. Data also indicated that a large disturbance moment had been applied to the roll axis 26 seconds after third-stage ignition. The moment, presumably due in some way to the Antares motor, was almost four times as large as the maximum control moment provided. The disturbance, which lasted about five seconds and caused the vehicle to roll through a very large angle, completely overpowered the controls. In addition to this primary disturbance, a small roll impulse was observed three seconds after ignition. It amounted to an angular impulse of six ft-lb-sec applied in an interval of 55 ms, causing a transient roll error of only a few degrees.

The unreliability and intermittent operation of the acceleration switch of the first flight was recognized, and all subsequent systems were changed from the boost to the coast configuration on a signal from

	FLIGHTS	
	Number 1	Number 2

DEADBANDS: (BOOST PHASE)
    Pitch and Yaw
    Roll
	.014 rad ± 10%
	.015 rad ± 10%
		same
		same

DEADBANDS: (COAST PHASE)
    Pitch and Yaw
    Roll
	.004 rad ± 10%
	.015 rad ± 10%
		.014 rad ± 10%
		.015 rad ± 10%

RATE-TO-POSITION GAIN RATIO: Both phases, all axes	0.4 ± 10%	same

REACTION JET THRUST LEVEL: (BOOST PHASE)
    Pitch and Yaw
    Roll
	44 lbs ± 10%
	2.2 lbs ± 10%
		same
		14 lb ± 10%

REACTION JET THRUST LEVEL: (COAST PHASE)
    Pitch
    Yaw and Roll (two jets)
	2.2 lb ± 10%
	2.2 lb ± 10% each
		same
		14 lb ± 10% each

REACTION JET TIME RESPONSES: (BOOST PHASE)
    Turn-on time: Pitch and Yaw
                     Roll
    Turn-off time: Pitch and Yaw
                      Roll
	.070 sec
	.05 sec
	.070 sec
	.09 sec
		same
		san e
		same
		same

REACTION JET TIME RESPONSES: (COAST PHASE)
    Turn-on time: Pitch
                     Yaw and Roll
    Turn-off time: Pitch
                      Yaw and Roll
	.05 sec
	.05 sec
	.09 sec
	.09 sec
		same
		same
		same
		same

METHOD OF CHANGE-OVER TO COAST OPERATION:	Acceleration switch set at 2 g's	Timer (43 seconds after stage ignition)
CONTROL-LOOP FILTER LAG TIME CONSTANT:	.0145 to .0195 sec	same
APPROXIMATE DURATION OF COAST PHASE:	25 sec	15 sec
TOTAL REACTION CONTROL IMPULSE AVAILABLE:	2,556	same
CALCULATED MAXIMUM CONTROL IMPULSE REQUIRED:	1,430 lb-sec	2,415 lb-sec

CALCULATED INITIAL TRANSIENT ERROR,
STANDARD CONDITIONS:
    Pitch or Yaw
    Roll
	2.4 deg
	8.5 deg
		same
		2 deg

Table 4 Third-Stage Control Parameters for Vehicle One

the timer. The huge roll moment, however, presented a more serious problem and its proper solution was not so obvious. It was finally decided that, although the disturbance was unsuspected and its source was not known, the safe approach would be to provide for its occurrence in the future. The peak moment observed on the first flight was about 21 ft-lbs, and it was felt that the system should be modified to cope with values of at least 30 ft-lbs. The alternative was to correct the fault which caused the disturbance, and that might have been a time consuming and expensive process.

The second SCOUT system was modified by increasing the third-stage roll jet thrust to 14 pounds nominal and changing the effective moment arm to 15.1 inches. This was considered to be an interim measure to operate the SCOUT until further information could be obtained. Naturally the large increase in roll jet thrust greatly affected the fuel consumption, even though the jet response times were improved. Fortunately the second flight requirements dictated a third-stage coast time of only 25 seconds, and sufficient fuel was available to operate even these large jets for a short time. The original roll deadband of 14 mr was used.

The second SCOUT firing on 4 October 1960 again showed a roll disturbance of nearly the same magnitude as the first. This time, however, the controls counteracted it and the mission was performed satisfactorily. The continued presence of the roll moment made it necessary to consider retaining the large roll jets during boost and developing a scheme for reducing their thrust level or switching to other jets for long coast periods. A thrust reduction technique was

devised for the third flight which would attenuate the 14-pound thrust to little more than five pounds. The technique consisted of lowering the effective fuel feed pressure by inserting a severe restriction in the peroxide line to the valves. This restriction was to be switched into the line at the beginning of the coast period. The actual behavior of the so-called "turned-down" jets was more complicated after this modification than before. The average thrust level of the jet depended upon the manner of operation, and reduced considerably if the jet was cycled rapidly. At the oscillation frequency and duty cycle expected during the third-stage coast, each pulse would have an average thrust of seven pounds. The response time was good, however; the turn-off times were found to be less than 60 ms. With the roll and yaw deadbands increased from those of previous flights, the third and subsequent systems would still be capable of a 600-second coast period. The roll deadband was increased to 35 mr nominal, and the yaw deadband was changed to 16 mr. These values were used for the entire flight, during second and third-stage boost and third-stage coast. The pitch axis, which still used a 2.2-pound jet, retained its dual deadband of 14 mr during second and third-stage boost, and 4 mr for third-stage coast.

The calculated behavior of the later third-stage roll control system can be seen from the transient-response and fuel-consumption curves of figures 39 through 41. The transient performance with the large jets was, of course, improved. The time response of figure 41 simulates the effect of a 21 ft-lb disturbing moment applied suddenly during burning. The calculated maximum fuel consumed during the boost phase was increased slightly to 1565 lb-sec, leaving 990 lb-sec
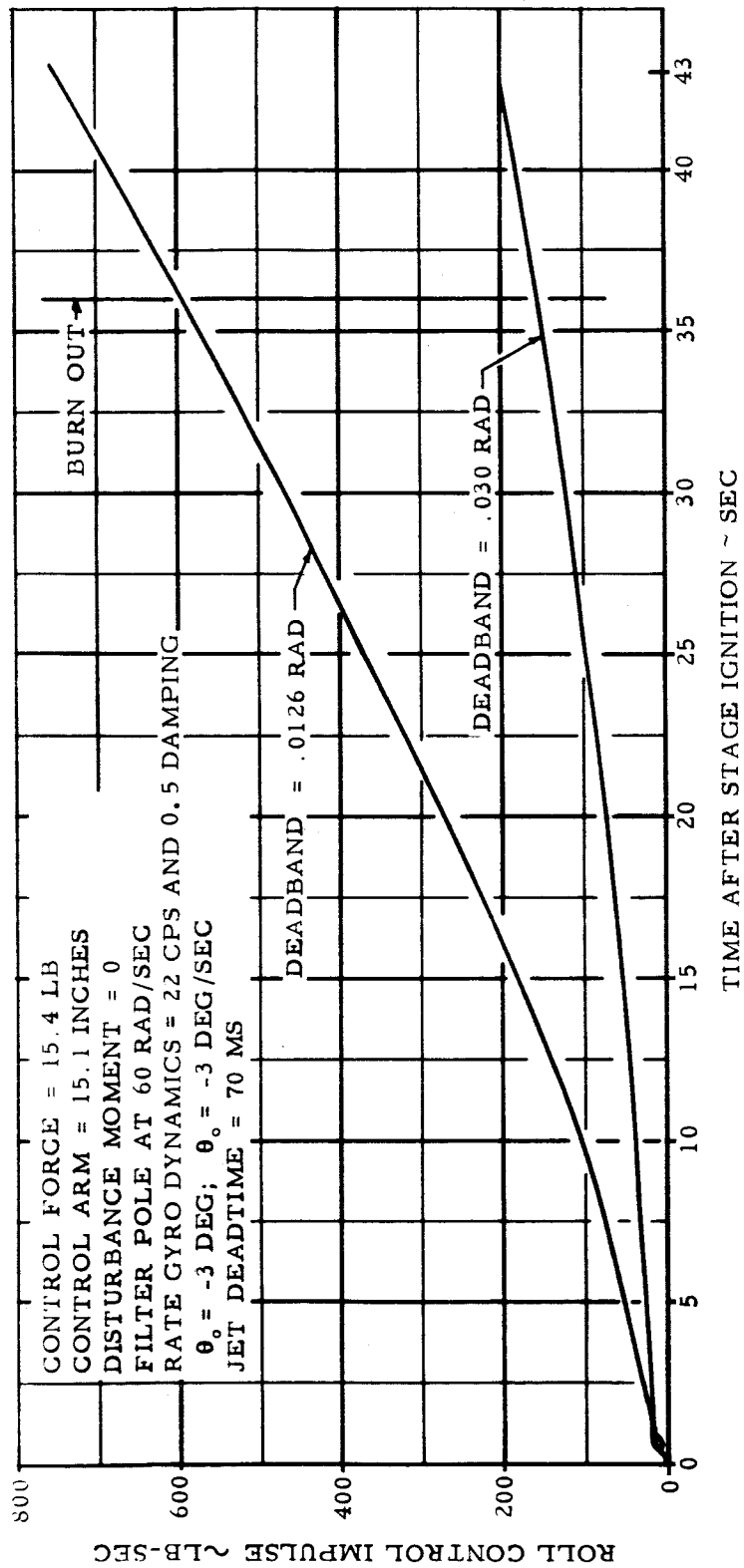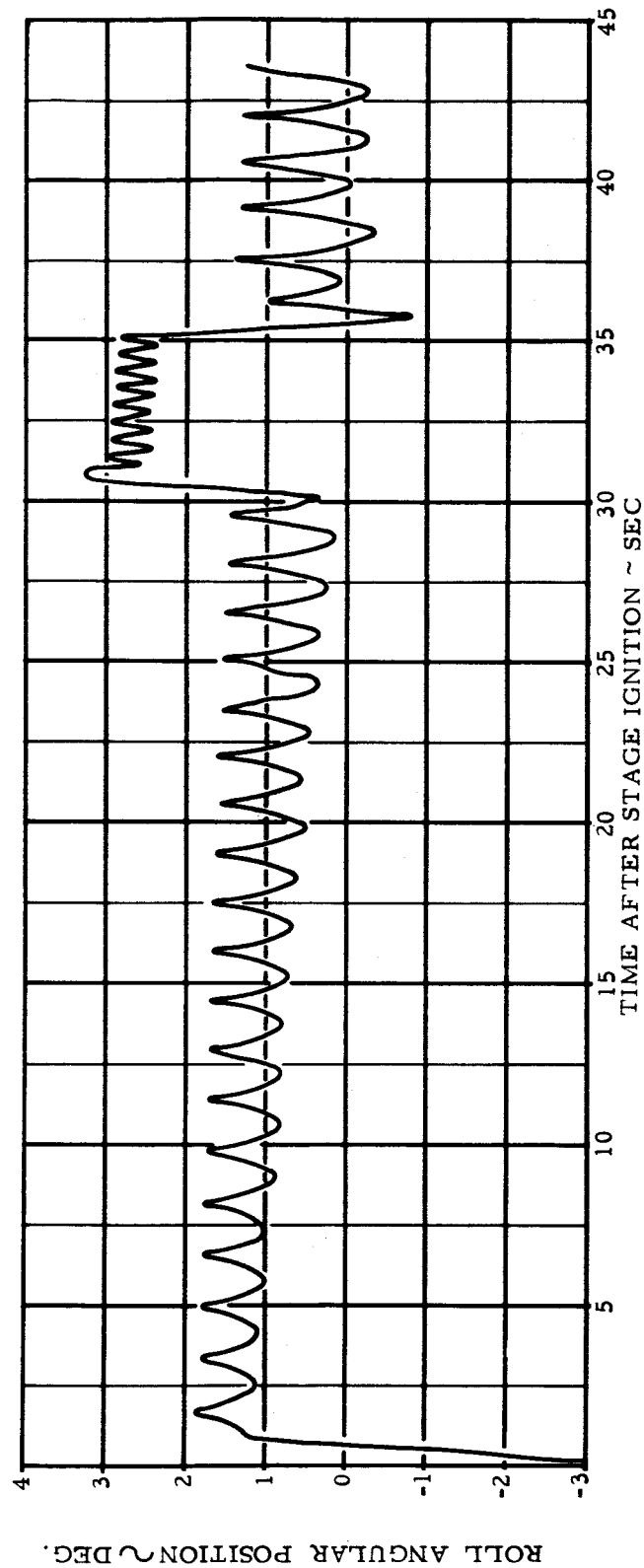
Figure 40   Third-Stage Roll Fuel Consumption

CONTROL FORCE = 12.6 LB
CONTROL ARM = 15.1 INCHES
DISTURBANCE MOMENT = 21 FT LBS
     APPLIED BETWEEN t = 30 AND t = 35 SECS.
DEADBAND = .0385 RADS; HYSTERESIS = 5%
FILTER POLE AT 60 RADS/SEC; RATE GYRO DYNAMICS = 22 CPS AND 0.5 DAMPING
ϕ_o = -3 DEG;   = -3 DEG/SEC
JET DEADTIME = 70 MS

Figure 41   Third-Stage Roll Transient Response to an External Disturbance

for coast. The pitch and yaw performance of the later systems is the same as that shown in figures 37 and 38. The maximum rate of impulse consumption during the coast period was calculated to be:

Pitch axis	.235 lb-sec/sec
Yaw axis	.535 lb-sec/sec
Roll axis	.725 lb-sec/sec

These figures include the effects of electronic and instrument lags, deadbands 10 percent less than nominal, switching hysteresis of five percent of the deadband, and jet thrusts higher than nominal. The pitch jet thrust was taken as 2.42 pounds, while the roll-yaw jets were assumed to produce eight pounds each. The noise-filter lag was switched out at the beginning of the coast period. It should be noted that the third and fourth flight systems were designed for a roll inertia of 38 slug-ft^2 at third-stage burnout in compliance with verbal instructions from NASA. If the original 27.4 slug-ft^2 had been used, the roll impulse consumption rate during coast would increase to approximately 1.0 lb-sec/sec and a 600-sec coast time would be difficult to meet.

A summary of the third and subsequent system parameters is given in table 5. Any changes performed on the fourth vehicle immediately prior to firing are not included in this document.

DEADBANDS: (BOOST PHASE)
   Pitch
   Yaw
   Roll
	.014 rad ± 10%
	.016 rad ± 10%
	.035 rad ± 10%

DEADBANDS: (COAST PHASE)
   Pitch
   Yaw
   Roll
	.004 rad ± 10%
	.016 rad ± 10%
	.035 rad ± 10%

RATE-TO-POSITION GAIN RATIO: Both phases, all axes	.04 ± 10%

REACTION JET THRUST LEVEL: (BOOST PHASE)
   Pitch and Yaw
   Roll
	44 lbs ± 10%
	14 lb ± 10%

REACTION JET THRUST LEVEL: (COAST PHASE)
   Pitch
   Yaw and Roll (two jets)
	2.2 lb ± 10%
	8.0 lb or less

REACTION JET TIME RESPONSE: (BOOST PHASE)
   Turn-on time: Pitch and Yaw
                 Roll
   Turn-off time: Pitch and Yaw
                 Roll
	.07 sec
	.06 sec
	.07 sec
	.06 sec

REACTION JET TIME RESPONSE: (COAST PHASE)
   Turn-on time: Pitch
                 Yaw and Roll
   Turn-off time: Pitch
                 Yaw and Roll
	.05 sec
	.06 sec
	.09 sec
	.06 sec

METHOD OF CHANGE-OVER TO COAST OPERATION:	Timer signal 43 seconds after ignition

CONTROL-LOOP FILTER LAG TIME CONSTANT:
   Boost phase
   Coast phase
	.0145 to .0195 sec
	.0015 sec

APPROXIMATE DURATION OF COAST PHASE:	420 sec
TOTAL REACTION CONTROL IMPULSE AVAILABLE:	2,556 lb-sec
CALCULATED MAXIMUM CONTROL IMPULSE REQUIRED:*	2,195 lb-sec

CALCULATED INITIAL TRANSIENT ERROR, STANDARD CONDITIONS:
   Pitch or Yaw
   Roll
	2.4 deg
	2 deg

* Based on a burnout roll inertia of 38 slug-ft^2 and a yaw inertia of 814 slug-ft^2.

Table 5 Third-Stage Control Parameters for Vehicles Three and Four